

Flow Boiling Heat Transfer and Two-Phase Flow Phenomena of CO₂ in Macro- and Micro-channel Evaporators: Fundamentals, Applications and Engineering Design

CHENG, Lixin, XIA, Guodong and THOME, John

Available from Sheffield Hallam University Research Archive (SHURA) at:

<https://shura.shu.ac.uk/28680/>

This document is the Accepted Version [AM]

Citation:

CHENG, Lixin, XIA, Guodong and THOME, John (2021). Flow Boiling Heat Transfer and Two-Phase Flow Phenomena of CO₂ in Macro- and Micro-channel Evaporators: Fundamentals, Applications and Engineering Design. Applied Thermal Engineering. [Article]

Copyright and re-use policy

See <http://shura.shu.ac.uk/information.html>

Flow Boiling Heat Transfer and Two-Phase Flow Phenomena of CO₂ in Macro- and Micro-channel Evaporators: Fundamentals, Applications and Engineering Design

Lixin Cheng^{1,2*}, Guodong Xia^{1*}, John R Thome³

¹Beijing Key Laboratory of Heat Transfer and Energy Conversion, Beijing University of Technology,
Beijing 100124, P. R. China

²Department of Engineering and Mathematics, Sheffield Hallam University, Howard Street,
Sheffield S1 1WB, UK

³Laboratory of Heat and Mass Transfer (LTCM), Faculty of Engineering (STI), École Polytechnique
Fédérale de Lausanne (EPFL), Station 9, Lausanne, CH-1015, Switzerland

Abstract

The paper presents a comprehensive review of fundamentals and engineering applications of CO₂ flow boiling heat transfer, flow patterns and two-phase pressure drops in macro- and micro-channel evaporators. First, distinctions of macro- and micro-channels are discussed. Second, the review addresses the extensive experimental studies on CO₂ flow boiling heat transfer and two-phase flow in macro- and micro-channels. **The effects of the physical properties on flow boiling heat transfer, flow patterns and pressure drops are analysed by simulations using various physical property packages. Furthermore,** analysis of the existing experimental studies of flow boiling heat transfer is presented and the physical mechanisms are discussed. Next, **generalized CO₂ flow pattern map and flow pattern based mechanistic flow boiling heat transfer and two phase pressure drop modelss specially developed for CO₂ are discussed. New experimental database of flow boiling heat transfer and**

* E-mail address: lixincheng@hotmail.com; xgd@bjut.edu.cn

diabatic two phase frictional pressure drop have been set up to evaluate the models. Comparative results of the flow pattern map, heat transfer and pressure drop models to the experimental database are analysed. In addition, studies of CO₂ flow boiling in enhanced channels are summarized. The oil effects on the flow boiling heat transfer and two phase frictional pressure drop are analyzed and simulated as well. According to the extensive analysis, the physical mechanisms and prediction models of the CO₂ flow boiling heat transfer and two phase flow phenomena in evaporators have been well understood. In the aspect of engineering application, comparisons of simulation results and the experimental data in the real thermal systems are discussed. Furthermore, research need of CO₂ evaporators is discussed. Some practical design methods of CO₂ evaporators are recommended according to the analysis. Finally, the potential application of CO₂ for high heat flux cooling, thermal and power systems are also discussed. Future research needs in flow boiling heat transfer and two phase flow of CO₂ in evaporators and engineering applications are discussed and recommended according to this comprehensive review.

Keywords: CO₂, flow boiling heat transfer, flow pattern map, two phase pressure drop, models, macro- and micro-channel evaporators

Table of Contents

1. Introduction
2. Criteria for distinction of macroscale and microscale channels
3. Fundamental issues of flow boiling and two-phase flow of CO₂ in macro- and micro-channels
 - 3.1. Analysis of the phenomena and physical mechanisms according to the thermal physical and transport properties of CO₂
 - 3.2. Analysis of experimental results of flow boiling heat transfer of CO₂ in macro- and micro-channel evaporators
4. **Generalized flow pattern based mechanistic** flow boiling heat transfer and two phase pressure drop prediction methods specially developed for CO₂ **inside macro- and micro-channels**
 - 4.1. Generalized prediction methods for CO₂ flow boiling heat transfer and two phase pressure drop
 - 4.2. The Cheng et al. [28, 30] diabatic flow pattern map for CO₂ flow boiling in macro- and micro-channels
 - 4.3. The Cheng et al. [31] flow pattern-based flow boiling heat transfer model for CO₂ **evaporation inside channels**
 - 4.4. The Cheng et al. [30] flow pattern based two-phase frictional pressure drop model for CO₂ for CO₂ two phase flow inside channels
5. **Current research status of** flow boiling and two-phase flow of CO₂ in enhanced channels
6. **Current research status of** research on the oil effect on CO₂ flow boiling heat transfer and two-phase pressure drop and prediction methods

- 6.1. Analysis of the experimental data of the oil effect on CO₂ flow boiling heat transfer and two-phase pressure drop
- 6.2. Analysis the oil effect on CO₂ flow boiling heat transfer and two-phase pressure drop prediction methods
7. CO₂ evaporator simulation and engineering design
 - 7.1. CO₂ evaporation and evaporator modeling
 - 7.3. CO₂ evaporator design and selection criteria
8. Potential application of CO₂ in cooling and thermal energy Systems
9. Concluding remarks and future research recommendations

1. Introduction

Over the past decades, CO₂ (R744) has been receiving renewed and intensive interest as an efficient and environmentally safe refrigerant in a number of applications, including mobile air conditioning, residential heat pump and hot water heat pump systems and as the secondary refrigerant in refrigeration systems at low temperatures [1-11]. Compared to other conventional refrigerants, flow boiling heat transfer, flow patterns and two-phase pressure drop are quite different from those of conventional refrigerants [1, 2, 14]. In order to design evaporators for these systems effectively, it is important to understand and predict the characteristics of flow boiling heat transfer, flow patterns and two-phase flow pressure drop of CO₂ evaporation inside horizontal tubes. As a natural working fluid, CO₂ is an ideal working fluid because it is non-explosive, non-flammable, non-toxic, and relatively cheap. CO₂ is also applicable to most thermal energy sources such as fossil fuel combustion, nuclear, solar, geothermal, and waste heat recovery. Therefore, use of CO₂ in a power system has been explored for decades, and it has undergone constant reinvention. Furthermore, it also has potential applications in cooling for electronic device, particle physics detectors and other high heat flux removal [12-19]. Considering the environmental and global warming issue, CO₂ has no ozone depletion potential (ODP = 0) and a negligible direct global warming potential (GWP = 1) when used as a working fluid. CO₂ has a low critical temperature ($T_{cr} = 31.1^{\circ}\text{C}$) and a high critical pressure ($p_{cr} = 7.38 \text{ MPa}$), therefore, CO₂ is utilized at much higher operating pressures in air-conditioning and heat pump systems compared to other conventional refrigerants. As the effects of good thermophysical properties, favorably evaporation heat transfer and two-phase flow characteristics of CO₂ can be achieved in its thermal systems. However, use of CO₂ in various systems requires well understanding and proper modelling of flow boiling heat transfer, two-phase flow patterns and pressure drops for achieving accurate designs of evaporators for high efficiency thermal cycles. Therefore, robust prediction methods for flow boiling heat transfer, two phase flow regimes and pressure drop are critical in design evaporators used in various practical application. Understanding

of the fundamentals of CO₂ flow boiling and two-phase flow phenomena through experimental and modelling is essential in achieving prediction tools for the complex flow boiling and two-phase processes in both macro- and micro-channels. General practical design criteria are needed to be addressed as well. All these aspects in the refrigeration, air-conditioning and heat pump systems are the focus of this timely comprehensive review paper.

CO₂ has favorable thermal performance when used in air-conditioning and heat pump systems as compared to conventional refrigerants. For example, in the CO₂ automobile air-conditioning system, for ambient air temperatures, the heat transfer process on the high pressure side of a CO₂ cycle is not a condensation process as in conventional systems but a supercritical gas cooling process [11]. Figure 1 shows a comparison of pressure-enthalpy diagrams of CO₂ and R134a in automobile air-conditioning systems. For the evaporation processes in the evaporator, CO₂ evaporates at much higher pressure than conventional refrigerant R134a. The physical and transport properties of CO₂ are quite different from those of conventional refrigerants at the same saturation temperatures. The physical properties have a significant effect on the evaporation processes. The characteristics of flow boiling heat transfer, flow patterns and two-phase frictional pressure drops in the compact heat exchangers with micro-channels are quite different from those in conventional channels. Therefore, conventional flow pattern maps, flow boiling heat transfer and two phase pressure drop correlations do not work for CO₂ in micro-channels.

Furthermore, CO₂ has positive attributes as a secondary refrigerant at low temperatures in commercial refrigeration used in supermarkets, shops and large kitchens etc., in indirect and low temperature cascade systems and as a primary refrigerant in all CO₂ centralized refrigeration systems. Figure. 2 shows an ammonia-CO₂ secondary loop of an indirect refrigeration system which operates at low temperatures. CO₂ evaporation and condensation processes are nearly at the same pressures. In particular, this system does not involve any oil effect for the CO₂ secondary loop. The main benefits for using CO₂ in indirect system arrangements include the simplicity of the system and the possibility of using components for other refrigerants to build the CO₂ circuit. In recent years, other

arrangements, such as cascade and multistage systems have been used commercially [10, 11]. Advantages of CO₂ cascade systems include greatly reduced low-temperature compressor size, the absence of a liquid pump and fewer stages of heat transfer. Furthermore, two-stage and multistage CO₂ centralized refrigerant systems are also used in supermarket refrigeration. These systems are most suitable for cold climates or where heat sinks are available [11]. The operation of such refrigeration systems is mostly in the sub-critical region. If the ambient temperature is higher than the critical temperature, the system will be super-critical and this generally should be connected to another thermal system such as hot water or space heating heat pumps for efficient energy use. Due to the high working pressure, CO₂ as a phase change secondary refrigerant has a high volumetric refrigeration capacity, which equates to approximately five times or more that of R22 and NH₃. Therefore, use of CO₂ in the refrigeration systems requires understanding and prediction of flow boiling heat transfer, flow patterns and two phase pressure drops at low temperatures for achieving accurate designs of evaporators and energy-efficient refrigeration system cycles using CO₂.

Both macro- and micro-scale channels are used in the CO₂ refrigeration, air-conditioning and heat pump systems. For example, in the automobile air-conditioning systems, micro-scale channels with diameters of 0.6 to 1 mm are generally used in evaporators while macro- and micro-channels are used for CO₂ refrigeration and heat pump systems. Due to the quite different phenomena and physical mechanisms of flow boiling in micro-scale channel evaporators as compared to macro-scale channel evaporators, emphasis has been put on the characteristics of flow boiling heat transfer and two phase in small and micro-scale flow passages due to the rapid development of micro-scale devices in recent years [3, 5, 11-20].

Although experimental studies and models on CO₂ flow boiling and two-phase flow characteristics have been conducted in macro- and microchannels over the past decades. There are quite different results for similar working conditions from various studies. Furthermore, some flow boiling heat transfer and two phase pressure drop correlations have been developed based only on specific or limited experimental results. These lack generality and in general they cannot be

extrapolated to other conditions. In particular, these correlations lack the connection to the flow regimes which represent the corresponding flow boiling heat transfer mechanisms. Some such methods only predict the experimental data globally to some extent but cannot predict the parametric trends of CO₂ flow boiling and two phase flow.

It is essential to understand the flow boiling heat transfer and two-phase flow processes and mechanisms at low and high saturation temperatures for properly designing the evaporators which use macro- micro-channels for the automobile air-conditioning, heat pump and refrigeration systems. From a predictive standpoint, many features of the existing flow pattern maps, flow boiling heat transfer and two-phase pressure drop correlations require refinement to attain the desired level of accuracy for refrigerant heat exchangers (evaporators, internal heat exchangers, gas coolers and condensers) design. Therefore, this review focuses on understanding the fundamentals, mechanisms and applications of flow boiling heat transfer and two phase pressure drop in macro- and micro-channels, simulations of flow boiling and two phase flow using the mechanistic models based on flow patterns, application of these methods in practical applications and design of evaporators. The flow boiling and two phase characteristics in evaporators with the effects of oil are also analyzed according the available experimental data and modeling. Design of CO₂ evaporators is discussed. According to this comprehensive review, the future research needs have been identified and recommended.

2. Criteria for distinction of macroscale and microscale channels

Both macro- and micro-scale channels are used in the CO₂ refrigeration, air-conditioning and heat pump systems. For example, in the automobile air-conditioning systems, micro-scale channels with diameters of 0.6 to 1 mm are generally used in evaporators, internal heat exchangers and gas coolers. Due to the significant differences of two-phase flow and evaporation heat transfer phenomena in micro-scale channels as compared to conventional size channels or macro-scale channels, emphasis has been put on the characteristics of two-phase flow and heat transfer in small and micro-scale flow

passages due to the rapid development of micro-scale devices. Experimental studies and models on CO₂ flow boiling, flow patterns and two-phase flow characteristics in both macro- and microchannels have been conducted over the past decades.

Due to the quite different flow boiling phenomena in microscale channels as compared to conventional size channels or macroscale channels, the first and most important issue should be clarified about the distinction between micro-scale channels and macro-scale channels. However, a universal agreement is not yet established so far. Instead, there are various definitions on this issue, which are based on the engineering applications, bubble confinements or others [12 - 22]. Here, just to show two examples, based on engineering practice and application areas such as refrigeration industry in the small tonnage units, compact evaporators employed in automotive, aerospace, air separation and cryogenic industries, cooling elements in the field of microelectronics and micro-electro-mechanical-systems (MEMS), Kandlikar and Grande [15] and Kandlikar [16] defined the following ranges of hydraulic diameters D_h which are attributed to different classifications:

- Conventional channels: $D_h > 3$ mm.
- Minichannels: $D_h = 200 \mu\text{ m} - 3$ mm.
- Microchannels: $D_h = 10 \mu\text{ m} - 200 \mu\text{ m}$.

According to this definition, the distinction between small and conventional size channels is 3 mm and the distinction between mini and micro channels is 200 μm .

Kew and Cornwell [20] earlier proposed the Confinement number Co for the distinction of macro- and micro-scale channels, as

$$Co = \frac{1}{D_h} \sqrt{\frac{4\sigma}{g(\rho_L - \rho_G)}} \quad (1)$$

which is based on the definition of the Laplace constant [17, 22]. Other different definitions are also proposed in the reviews [13, 17, 18, 22]. Obviously, there is no agreement on the definition of a

micro-scale channel so far. Figure 3 shows the comparable definitions macro- and micro-scale channels for CO₂ according to Kandlikar and Grande [15] and Kandlikar [16] and the Confinement number Co which shows the big difference among these criteria.

However, it should be realized that the transition from macro-to-micro scale is a continuous and progress process which corresponds to the flow regime, flow boiling heat transfer behaviors and mechanisms. Therefore, the most important point is to relate flow regimes to flow boiling heat transfer and two phase pressure drop behaviors [13, 22, 27 - 31]. Relating flow regime behaviors to the corresponding flow boiling heat transfer and gas liquid two phase flow behaviors is a practical and effective method to develop mechanistic or phenomenal predictions for both macro- and micro-channels due to the continuously progressive change from macro- channels to micro-channels. This has been validated by the flow pattern based CO₂ flow boiling model of Cheng et al. [28-31], which covers both macroscale and microscale channels for CO₂ flow boiling heat transfer and two phase flow. Their generalized flow pattern based CO₂ flow boiling heat transfer model predicts both macro- and micro-channel flow patterns and heat transfer reasonably well. Especially, their CO₂ flow pattern map captured well the independent flow pattern observations in microscale channels by Gasche [76] and Mastrullo et al. [100]. It gives a hint that the macro- and micro-channels may be determined according to the flow boiling heat transfer behavior due to the intrinsic links between the heat transfer mechanisms and the flow structures in both macro- and micro-channels. A mechanistic distinction criterion may be more of practice and effectiveness in developing new flow boiling heat transfer prediction methods. However, such criteria need to be further developed in future. To some extent, using Kandlikar's criterion of 3 mm to distinct the macro- and micro-channels is reasonable when developing mechanistic models because it covers the transitional region from macroscale to microscale flow boiling. It should be realized that the transition between microscale and macroscale channels has neither been well defined nor seriously experimentally investigated as evidence as mentioned by Cheng and Xia [13]. However, one may distinguish between flow boiling behaviors such as heat transfer, flow patterns and pressure behaviors in macro- and micro- channels. It is

definitely effective from the viewpoint of practical applications if the flow patterns can be incorporated into flow boiling heat transfer and two phase frictional pressure drop prediction methods simultaneously with the corresponding heat transfer mechanisms such as those by Katten et al. [50-52], Wojtan et al. [48, 49], Cheng et al. [28-31], Moreno Quibén and Thome [63, 64] and Moreno Quibén et al. [68, 69]. Such a prediction method actually works reasonably well if they are related flow regimes and bubble dynamics to the corresponding heat transfer behaviors.

The dimensionless number such as the confinement number has been given different values according to individual observations and experimental data with limited test fluids, test channels and test conditions. Although a number of such criteria have been proposed by various researchers so far, it is obvious that no universal agreement has been reached according to the dimension less numbers. The main reason is due to the limited experimental parameter ranges and test channel sizes and shapes. In the present paper, the distinction between macro- and micro-channels by the threshold diameter of 3 mm is adopted due to the lack of a well-established theory, but is in line with that recommended by Kandlikar and Grande [15] and Kandlikar [16]. Using this threshold diameter enables more relevant studies to be included and thus the different flow boiling heat transfer characteristics, mechanisms and models in various channels with different sizes can be compared and analyzed. This distinction is also reasonable and valid for the practical use in the CO₂ air-conditioning, heat pump and refrigeration systems.

3. Fundamental issues of flow boiling and two-phase flow of CO₂ in macro- and micro-channels

3.1. Analysis of the the phenomena and physical mechanisms according to the thermal physical and transport properties of CO₂

The existing experimental studies have shown that CO₂ has higher flow boiling heat transfer coefficients and lower pressure drops than those of conventional refrigerants at the same saturation

temperatures. The available flow boiling heat transfer correlations developed for conventional low pressure refrigerants generally significantly underpredict the experimental data of CO₂. Furthermore, dryout may occur much earlier (at moderate vapor quality) in CO₂ flow boiling, particularly at high mass flux and high temperature conditions [6]. Significant deviations for the two phase flow patterns of CO₂ compared to the flow pattern maps that were developed for other fluids at lower pressures have been observed as well. Two-phase pressure drops of CO₂ are also much lower than those for conventional low pressure refrigerants [6].

Thermal physical and transport properties of CO₂ have a significant effect on the flow patterns, two phase flow and evaporation heat transfer characteristics and the corresponding prediction models in the evaporator tubes. CO₂ has higher liquid and vapor thermal conductivities, a lower vapor-liquid density ratio (lower liquid and higher vapor densities), a very low surface tension, and a lower liquid-vapor viscosity ratio (lower liquid and higher vapor viscosities) than conventional refrigerants. As a result, the flow boiling heat transfer, two-phase flow pattern and pressure drop characteristics are quite different from those of conventional low pressure refrigerants. CO₂ has a much higher saturation pressure than R134a at the same saturation temperature. CO₂ has a much lower vapor-liquid density ratio (lower liquid and higher vapor densities), higher liquid and vapor specific heats, a lower liquid-vapor viscosity ratio (lower liquid and higher vapor viscosities), a higher latent heat (only near the critical point, the CO₂ latent heats are lower than R134a), much higher liquid and vapor thermal conductivities and much lower surface tensions than R134a. The different physical properties result in quite different flow boiling heat transfer, two-phase flow pattern and pressure drop behaviors as compared to those of R134a. The different thermal physics and transport properties of CO₂ at low and high reduced pressures may be used to explain the different flow boiling and two phase mechanisms at various working conditions and further to develop mechanistic models based on flow patterns.

The thermal physical properties of CO₂ may be obtained from several software packages [23 - 26]. There are some differences among these software packages. The physical properties have some

effect on reducing experimental results and implementation of prediction methods. The CO₂ flow pattern map, evaporation heat transfer and two-phase pressure drop models [28 - 31] were developed using the physical properties from REFPROP.NIST version 6.01 [25]. Since the Cheng et al. models were developed in 2006 and 2008 [28-31], there have been a number of experimental studies on CO₂ flow boiling and two phase flow. It is essential to evaluate the Cheng et al. models with the new data. First, evaluation of the effects of the physical properties from different property packages on flow boiling heat transfer and flow patterns has been done here. Figure 4 shows the simulated results by the Cheng et al. model [30, 31] using various physical properties of EES [24], REFPROP 6.01 [25], REFPROP 7.0 [26] and REFPROP 9.1 [27] at the indicated working conditions. Figure 4 (a) shows the simulated flow boiling heat transfer coefficients of CO₂ versus vapor quality at the indicated conditions and it indicates that using REFPROP 6.01 gives slightly different simulated results while other property packages give the same results. The difference of the simulated heat transfer coefficients is less than 8%, which is insignificant for flow boiling heat transfer. Figure 4 (b) shows the corresponding flow pattern map where the vertical dash line represents the intermittent to annular flow (I to A) and the Stratified-wavy and Slug flow to stratified-wavy flow transition using EES, REFPROP 7.0 and REFPROP 9.1 and the solid vertical line represents the I to A transition using REFPROP 6.01. The difference of the transition vapor quality is only 0.01 which is negligible for flow boiling processes. To further analyze the physical property effects on flow boiling heat transfer and flow patterns, the predicted results using REFPROP 6.01 and REFPROP 9 are compared to the experimental data for different diameter channels from macro-channels to microchannels, different saturation temperatures, heat fluxes and mass flow rates as shown in Figs. 5 to 9. It shows that using different property packages may produce slightly different heat transfer results or the same results depending on the experimental conditions while it predicts the same flow pattern maps. Furthermore, the CO₂ two phase pressure drop model of Cheng et al. [30] has also evaluated with these property packages and it gives the same predicted results for flow pattern map as shown in Figs. 5(b) to 9(b). Therefore, no predicted results are shown here.

Furthermore, lubricant oil has great effect on heat transfer and pressure drop, which should be clarified for both flow boiling heat transfer and two phase pressure drops of CO₂. Therefore, it is important to understand and to predict the two phase flow patterns, pressure drop and heat transfer in flow boiling without and with the oil effect in evaporators.

3.2. Analysis of experimental results of flow boiling heat transfer of CO₂ in macro- and micro-channel evaporators

Table 1 lists selected experimental study of flow boiling heat transfer in the literature before 2007, which were used in the development of the Cheng et al. [28 – 31] flow pattern map, heat transfer and pressure drop models developed in 2006 and 2008. Table 2 lists the selected experimental studies on flow boiling heat transfer and two phase flow of CO₂ inside macro- and micro-channels after 2007. It is interesting to see that a number of studies before 2007 are related to flow boiling in multi-microchannels before 2007 while nearly all the studies after 2007 are related to flow boiling in single circular channels. It essential to conduct research of flow boiling and two phase flow in multi-channels in order to understand the phenomena and mechanisms but all the latest studies are related to single circular channels. According to the available studies in the literature, quite different evaporation heat transfer and two-phase flow behaviors of CO₂ have been shown for high and low reduced pressures [28-31].

The flow boiling heat transfer and two-phase flow characteristics of CO₂ at the saturation temperatures ranging from 0 to 25°C show quite different characteristics as compared to those of conventional refrigerants due to the significant differences in physical properties. Generally, CO₂ has much higher evaporation heat transfer and much lower pressure drops than other low-pressure refrigerants. One feature is the dominance of the nucleate boiling at low/moderate vapor qualities prior to dryout [32 - 36]. Another feature is that the dryout in CO₂ flow boiling occurs much earlier (at relatively lower vapor qualities) than conventional refrigerants. **Nucleate boiling is the dominant heat transfer mechanisms for CO₂ evaporation at low vapor qualities. Del Col [102] conducted**

experimental study of flow boiling of R410A at high saturation temperature (40°C) and found the similar observation for R410A. For carbon dioxide and for R410A, the decreasing trend of the heat transfer coefficient with vapor quality is due to the large dominance of nucleate boiling at low vapour qualities and to partial dryout of the liquid film. Therefore, Similarities between R410A and carbon dioxide can be seen from this research.

Furthermore, the effect of the saturation temperature on the evaporation heat transfer coefficients is noticeable. At higher saturation temperatures, the nucleate boiling is more pronounced and plays an important role at the low vapor quality. However, the experimental data from the different independent studies show somewhat quite different evaporation heat transfer trends at similar test conditions. Just to show several examples here, Figure 10 two opposite evaporation heat transfer behaviors with the saturation temperature in the studies of Pettersen [32] and Yoon et al. [36]. Heat transfer coefficients increase with increasing saturation temperature in the study of Pettersen while they decrease in the study of Yoon et al. The only big difference between the two studies is the diameter of the test channels as indicated in Fig. 10. Figure 11 shows comparison of the experimental data of Yun et al. [37] for two diameters of 1.53 mm and 1.54 mm at the same test conditions. According to their results, the evaporation heat transfer coefficients can be higher up to 80% with a very little change of hydraulic diameter from 1.53 mm to 1.54 mm at the same test conditions. The uncertainty of heat transfer coefficient is 12.9% reported in their study. No explanation why there is such a big difference even was offered in their paper. Other different results are also analyzed here. By comparing the heat transfer coefficients of Pettersen [32] with those of Koyama et al. [38, 45], the biggest difference between them is that in Koyama et al. the heat flux is 32.06 kW/m² while in Pettersen it is 10 kW/m² but the heat transfer coefficients fall off at a vapor quality of about 0.7 in the study of Pettersen while the heat transfer coefficients increase even at qualities larger than 0.7 in the study of Koyama et al. It is difficult to explain why the heat transfer coefficients fall off at the lower heat flux in one study while they still increase at the higher heat flux in the other study. This could be an effect of the heating methods or because of multi-channel vs. single channel test setups. For the

heat transfer results of Hihara [39] at a mass velocity of $360 \text{ kg/m}^2\text{s}$, a saturation temperature of 15°C and a heat flux of 18 kW/m^2 with two different tube diameters, 4 and 6 mm, the heat transfer coefficients of the 4 mm tube are twice those of the 6 mm tube. In addition, the trends of the heat transfer coefficients are totally different. As both diameters are in the range of macro scale, it is surprising that the diameter has such a big effect on the heat transfer values and trends. Hence, in summary, there is still not a clear view of why CO_2 data do not conform to conventional trends and also differ widely from one study to another.

Furthermore, the available studies have shown different heat transfer behaviors at lower saturation temperatures from those at higher saturation temperatures. In fact, at low evaporation temperatures down to -40°C , the CO_2 reduced pressures (e.g. the reduced pressure $p_r = 0.136$ at -40°C) are still much higher than those of conventional refrigerants such as R134a (e.g. the reduced pressure $p_r = 0.0126$ at -40°C). The physical properties at the lower temperatures are much different from those of R134a but similar trends as those of CO_2 at higher temperatures are shown. It is difficult to explain the experimental results in some studies at low temperatures. For example, Bredensen et al. [40] performed the boiling heat transfer experiments with CO_2 at temperatures of -10°C and -25°C . The experimental results show the heat transfer coefficient increases with vapor quality until dryout, which is opposite to the trend of their data at 0°C . Knudsen and Jensen [41] measured flow boiling heat transfer coefficients of CO_2 in a horizontal tube of diameter 10.06 mm at the saturation temperatures of -28°C and -30°C . Their boiling heat transfer coefficients are much lower than others' data. Zhao and Bansal [42] presented experimental heat transfer data at -30°C . Park and Hrnjak [43, 44] showed the heat transfer coefficients in a 6.1 mm inner diameter tube at -30 and -15°C for various mass fluxes and heat fluxes. Quite big differences among these data are found. It is difficult to explain why there are such big differences although the test conditions are similar. Zhao and Bansal [42, 46] also found that the Liu and Winterton [57] correlation predicted their data rather well while it does not predict other data [40, 41]. In fact, there are only few data points in their study. Considering the

big differences among the available data, it is recommended that more and accurate experimental data at low temperatures are needed by careful and properly designed experiments and documented research papers. There are several experimental studies of CO₂ flow boiling heat transfer and two-phase pressure drop in micro-channels at low temperature available after 2007 as summarized in table 2.. It is interesting to evaluate the Cheng et al. CO₂ flow boiling and pressure drop models with the new experimental data, which helps to further understand the physical mechanisms and identify future development of new prediction methods. The comparative results of the predicted and experimental data are presented and analyzed in the following sections.

Heat flux has a significant effect on the heat transfer trends as reported by Jiang et al. [96] and Kenia et al. [114]. With increasing heat flux, heat transfer coefficient increases in both studies. It indicates that the heat transfer mechanism is nucleate boiling dominant for CO₂ flow boiling in their studies. The results of Jiang et al. show that the dryout occurs at a low vapor quality as indicated to a sharp decrease in heat transfer coefficient while the results of Kenia et al. do not show that the dryout occurs. It is difficult to explain the results of Kenia et al. because dryout is typical phenomenon in flow boiling of CO₂.

Contradictory experimental data at the same conditions from different studies make it difficult to understand the physical mechanisms and develop accurate prediction methods if improper data are used in developing the methods. Evaluation of various available prediction methods has indicated different results by different results. Table 3 listed the selected research on evaluation of flow boiling heat transfer correlations and development of new flow boiling heat transfer correlations. It can be seen that the evaluations of the available correlations and models give quite diverse results. In general, the available correlations were originally developed for low reduced pressure fluids do not work for CO₂ due to the quite different physical properties. Some researchers simply modified the available correlations based on their own experimental data which do not cover a wide range of channel size, saturation temperatures and mass flow rates. Such correlations do not work properly. In particular, most of the correlations do not include the physical mechanisms and cannot capture the sharply

change between the dryout and mist flow regimes. Nearly all these correlations do not include underneath flow structures and therefore lack the proper physical mechanisms. Therefore, it is essential to develop prediction methods based on the corresponding flow patterns.

Furthermore, empirical heat transfer methods do not capture the parametric trends in dryout and mist flow regimes and cannot explain the physical mechanisms although they predict some data well in some cases. Therefore, an improved heat transfer model based on flow regimes for flow boiling is needed, but first accurate experimental data under wide test conditions are needed. Furthermore, no two-phase pressure drop data at low temperatures are available so far. Regarding the flow boiling heat transfer mechanisms, high reduced pressures and low surface tensions for CO₂ compared to conventional refrigerants have major effects on nucleate boiling heat transfer characteristics. Previous studies have suggested a clear dominance of nucleate boiling heat transfer even at very high mass flux. Therefore, CO₂ has much higher heat transfer coefficients than those of conventional refrigerants at the same saturation temperature and the available heat transfer correlations generally underpredict the experimental data of CO₂. In addition, previous experimental studies have demonstrated that dryout trends occur earlier at moderate vapor qualities in CO₂, particularly at high mass flux and high temperature conditions. However, it is difficult to explain the available boiling data at low temperatures according to these mechanisms although nearly all these studies pointed to nucleate boiling dominant mechanism with respect to their data. From the physical properties at low temperatures, it seems that these heat transfer behaviors should be similar to those at high saturation temperatures but they are not indeed. Thus, understanding of the two-phase flow and heat transfer characteristics of CO₂ at low temperatures is essential.

In summary, flow boiling and two phase flow of CO₂ in macro- and micro-channels at low and high temperatures (corresponding to low and high reduced pressures) are important in evaporator design and simulation. It is essential to understand the mechanisms governed by the channel size and at low and high saturation temperatures. In particular, accurate mechanistic prediction methods for

flow patterns, flow boiling heat transfer and two phase pressure drops are required under a wide range engineering application operation conditions.

4. Generalized flow pattern based mechanistic flow boiling heat transfer and two phase pressure drop prediction methods specially developed for CO₂ inside macro- and micro-channels

4.1. Generalized prediction methods for CO₂ flow boiling heat transfer and two phase flow pressure drop

Cheng et al. [28 - 31] did comprehensive literature review on the relevant topics, collected the experimental results from different studies and critically analyzed the results in developing new flow pattern map and models for evaporation heat transfer and frictional pressure drops of CO₂ inside horizontal tubes in 2006 and 2007. Based on the database setup, Cheng et al. have developed a general flow pattern map covering all flow patterns, flow pattern based evaporation heat transfer and two phase frictional pressure drop models for CO₂ evaporating inside horizontal models. Fang et al. [58 - 60] developed several correlations for CO₂ flow boiling heat transfer correlations over the past years and compared a large number of prediction methods. They have concluded that their correlations are the best methods with a large amount of database collected from the literature. In particular, their last version of correlation developed for 18 fluids predicts 93.5% of the database within $\pm 10\%$. It should be realized the measured uncertainty of flow boiling heat transfer is large than $\pm 10\%$. In particular, with such a large of database of 18 different fluids, it is essential to validate this model in future to see if the correlation capture the parametric trends. It is important to show the predicted heat transfer trends against the experimental data while quite a large of number of the available studies do not present such results. In particular, dryout occurs much earlier for CO₂ than other fluids as evidenced by many studies. Jiang et al. [96] compared their experimental data with the Fang et al. [59] correlation. **It can be clear that there are big errors in both pre-dryout and dryout regions although**

they claim the Fang et al. correlation predicts their data well. However, such detailed analysis and discussion are not presented in their paper. Most recently, Mastrullo et al. [6] evaluated a number of methods and have found that the Fang et al. [60] correlation is the best method which predicts 80% of their database with $\pm 30\%$. Again, it would be interesting to show some predicted parametric trends for specific working conditions and also propose the physical mechanisms underneath the correlation. The classic Chen [53] correlation clearly indicates two heat transfer mechanisms of nucleate boiling and convective boiling which have been adopted by most of the researchers. Sometimes, they predict the data globally but it is unknown if they are able to capture the parametric trends. A number of researchers evaluated the flow pattern based heat transfer model of Cheng et al. [28-31] with their experimental data find their models not only favorably predict their data but also capture the trends while others show some different results. It is important to consider the flow regimes in developing the prediction methods. A comprehensive flow pattern map is needed for such a purpose.

Here we do not present another comprehensive review but concisely present a systematic knowledge on this topic covering the behaviors of flow boiling heat transfer, two-phase flow patterns and two-phase pressure drops without oil effect are briefly summarized according to the available studies. The CO₂ flow map, flow pattern based flow boiling heat transfer model and phenomenological two-phase frictional pressure drop model are mainly presented in the following sections.

According to the overall review of evaporation heat transfer and two-phase flow of CO₂ in the literature conducted by Thome and Ribatski [5], none of the available prediction methods was able to predict the experimental data of CO₂ well. Therefore, they suggested that a new evaporation heat transfer prediction method should be developed and the evaporation heat transfer model should include the CO₂ effects on the annular to dryout and dryout to mist flow transitions in order to more accurately predict heat transfer coefficients at moderate/high vapor qualities. In response, Cheng et al. [28, 29] proposed a new flow pattern map and a new evaporation heat transfer model based on the

flow patterns for CO₂ evaporating inside horizontal tubes. The flow map and flow pattern based mechanistic heat transfer model were developed by modifying the methods of Wojtan et al. [48, 49], which is an updated version of the Kattan et al. [48-50] flow pattern map and evaporation heat transfer model which were developed for five conventional refrigerants. Cheng et al. [28, 31] related the flow patterns to the corresponding evaporation heat transfer mechanisms for CO₂, thus, different from the numerous empirical models, such as the correlations of Chen [53], Shah [54], Gungor and Winterton [55], Kandlikar [56] and Liu and Winterton [57], Steiner and Taborek model [68], Kim and Mudawar [5], Jung et al. [103], Hihara and Tanaka [104] et al., which do not include flow pattern information. In fact, some of these correlations predicted the data well to some extent but fail to capture the parametric trends or ignore the dryout and mist flow regimes which are typical working conditions for CO₂ evaporating in horizontal channels. The Cheng et al. [28] CO₂ flow boiling heat transfer model is applicable to a wide range of conditions: tube diameters (equivalent diameters defined by Eq. (2) is used for non-circular channels) from 0.8 to 10 mm, mass fluxes from 80 to 570 kg/m²s, heat fluxes from 5 to 32 kW/m², saturation temperatures from -28 to 25°C (the corresponding reduced pressures are from 0.21 to 0.87). The model reasonably predicts the database and it covers channel diameters found in most CO₂ evaporation applications. However, their model is limited by its parameter ranges from being applicable to some important applications, for example, the mass velocity ranges from 50 to 1500 kg/m²s in CO₂ automobile air conditioning systems and other thermal systems. In addition, the heat fluxes in some applications go beyond the maximum value in the Cheng et al. evaporation heat transfer model. Furthermore, the model does not extrapolate well to these conditions. In addition, the heat transfer model does not include heat transfer methods for CO₂ in mist flow and bubbly flow regimes due to the lack of the experimental data in these regimes, which were not available at that time. Therefore, it is necessary to update the heat transfer model for CO₂ to cover a wider range of conditions and these flow regimes and an updated version of the Cheng et al. [30, 31] evaporation model was developed. Furthermore, a flow pattern based two-phase pressure drop model was also needed for CO₂ was developed by Cheng et al. [30]. Over the past decades, these

methods have been verified to be the most favorable methods for CO₂ flow boiling heat transfer and two phase flow in both macro- and micro-channels. However, improvement of the methods in some flow patterns such as dryout and mist flow is needed due to the inaccurate and less experimental data in these regimes.

4.2. The Cheng et al. [28, 30] diabatic flow pattern map for CO₂ flow boiling in macro- and micro-channels

There are a large number of correlations and models available in the literature for flow boiling of saturated liquids in conventional channels. A number of researchers have developed correlations or models for microchannel flow boiling on the basis of these for macroscale channel flow boiling. Most of these consider the contribution of two flow boiling heat transfer mechanisms: nucleate boiling dominant and convective boiling dominant. The heat transfer coefficient correlations can generally be divided into three groups: (i) The summation correlations: The heat transfer coefficient is considered to be the addition of the nucleate and convective boiling contribution such as the Chen correlation [53]; (ii) The asymptotic model: The heat transfer coefficient is calculated using the asymptotic model such as the Steiner and Taborek model [68]; (iii) The flow pattern based model: This model consists of a flow pattern map and flow pattern specific models and correlation for the heat transfer such as the prediction methods by Kattan et al. [50-52] and Wojtan et al. [48, 49].

Flow patterns are very important in understanding the very complex two-phase flow phenomena and heat transfer trends in evaporation heat transfer. To predict the local flow patterns in a channel, a flow pattern map is used. In fact, successful flow pattern based evaporation heat transfer and two-phase frictional pressure drop models [48-52, 63-64, 69, 70] have been proposed in recent years. Over the past decades, many flow pattern maps have been developed to predict two-phase flow patterns in horizontal tubes, such as those by Baker [65], Taitel and Dukler [66], Hashizume [67], Steiner [68] and so on, just to name a few. Most were developed for adiabatic conditions and then extrapolated by

users to diabatic conditions, thereby creating big discrepancies. For this reason, a number of diabatic flow pattern maps related to the corresponding heat transfer mechanisms have been developed [48-52]. However, none of these is applicable to CO₂ evaporation in horizontal tubes because the two-phase flow characteristics of CO₂ evaporation are greatly affected by the very high reduced pressures and low surface tensions of CO₂. In addition, the very low viscosities of CO₂ at high reduced pressures may affect the two-phase pressure drop greatly.

Cheng et al. [30, 31] proposed a new flow pattern map and a new general evaporation heat transfer model, flow pattern map and two-phase frictional pressure drop model for CO₂ in macro- and micro-scale channels to meet the wide range of parameters used in practical applications. The details of the flow pattern map are presented at first, then the evaporation and two phase pressure drop models are respectively presented in the following the flow pattern map. The physical properties of CO₂ have been obtained from REFPROP version 6.01 of NIST [25]. The flow pattern map is intrinsically related to the evaporation heat transfer model and the two phase frictional pressure drop model which are mechanistic based prediction methods and different from conventional empirical correlations.

Both circular and non-circular channels are used in CO₂ evaporators. For non-circular channels, equivalent diameters rather than hydraulic diameters were used in the flow pattern map [28, 30, 31, 69, 70] as follows:

$$D_{eq} = \sqrt{\frac{4A}{\pi}} \quad (2)$$

Using the equivalent diameter gives the same mass velocity as in the non-circular channel and thus correctly reflects the mean liquid and vapor velocities, something using hydraulic diameter in a two-phase flow does not. In the updated CO₂ flow pattern map, several new features were developed as compared to the Cheng et al. flow pattern map [28, 30]:

- (1) Combining with the updated flow boiling heat transfer model for CO₂, the annular flow to dryout region (A-D) transition boundary was further modified so as to better fit the sharp changes in flow boiling heat transfer characteristics for higher mass velocities.
- (2) Based on experimental heat transfer data, a new criterion for the dryout region to mist flow (D-M) transition was proposed.
- (3) Bubbly flow occurs at very high mass velocities and very low vapor qualities and a bubbly flow pattern boundary was integrated into the map to make it more complete.

With these modifications, the updated flow pattern map for CO₂ is now applicable to much higher mass velocities. Complete flow pattern transition criteria of the updated flow pattern map for CO₂ are described here for the convenience of researchers' use of the flow map.

As a practical option and for consistency between the flow pattern map and the flow boiling heat transfer model, an easier to implement version of the flow map was proposed by Thome and El Hajal [71]. The void fraction ε which is determined with the Rouhani-Axelsson drift flux model [72] by Thome and El Hajal is kept the same in the present new flow map for CO₂. The wet angle is calculated with an explicit correlation of Biberg [73]. Taking into account the modifications in the annular flow to dryout (A-D), dryout to mist flow (D-M) and intermittent flow to bubbly flow (I-B) transition curves, a new diabatic flow map was developed. The key points are given as:

The intermittent to annular flow (I-A) transition boundary is calculated with the Cheng et al. criterion [28, 30]:

$$x_{IA} = \left[1.8^{1/0.875} \left(\frac{\rho_V}{\rho_L} \right)^{-1/1.75} \left(\frac{\mu_L}{\mu_V} \right)^{-1/7} + 1 \right]^{-1} \quad (3)$$

The annular flow to dryout region (A-D) transition boundary is calculated with the new modified criterion for CO₂ as

$$G_{dryout} = \left\{ \frac{1}{0.236} \left[\ln \left(\frac{0.58}{x} \right) + 0.52 \right] \left(\frac{D_{eq}}{\rho_V \sigma} \right)^{-0.17} \left[\frac{1}{g D_{eq} \rho_V (\rho_L - \rho_V)} \right]^{-0.17} \left(\frac{\rho_V}{\rho_L} \right)^{-0.25} \left(\frac{q}{q_{crit}} \right)^{-0.27} \right\}^{1.471} \quad (4)$$

which is extracted from the new dryout inception equation as follows:

$$x_{di} = 0.58 e^{\left[0.52 - 0.236 We_V^{0.17} Fr_{V,Mori}^{0.17} (\rho_V / \rho_L)^{0.25} (q / q_{crit})^{0.27} \right]} \quad (5)$$

The vapor Weber number We_V and the vapor Froude number $Fr_{V,Mori}$ defined by Mori et al. [74] are calculated as

$$We_V = \frac{G^2 D_{eq}}{\rho_V \sigma} \quad (6)$$

$$Fr_{V,Mori} = \frac{G^2}{\rho_V (\rho_L - \rho_V) g D_{eq}} \quad (7)$$

and the critical heat flux q_{crit} is calculated with the Kutateladze [75] correlation as

$$q_{crit} = 0.131 \rho_V^{0.5} h_{LV} \left[g \sigma (\rho_L - \rho_V) \right]^{0.25} \quad (8)$$

The dryout region to mist flow (D-M) transition boundary is calculated with the new criterion developed based on the dryout completion data for CO₂:

$$G_M = \left\{ \frac{1}{0.502} \left[\ln \left(\frac{0.61}{x} \right) + 0.57 \right] \left(\frac{D_{eq}}{\rho_V \sigma} \right)^{-0.16} \left[\frac{1}{g D_{eq} \rho_V (\rho_L - \rho_V)} \right]^{-0.15} \left(\frac{\rho_V}{\rho_L} \right)^{0.09} \left(\frac{q}{q_{crit}} \right)^{-0.72} \right\}^{1.613} \quad (9)$$

which is extracted from the dryout completion (which means the wall remains completely dry) equation developed in this study by solving for G_M from:

$$x_{de} = 0.61 e^{\left[0.57 - 0.502 We_V^{0.16} Fr_{V,Mori}^{0.15} (\rho_V / \rho_L)^{-0.09} (q / q_{crit})^{0.72} \right]} \quad (10)$$

Several studies on flow pattern visualization of flow boiling of CO₂ inside channels were conducted and compared to the Cheng et al. flow pattern map. Gashe [76] conducted an experimental study of CO₂ evaporation inside a 0.8 mm diameter rectangular channel for various mass velocities and observed flow patterns by flow visualization as well. The Cheng et al. CO₂ flow pattern map was compared to his observations. It should be mentioned that the observed slug/annular flow of Gashe is counted as an annular flow in the updated flow pattern map. In his study, annular flow is the predominant flow in the slug/annular flow defined by Gashe. The observations (3) and (4) are near their correct regimes, especially by the typical flow pattern map standards. Statistically, 82% of the total 28 flow pattern data of Gashe [76] are identified correctly by the Cheng et al. flow pattern map. Furthermore, it is commonly understood that flow pattern transitions do not occur abruptly but over a range of conditions to complete the transition from one stable regime to the other, whereas transition lines on a map only represent the probable “centerline” of this transition range. With the limited data available for CO₂ at this point, predicting the “width” of a transition zone around the transition line is not yet feasible, but it should be a good topic for future research.

Ozawa et al. [101] conducted flow visualization of CO₂ flow boiling in three horizontal tubes with diameters of 1 mm, 2 mm and 3mm. Typical flow patterns in 2-mm tube at 5.0 MPa and 6.5 MPa are shown in Fig. 12 as a function of vapor quality and mass flux. The observed flow patterns in the 2 mm tube cover the whole range of experimental findings including the results in 1 mm and 3 mm tubes. The flow patterns observed in the 2 mm tube at 5.0 MPa are quite similar to macro-channels, while in 1.0 mm tube as shown in Fig. 13, the geometrical configuration of, typically, slug flow is clearly different from that in 2 mm tube. The gas–liquid interface or large bubble shape is seemingly axis-symmetric which shows the behavior of flow regimes in microchannels. However, there exists no substantial difference on flow configuration between 2 mm and 3 mm tubes. The Cheng et al. [30] flow pattern map was used to compare to the observed flow patterns and predicts most of the flow patterns as shown in Fig. 14. The solid lines are transition boundaries given by Cheng et al. [30].

Comparing the observed flow pattern at 5.0 MPa with the transition curves by Cheng et al. , the bubbly and intermittent flows including plug and slug flows are nearly involved in or close to the respective region, while the slug–annular flow regime penetrates into the predicted annular flow region. The annular flow region extends toward lower quality at high mass flux, and the mist flow appears reasonably at high quality. Another flow pattern transition shown by dashed lines of Revellin and Thome’s [105] for micro-channel, are drawn as well. Overall feature is consistent with those predicted, i.e. the bubbly and plug flows well corresponds to *isolated bubble (IB)* regime, and *coalescing bubble (CB)* regime well includes the slug flow. The slug to slug–annular boundary well corresponds to *coalescing bubble-to-annular (CB-A)* boundary, while the transition mode, i. e. slug–annular, is not considered in the Revellin and Thome’s flow pattern criteria. It should be pointed out that the Cheng et al. [30] flow map is diabatic map which is related to flow boiling heat transfer. It is essential to modify the flow pattern map for adiabatic flow conditions, which should be done in future.

It should be mentioned that different flow regime definitions may represent the same flow regimes. They also mentioned the heat transfer mechanisms are related to the flow patterns. Therefore, it is very important to relate flow boiling heat transfer prediction methods to the flow patterns as the Cheng et al. heat transfer model developed for CO₂ flow boiling which has been validated to be one of the most accurate prediction methods by many researchers.

Mastrullo et al. [100] conducted two-phase flow visualizations and flow boiling measurements at medium (0.50) reduced pressure. They have confirmed that the Cheng et al. [30] flow pattern map favorably predicts their observed CO₂ flow patterns as shown in Table 3. Furthermore, they measured and analyzed the local peripheral heat transfer coefficients at large range of vapor qualities and concluded that the heat transfer coefficients at the bottom of the tube are mainly influenced by nucleate boiling contribution due to the high liquid hold-up, and hence it has the predominant effect for CO₂, remarking the strong dependence on the heat flux and the almost independence on the mass flux for CO₂ at their test conditions. Ozawa et al. [101] also observed this phenomena and nucleate boiling still occurs in the liquid at the bottom even when the top surface is dry. This can reasonably

explain why the CO₂ has much higher heat transfer coefficients than conventional refrigerants such as R410A as the dominant heat transfer mechanism is convective evaporation process.

Zhang et al. [115] conducted experimental study of the frictional pressure drop characteristics of flow boiling heat transfer of CO₂ in a horizontal microchannel with an inner diameter of 1.5 mm. They observed flow regimes and analyzed the effect of flow regime on the pressure drop. Figure 15 shows their observed flow regime evolution from the bubble dynamic growth of CO₂ in the microchannel. As in Fig, 15, the vapor-liquid interface is noted with red lines. The bubble dynamically grows in the microchannel. As the effect of buoyancy, the bubbles detach from the wall surface and float above the bottom surface of the channel. The bubbles grow rapidly due to the flow boiling heat transfer process and the size of the bubble is less than the channel diameter as shown in (a) and (b). Due to the heat transfer, the bubbles continue to grow to the channel diameter size. The small bubbles formed on the wall are merged to form larger bubbles before they are detached. The larger bubbles can trap more bubbles. Due to the confinement in the microchannel, the bubble can only extend in the axial direction. The shape of the bubble has also changed from a circle to elongated bubbles and the flow pattern also appears as a plug flow or intermittent flow in the microchannel, as shown in (c) - (h). Furthermore, the liquid around the bubbles evaporate, and bubbles merge together. At low mass flow velocity, due to the buoyancy and gravity effect, the vapor is concentrated in the upper part of the microchannel, and the liquid is at the bottom of the channel. The vapor-liquid two-phase interface is relatively smooth, as shown in (i) - (j). With increasing the mass flow velocity and the vapor quality, the gas phase flow velocity increases significantly, which causes the surface liquid to tumble in the flow direction and forms waves on the vapor-liquid interface. The wave transmits downstream in the flow direction to form a wave flow, as shown in (k). The flow patterns (i) - (j) occur only when the flow rate and the heat flow flux is low, and these are main flow patterns during the heat transfer process. When the mass flow rate is greater than a critical value, these flow patterns usually last only a short time as heat transfer process. Furthermore, the liquid on the bottom surface is pushed to the sides of the channel wall. When the vapor velocity is high enough and forms a

continuous annular liquid film in the microchannel with high-speed vapor in the center. There is a strong disturbance between the annular liquid film and the vapor core. At the later stage of the annular flow, the central high-speed flow entrained the liquid on the vapor-liquid interface and dispersed in the central flow as droplets, as shown in (l). In the final stage of heat transfer, the liquid film gradually becomes thin. The liquid is completely dispersed in the form of droplets, and a continuous gas-phase mist flow is formed in the microchannel, as shown in (m). Most of the existing models are used to predict the pressure drop for the annular flow. Moreover, experimental research shows that the effect of the dryout phenomenon on the pressure drop is not as large as that of heat transfer. Further improvements based on existing models can better predict the pressure drop for this flow pattern. At this stage, the pressure drop is stabilizing. A homogeneous vapor fluid model can be used to predict pressure drop. However, the transition model of annular flow to mist flow needs further study. The visualization experimental results show that there is a corresponding relationship between the frictional pressure drop and the flow pattern of CO₂ during flow boiling heat transfer process. The flow visualization study shows that the Cheng et al. flow pattern map can better reflect the flow pattern of CO₂ in the phase-change heat transfer process and the transition trend of flow pattern under different working conditions.

Furthermore, the Cheng et al. [28, 30] flow pattern map is widely used to identify flow patterns for enhanced tubes. It is also used together with the mechanistic flow boiling heat transfer model and pressure drop model based on flow patterns in predicting flow boiling heat transfer and two phase frictional pressure drop in macro- and micro-channels with good results as presented the following sections respectively.

4.3. The Cheng et al. [30, 31] flow pattern-based flow boiling heat transfer model for CO₂ evaporation inside channels

To meet the engineering practical application with a wide range of parameters and working conditions, a generalized updated general flow boiling heat transfer model was developed by

modifying the Cheng et al. [28, 29] flow boiling heat transfer model [30]. By incorporating the Cheng et al. [31] flow pattern map presented in the above section, the Cheng et al. CO₂ flow boiling heat transfer model is physically related to the flow patterns of CO₂, and thus correspondingly the model has been extended to a wider range of conditions and to include new heat transfer methods in mist flow and bubbly flow regimes. The heat transfer database used in their heat transfer model is listed in Table 1. The generalized flow boiling heat transfer model has predicted reasonably well an extensive experimental database derived from the literature and widely used for academic research, engineering simulation and design of evaporators and thermal systems over the past decade.

To develop a general evaporation heat transfer prediction method, it is important that the method is not only numerically accurate but that it also correctly captures the trends in the data to be useful for heat exchanger optimization. Most importantly, the evaporation heat transfer mechanisms should be related to the corresponding flow patterns and be physically explained according to flow pattern transitions. Besides significantly extending the range of the heat transfer database here, several new modifications were implemented in the updated general evaporation heat transfer model and will be presented below. Changes to the flow pattern map also have an effect on the heat transfer model: the new dryout inception vapor quality correlation and a new dryout completion vapor quality correlation are used to better segregate the data into these regimes, which have sharply different heat transfer performances. Accordingly, the evaporation heat transfer correlation in the dryout region was updated. In addition, a new mist flow heat transfer correlation for CO₂ was developed based on the CO₂ data and a heat transfer method for bubbly flow was adopted for completeness sake. With these modifications, a new general evaporation heat transfer model for CO₂ was developed to meet a wider range of conditions and to cover all flow regimes [30, 31].

The general equation for the local flow boiling heat transfer coefficients h_p in a horizontal tube is used as follows:

$$h_p = \frac{\theta_{dry} h_v + (2\pi - \theta_{dry}) h_{wet}}{2\pi} \quad (11)$$

where θ_{dry} is the dry angle. The dry angle θ_{dry} defines the flow structures and the ratio of the tube perimeter in contact with liquid and vapor. The vapor phase heat transfer coefficient on the dry perimeter h_v is calculated with the Dittus-Boelter [77] correlation assuming tubular flow in the tube. The heat transfer coefficient on the wet perimeter h_{wet} is calculated with an asymptotic model that combines the nucleate boiling and convective boiling heat transfer contributions to flow boiling heat transfer by the third power:

$$h_{wet} = \left[(S h_{nb})^3 + h_{cb}^3 \right]^{1/3} \quad (12)$$

where h_{nb} , S and h_{cb} are respectively nucleate boiling heat transfer coefficient, nucleate boiling heat transfer suppression factor and convective boiling heat transfer coefficient and are determined in the following equations

The nucleate boiling heat transfer coefficient h_{nb} is calculated with the Cheng et al. [28] nucleate boiling correlation for CO₂ which is a modification of the Cooper [78] nucleate pool boiling correlation:

$$h_{nb} = 131 p_r^{-0.0063} (-\log_{10} p_r)^{-0.55} M^{-0.5} q^{0.58} \quad (13)$$

The Cheng et al. [28] nucleate boiling heat transfer suppression factor S for CO₂ is applied to reduce the nucleate boiling heat transfer contribution due to the thinning of the annular liquid film:

$$\text{If } x < x_{IA}, S = 1 \quad (14)$$

$$\text{If } x \geq x_{IA}, S = 1 - 1.14 \left(\frac{D_{eq}}{0.00753} \right)^2 \left(1 - \frac{\delta}{\delta_{IA}} \right)^{2.2} \quad (15)$$

Furthermore, if $D_{eq} > 7.53 \text{ mm}$, then set $D_{eq} = 7.53 \text{ mm}$. The liquid film thickness δ shown in Fig. 1 is calculated with the expression proposed by El Hajal et al. [79]:

$$\delta = \frac{D_{eq}}{2} - \sqrt{\left(\frac{D_{eq}}{2}\right)^2 - \frac{2A_L}{2\pi - \theta_{dry}}} \quad (16)$$

where A_L , based on the equivalent diameter, is cross-sectional area occupied by liquid-phase.

The convective boiling heat transfer coefficient h_{cb} is calculated with the following correlation assuming an annular liquid film flow from the original model [52]:

The heat transfer coefficient in mist flow is calculated by a new correlation which is a modification of the correlation by Groeneveld [80], with a new lead constant and a new exponent on Re_H according to CO₂ experimental data:

$$h_M = 2 \times 10^{-8} Re_H^{1.97} Pr_V^{1.06} Y^{-1.83} \frac{k_V}{D_{eq}} \quad (17)$$

where the homogeneous Reynolds number Re_H and the correction factor Y are calculated as follows:

$$Re_H = \frac{GD_{eq}}{\mu_V} \left[x + \frac{\rho_V}{\rho_L} (1-x) \right] \quad (18)$$

$$Y = 1 - 0.1 \left[\left(\frac{\rho_L}{\rho_V} - 1 \right) (1-x) \right]^{0.4} \quad (19)$$

The heat transfer coefficient in the dryout region is calculated by a linear interpolation proposed

The Cheng et al. [30, 31] generalized flow boiling heat transfer model was compared to an extensive database in Table 1. The updated general flow boiling heat transfer model not only captures

the heat transfer trends well but also predicts the experimental heat transfer data well. As it is harder to predict (and harder to accurately measure) heat transfer data in the dryout and mist flow regimes, the updated general heat transfer model does not always predict the experimental data in these two flow regimes satisfactorily. Some examples of such comparisons can be found in [31]. In further analysis, comparisons have also been made by classes of flows, i.e. the predictions versus all the heat transfer data excluding dryout and mist flow data (essentially the all wet perimeter data), versus all dryout heat transfer data (the partially wet perimeter data) and versus the mist flow data (all dry perimeter data) [31]. The statistical analysis has shown the following fraction of the database are predicted within $\pm 30\%$: 71.4% of the entire database in Table 1 (1124 points), 83.2% of the all wet wall data points (773 points), 47.6% of the partially wet wall data points (191 points) and 48.2% of the all dry wall data points (160 points).

Overall, the updated general flow boiling heat transfer model predicts the overall database quite well. However, for the dryout and mist flow regimes with partially or all dry perimeters, the heat transfer model is only partially satisfactory. For these last two regimes, many of the experimental data sets have a level of scatter ranging up to 40% themselves. In part, the larger errors are due to the very sharp change in trend in these data with vapor quality, where an error of a 2-3% in vapor quality in the energy balance of the experiments or in the prediction of x_{di} and/or x_{de} immediately results in a heat transfer prediction error of 50%. Therefore, more careful experiments are needed in these two regimes to provide more accurate heat transfer data, with attention to also determine the transitions x_{di} and x_{de} , because they are typical working conditions in the micro-scale channels of extruded multi-port aluminum tubes used for automobile air-conditioners that operate over a wide range of mass velocities up to as high as 1500 kg/m²s.

Furthermore, one example of simulation for CO₂ evaporation and corresponding flow patterns is shown here to illustrate and understand the method. Figure 16 shows simulation of the updated flow pattern map and flow boiling model for CO₂ at the indicated conditions, superimposed on the same graphs by Cheng et al. [81]. The process path for the vapor quality variation from $x = 0.01$ to $x = 0.99$

is shown as the horizontal broken line (dash-dot line) while the variation in the heat transfer coefficient as it changes vapor quality and flow pattern is depicted by the dashed line. The flow pattern boundaries are in solid lines. The line (dash line with arrows) indicates the calculated heat transfer coefficient at the indicated mass velocity and vapor quality. Notice the various changes in trends in the heat transfer coefficient as this occurs. For example, when the flow regime passes from annular flow into the dryout regime, there is a sharp inflection in the heat transfer coefficient as the top perimeter of the tube becomes dry.

Over the past decade, a number of experimental studies have confirmed that the Cheng et al. flow pattern based heat transfer model for CO₂ flow boiling favorably predicts their experimental data. All these studies have confirmed that the Cheng et al. model gives to the best prediction for their experimental data [91-94, 97-98, 104, 111, 116] while some studies do not.

Oh and Son [111] conducted experiments of CO₂ flow boiling in a horizontal channel with a diameter of 4.57 mm at heat fluxes ranging from 10 to 40 kW/m² K, mass fluxes ranging from 200 to 1000 kg/m²s, and saturation temperatures ranging from 0 to 40°C. The boiling heat transfer of CO₂ has a greater effect on nucleate boiling than convective boiling and highly depends on the vapor quality, heat flux, and saturation temperature. They compared their experimental data to nine flow boiling heat transfer correlations and model. The Cheng et al. [31] model showed the best agreement with the experimental data for CO₂. Zhang et al. [109] conducted experimental study of characteristics of heat transfer for CO₂ flow boiling in a horizontal microchannel with a diameter of 1.5 mm at saturated temperature of -40 – 0 °C, heat flux of 5 – 35 kW/m² and mass flux of 200 – 1500 kg/m²s. They compared their experimental data with the Cheng et al. model which has a higher prediction accuracy. It predicts 77.1% of the heat transfer within ± 30% error band before dryout regime as shown in Fig. 17 while it only predicts 22.9% of the data after dryout phenomenon as shown in Fig. 18. This is similar to the results in the study of Cheng et al. [30, 31] as they have recommended improvement is needed in these two flow regimes. **As the Cheng et al. [30, 31] model is extrapolated to microchannels at low temperature, the dryout occurrence and completion are not captured.**

Therefore, anomalous results have been obtained in their study as shown in Fig. 18. It is essential to develop new prediction methods to cover a wide range of parameters and conditions.

Jiang et al. [97] conducted an experimental investigation on two-phase flow boiling heat transfer with CO₂ or R744) in two horizontal microchannels of diameters of 0.6 mm and 1.5 mm at heat flux of 7.5 – 30 kW/m², mass flux of 300 – 600 kg/m²s and saturation temperature of 233–273 K. They compared their measured data to the Cheng et al. flow boiling heat transfer model and the model predicts 79.8% of the data points within $\pm 30\%$ and has a deviation of 21.8% before the dryout while it only predicts 18.4% of the data points and has a mean deviation of 59.9% after the dryout. Again, the heat transfer prediction methods in the dryout and mist flow regimes need to be improved in future. This was also observed by Wu et al. [95] that the model does not capture the dryout for some conditions although the model captures the parametric trends. Yun and Kim [111] investigated the post-dryout heat transfer behaviors and also find the Cheng et al. model needs to be improved in prediction of the dryout occurrence. Similar results have been obtained by Ducoulombier et al. [112]. As the dryout heat transfer is a dynamic and unstable process, there are big differences from one study to another one. It is suggested that the mechanisms of dryout should be further investigated and a new mechanistic approach should be developed to capture the heat transfer in the dryout region in future.

In order to identify future research needs and model development, the Cheng et al. CO₂ flow boiling heat transfer model has been evaluated with the new experimental data after 2007. A total of 3609 new heat transfer data from table 2 have been compared to the predicted heat transfer coefficients by the Cheng et al. [30, 31] model. Table 5 shows the statistical analysis of the predicted flow boiling heat transfer coefficients by the Cheng et al. heat transfer model. For the entire new experimental data after 2007, the model predicts 56.9% of the data within $\pm 30\%$ while it predicts 81.3% of the entire data without dryout and mist flow data within $\pm 30\%$. For the heat transfer data in the dryout and mist flow regions, the model only predicts 21% of the data within $\pm 30\%$. It should be realized that the Cheng et al. model has been extrapolated beyond its original conditions. In particular,

it does not capture the dryout and mist flow regimes properly and therefore predicts the database unsatisfactorily. Furthermore, the whole data points including all the new data points and previous data used in their model, it predicts 62.9% of the whole data within $\pm 30\%$, 81.8% of those without dryout and mist flow data points and 29.3% of the dryout and mist flow data. Therefore, the heat transfer model and flow pattern map need to be improved in future.

Overall, the flow pattern based heat transfer prediction method is related to the corresponding mechanisms and works correctly for CO₂ flow boiling. According to the afore-going analysis, the Cheng et al. [31] CO₂ flow boiling heat transfer model is recommended for evaporator design and simulation. Further improvement should be done for the dryout and mist flow regimes with sufficient accurate experimental data in these regions.

4.4. The Cheng et al. [30] flow pattern based two-phase frictional pressure drop model for CO₂

The predictions of two-phase flow frictional pressure drops with the leading methods often cause errors of more than 50% [62-64], therefore, efforts are increasingly being made to improve on the two phase frictional pressure drop prediction methods and models. Furthermore, the leading two phase frictional pressure drop prediction methods do not usually contain any flow pattern information, which is intrinsically related to the two-phase frictional pressure drop. Due to the effects of thermal physical and transport properties of CO₂, the leading prediction two phase frictional pressure drop methods do not work well. The reason is that these methods do not usually cover the much lower liquid-to-vapor density ratios and very small surface tension characteristics of CO₂ at high pressures. In general, the two-phase frictional pressure drops of CO₂ are much lower than those of other refrigerants [30, 31]. Significantly, there is no proven generally applicable two-phase frictional pressure drop prediction method for CO₂, although there are a number of studies on CO₂ two phase frictional pressure drops in the literature [36, 85-89]. Some researchers proposed two phase frictional pressure drop correlations for CO₂ based on their own experimental data but such methods do not

work properly when extrapolated to other conditions. For example, Yoon et al. [36] proposed a modified Chisholm method [118] to fit their data in a macro-channel but it cannot be applied to other conditions because they tested only one tube diameter. In the practical applications, both macro- and micro-scale tubes are used in the CO₂ evaporators and heat exchangers.

As opposed to the completely empirical two-phase frictional pressure drop methods, a flow pattern based phenomenological frictional pressure drop model relating the flow patterns to the corresponding two-phase frictional pressure drops is a promising approach in the two-phase pressure drop predictions. Ould Didi et al. [62] used local flow patterns to analyze two-phase flow pressure drops, which resulted in a significant improvement in accuracy. Based on that, a new flow pattern based phenomenological model of two-phase frictional pressure drops was recently developed by Moreno Quibén and Thome [63, 64]. The model physically respects the two-phase flow structure of the various flow patterns while maintaining a degree of simplicity as well. The model predicts their experimental data well but not the CO₂ experimental database in table 6 which was used in developing the Cheng et al. [30] pressure drop model.

Cheng et al. [30] compiled a large database of CO₂ two-phase frictional pressure drop and compared the database to the leading two-phase frictional pressure drop methods: the empirical two-phase frictional pressure drop methods by Chisholm [118], Friedel [119], Grønnerud [120] and Müller-Steinhagen and Heck [121], Ciccitti et al. [122], a modified Chisholm correlation by Yoon et al. [36] and the flow patterned based pressure drop model by Moreno Quibén and Thome [63, 64]. The CO₂ database includes the experimental data of Bredesen et al. [40], Pettersen [32], Pettersen and Vestbøstad [88], Zhao et al. [86, 87] and Yun and Kim [89, 117] before 2007 as in Table 6. The test channels include single circular channels and multi-channels with circular, triangular and rectangular cross-sections and electrical and fluid heated test sections. The data were taken from tables where available or by digitizing the pressure drops from graphs in these publications. All together 387 two-phase pressure drop data points were obtained.

Figure 19 shows the comparison of these leading pressure drop methods to the experimental data of Bredesen et al. [40] at the indicated test conditions. There are big differences among these methods. Overall, not one of these models is able to predict the CO₂ two-phase frictional pressure drop database in table 6 well (note that all have been extrapolated beyond their original conditions to make this comparison for CO₂), e. g. the Friedel method gave reasonably good predictions, but it failed to predict the pressure drop in smaller channels as in the Cheng et al [30] study. Therefore, it is necessary to develop a new general two-phase frictional pressure drop model model for CO₂ two-phase flow in macroscale- and microscale-channels. Cheng et al. [30] developed a flow pattern based two phase frictional pressure drop model specially for CO₂ using their general flow pattern map for CO₂. It indicates that various correlations give quite different prediction trends. Therefore, it is essential to evaluate the correlations for different fluids and conditions. Table 6 lists the selected research on evaluation of two phase frictional pressure drop correlations after 2007. It can be seen that quite different results for different correlations used to predict the CO₂ two phase flow pressure drop data. Some researchers modified the correlations to fit their own data but such kind of correlations are not applicable to a wide range of working conditions and channel sizes. It is obvious that there are not many studies on CO₂ two phase flow pressure drops since 2007. Furthermore, limited studies have considered the flow regime observation simultaneously. The data reduction methods are not clear in many papers because it is unclear if these data are frictional pressure drops or total pressure drops.

The Cheng et al. two-phase frictional pressure drop model for CO₂ was developed by modifying the model of Moreno Quibén and Thome developed for R-22, R-410a and R-134a and incorporating the updated Cheng et al. CO₂ flow pattern map, using the CO₂ pressure drop database by Cheng et al. [30]. In developing this pressure drop model, two-phase frictional pressure drop data were used. The total pressure drop is the sum of the static pressure drop (gravity pressure drop), the momentum pressure drop (acceleration pressure drop) and the frictional pressure drop:

$$\Delta p_{total} = \Delta p_{static} + \Delta p_m + \Delta p_f \quad (20)$$

For horizontal channels, the static pressure drop equals zero. Furthermore, the momentum pressure drop can be calculated as

$$\Delta p_m = G^2 \left\{ \left[\frac{(1-x)^2}{\rho_L(1-\varepsilon)} + \frac{x^2}{\rho_V \varepsilon} \right]_{out} - \left[\frac{(1-x)^2}{\rho_L(1-\varepsilon)} + \frac{x^2}{\rho_V \varepsilon} \right]_{in} \right\} \quad (21)$$

Thus, diabatic experimental tests that measure total pressure drops can be reduced using the above expressions to find the two-phase frictional pressure drops.

In the Cheng et al. [30] pressure drop model, for non-circular channels, the equivalent diameter D_{eq} is used in the two-phase frictional pressure drop model to remain consistent with that in the flow pattern map. Using the equivalent diameter gives the same mass velocity as in the non-circular channel and thus correctly reflects the mean liquid and vapor velocities, something using hydraulic diameter in a two-phase flow does not. Thus, equivalent diameter D_{eq} is used in the following method.

1) CO₂ frictional pressure drop model for annular flow (A): The basic equation of the two phase frictional pressure drop model is as follows:

$$\Delta p_A = 4 f_A \frac{L}{D_{eq}} \frac{\rho_V u_V^2}{2} \quad (22)$$

where the two-phase flow friction factor of annular flow f_A was correlated according to CO₂ experimental data here (considering the main parameters which affect the two-phase pressure drops for CO₂) as:

$$f_A = 3.128 Re_V^{-0.454} We_L^{-0.0308} \quad (23)$$

2) CO₂ frictional pressure drop model for slug and intermittent flow (Slug+I): A proration is proposed to avoid any jump in the pressure drops between these two flow patterns as follows:

$$\Delta p_{SLUG+I} = \Delta p_{LO} \left(1 - \frac{\varepsilon}{\varepsilon_{IA}} \right) + \Delta p_A \left(\frac{\varepsilon}{\varepsilon_{IA}} \right) \quad (24)$$

where Δp_A is calculated with Eq. (22) and the single phase frictional pressure drop considering the total vapor-liquid two-phase flow as liquid flow Δp_{LO} .

The two-phase friction factor of stratified-wavy flow f_{SW} is calculated with the following interpolating expression based on the CO₂ database:

$$f_{SW} = \theta_{dry}^*{}^{0.02} f_V + (1 - \theta_{dry}^*)^{0.02} f_A \quad (25)$$

and the dimensionless dry angle θ_{dry}^* is defined as

$$\theta_{dry}^* = \frac{\theta_{dry}}{2\pi} \quad (26)$$

where θ_{dry} is the dry angle. The dry angle θ_{dry} defines the flow structure and the ratio of the tube perimeter in contact with vapor. f_V is the single-phase friction factor of the vapor phase.

CO₂ frictional pressure drop model for slug-stratified wavy flow (Slug+SW): It is proposed to avoid any jump in the pressure drops between these two flow patterns as:

$$\Delta p_{SLUG+SW} = \Delta p_{LO} \left(1 - \frac{\varepsilon}{\varepsilon_{IA}} \right) + \Delta p_{SW} \left(\frac{\varepsilon}{\varepsilon_{IA}} \right) \quad (27)$$

3) CO₂ frictional pressure drop model for mist flow (M): the friction factor of mist flow f_M was correlated according to the CO₂ experimental data as:

$$f_M = \frac{91.2}{\text{Re}_M^{0.832}} \quad (28)$$

The Cheng et al. CO₂ two-phase frictional pressure drop model was compared to the CO₂ two-phase pressure drop database [30]. Figure 20 shows the comparison of the Cheng et al. CO₂ frictional pressure drop model to the experimental data of Bredesen et al. [40] at the indicated experimental conditions and the corresponding flow pattern map. The model predicts the data well and also captures the pressure drop trend. Figure 21 shows the comparative results of the predicted frictional pressure gradients by the new model to the entire database in their study [30]. Table 7 shows the statistical analysis of the two-phase frictional pressure drop predictions for all data points in the database in table 6 with the selected prediction methods. Generally, the new pressure drop model reasonably predicts the database and importantly captures the trends in the data too. Nonetheless, there are not many experimental data available covering some flow patterns and future experimental work is recommended to address these conditions.

The Cheng et al. pressure drop [30] model has been used to evaluate the experimental two phase pressure drop data by several researchers. Some studies have shown good prediction [99, 110]. However, improvement of the model is needed, in particular, in the dryout and mist regimes [95, 115, 116]. Just to show one example here, Zhang et al. [115] conducted experimental study of the frictional pressure drop characteristics of flow boiling heat transfer of CO₂ in a horizontal microchannel with an inner diameter 1.5 mm at heat flux of 7.5 - 30 kW/m², mass flux of 50 - 600 kg/m²s, saturation temperature of -40 - 0 °C and vapor quality from 0 to 1. Figure 22 shows the comparison between the experimental results and the Cheng et al. [30] theoretical flow pattern map. The heat flux has little effect on the frictional pressure drop at high vapor quality which can be found in the paper of Zhang et al. [115] but it has a decisive effect on the dryout and mist flow as shown in Fig. 22 at the indicated test conditions. Before the dryout, the Cheng et al. model favorably predicts the two phase pressure drop data with 81% in annular flow while it does not capture the data in the dryout and mist flow

regimes as in the paper of Zhang et al. [115]. The reason is mainly due to the lack of experimental data in their model development. It should also be noted that a linear relationship is adopted in their model. However, according to the available data as shown in Fig. 22, the linear correlation does not represent the actual pressure drop trends in these two regions. Therefore, the original method in these two regimes is only applicable to their own database. Therefore, Zhang et al. [115] modified the model in these regimes according to the experimental data and the modified model favorably predicts their data. Wu et al. [99] have also obtained a similar conclusion that the Cheng et al. [30] model does not capture their pressure drop data and modified the mist flow pressure drop of Cheng et al. The modified model by Wu et al. [99] has favorably predicted their two phase pressure drop data reported in their paper. Ducoulobier et al. [112] evaluated the Cheng et al. pressure drop model with the microchannel pressure drop data and have found that the model gives very big errors. It should be mentioned that new mechanistic prediction methods in these two regimes should be developed according to physical mechanisms and parametric trends in the experimental data.

In this review, the Cheng et al. CO₂ flow boiling heat transfer model has been evaluated with the new experimental data after 2007. A total of 463 new diabatic two phase frictional pressure drop data from table 8 were digitized and used to compare to the predicted two phase pressure drop by the Cheng et al. [30] two phase pressure drop model. Table 9 shows the statistical analysis of the predicted two phase pressure drop data by the Cheng et al. [30] model. For all new experimental data, the model predicts 40.8 % of all the new data within $\pm 30\%$, 62.7% of the data without dryout and mist flow data within $\pm 30\%$ and only 4.6% of the dryout and mist flow data within $\pm 30\%$. It should be realized that the Cheng et al. model has been extrapolated to its original conditions. In particular, it does not capture the dryout and mist flow data. Furthermore, the whole data points including all the new data points and previous data used in their model, it predicts 56.2% % of the whole data within $\pm 30\%$, 68.9% of those without dryout and mist flow data within $\pm 30\%$ and 25.7% of all the dryout and mist flow data within $\pm 30\%$. Therefore, it is essential to improve the model by using the current experimental data

in table 8. It should be mentioned that the Cheng et al. model is diabatic model and adiabatic pressure drop model together with adiabatic flow pattern map should also be developed.

In summary, the Cheng et al. [30] CO₂ two-phase frictional pressure drop model predicts the CO₂ pressure drop database better than the existing methods in their original study. Due to the limited and less accurate experimental data in micro-scale channels available in the literature, the CO₂ pressure drop model does not predict these data satisfactorily. It is suggested that additional, more accurate experimental CO₂ pressure drop data be obtained through well designed measurement facilities to further test or improve the model in the future.

5. Current research status of flow boiling and two-phase flow of CO₂ in enhanced channels

Although only limited studies of CO₂ flow boiling and two phase flow in enhanced channels are available in the literature, it is worth to mention these studies here because quite contradictory conclusions have been obtained from the available studies [45, 90, 104-106, 131, 132, 137, 138]. Koyama et al. [131, 132] conducted experiments on flow boiling in a smooth copper tube and in a micro-fin copper tube at 5.3°C. From their results, the heat transfer coefficients are only slightly higher than in the microfin tubes with a slight pressure drop increase as well. In this case, microfin tubes are not appropriate for CO₂ flow boiling heat transfer. However, several studies have shown that CO₂ flow boiling heat transfer can be enhanced significantly. Cho and Kim [90] conducted experimental studies of CO₂ for micro-channels and their data show that the average evaporation heat transfer coefficients are 150 to 210 % higher than those of smooth tubes. The increase of pressure drop was much lower than the heat transfer increase. So far, only limited studies of CO₂ flow boiling in micro-fin tubes are available. Whether they significantly enhance CO₂ flow boiling heat transfer or not is still unclear due to the lack of such information. Furthermore, Koyama et al. [131, 132] conducted experimental studies of flow boiling of CO₂-oil mixture in micro-fin tubes. Similar conclusions to those in smooth tube were obtained.

However, several studies have shown that significant heat transfer enhancement with microfin tubes have been achieved. Dang et al. [106] investigated flow boiling heat transfer of carbon dioxide inside a small-sized microfin tube (mean inner diameter: 2.0 mm; helix angle: 6.3) at a saturation temperature of 15°C, heat and mass flux of 4.5–18 kW/m² and mass flux of 360–720 kg/m²s. Their experimental results have indicated that heat flux has a significant effect on the heat transfer coefficients but the heat transfer coefficient does not always increase with mass flux as shown in Fig. 23 (a). Under certain conditions, the heat transfer coefficients at a high mass flux are lower than those at a lower mass flux, indicating that convective heat transfer had a suppression effect on nucleate boiling. The heat transfer coefficients in the microfin tubes were 1.9 to 2.3 times the values in smooth tubes of the same diameter under the same experimental conditions. The dryout vapor quality ranges from 0.9 to 0.95. The experimental results indicated that using microfin tubes may considerably increase the overall heat transfer performance. Kim and Hrnjak [138] also observed heat transfer enhancement in a large diameter channel with a diameter of 11.2 mm as shown in Fig. 23 (b).

Wu et al. [105] conducted experimental study on heat transfer and pressure drop characteristics of CO₂ flow boiling in mini tube with a diameter of 1.7 mm and micro fins of zero helix at mass flux from 100 to 600 kg m²s, heat flux from 1.67 to 8.33 kWm², vapor quality from 0 to 0.9 and saturation temperature from 1 to 15 °C. Their results show that the heat transfer coefficient increases with increasing vapor quality, but sharply decreases at vapor quality around 0.2 - 0.4 under most conditions, and the dryout vapor quality decreases with the increasing heat flux and saturation temperature. Pressure drop increases with increasing mass flux and heat flux, or decreasing saturation temperature, and mass flux is the major influence factors. There are two major differences between the trends: (1) The heat transfer coefficient decreases at vapor quality of 0.2–0.4 in micro-fin tube, while that is nearly unchanged at low vapor quality in smooth tube; (2) the heat transfer coefficient does not decrease a lot at high vapor quality in micro-fin tube, while that decrease sharply at high vapor quality in smooth tube, especially at higher heat flux conditions. The difference between the heat transfer characteristic in micro-fin tube and that in smooth tube can be partially explained by the

two-phase flow pattern and the special geometry of the micro-fin tube. The Cheng et al. [30] flow pattern map is used to predict the flow patterns. The flow pattern transits from intermittent flow to annular flow at around 0.2 vapor quality. The transition criteria from intermittent flow to annular flow in micro-fin tube of this study can be similar with those in smooth tube because the influence of 0° helix angle fins on flow pattern is not much. In micro-fin tube, before 0.2 vapor quality the flow pattern is intermittent flow and all inner surface is wetted by liquid; after 0.2 vapor quality the flow pattern transits to annular flow, and the liquid may accumulate between fins which makes tops of the fins touches the vapor. With the increase of vapor quality, the liquid becomes less and more surface of the fins is occupied by vapor. As a result the heat transfer coefficient presents a decline trend at the vapor quality of 0.2–0.4. The inner surface of smooth tube is more easily to be dry-out than that in micro-fin tube because the liquid is uniformly distributed on the inner surface of the tube. As a result, the heat transfer coefficient quickly falls off at high vapor quality. Furthermore, a heat transfer coefficient correlation and a pressure drop correlation for 0° helix angle micro-fin tube were developed, and they agree well with the experimental data.

Regarding heat transfer enhancement mechanisms, the increase in the flow boiling heat transfer coefficient for a micro-fin tube can be explained by (1) an increase in the wetted surface area, (2) an increase in the liquid-phase convective heat transfer, (3) an increase in the wetting around the circumference of the tube, (4) an increase in the nucleate boiling heat transfer, and (5) the effect of swirl on mist flow at high vapor qualities. The effect of swirl on the liquid-phase convective heat transfer is negligible due to the zero helix angle.

Mastrullo et al. [6] have recently presented a comprehensive review on CO_2 flow boiling in enhanced channels in their review paper from different viewpoints. It is valuable to contribute to understanding the current research, mechanisms and prediction methods on this topic. Furthermore, they assessment several heat transfer correlations and apparently there are big errors for the existing calculation methods.

Due to the limited studies of CO₂ flow boiling and two phase flow in enhanced channels, it is difficult to reach generally acceptable conclusions from these studies because limited experimental data and also contradictory results from one to another. It is essential to evaluate if it is needed to apply enhanced tubes for CO₂ flow boiling. In particular, at high saturation temperatures and microchannels, it might not be needed to use enhanced channels due to the high heat transfer coefficient achieved in the channels at the high saturation temperatures while it might be significant to use enhanced channels for CO₂ flow boiling in macrochannels at low saturation temperatures. Further exploration and research should be done in this topic and the feasibility of using enhanced channels for CO₂ flow boiling.

6. Current research status of the oil effect on CO₂ flow boiling heat transfer and two-phase pressure drop and prediction methods

6.1. Analysis of the experimental data of the oil effect on CO₂ flow boiling heat transfer and two-phase pressure drop

Flow boiling heat transfer and two-phase flow of refrigerant-lubricating oil mixtures are very complex phenomena but very important topics for air-conditioning, heat pump and refrigeration systems. The presence of lubricating oil may considerably affect the transport properties of a refrigerant and have a significant effect on the evaporation heat transfer, two-phase pressure drop and flow pattern characteristics and thus the design of evaporators in the relevant systems. Due to its large viscosity, surface tension and insulating effects, lubricating oil tends to decrease the flow boiling heat transfer coefficient of a refrigerant in most cases while it may increase the flow boiling heat transfer coefficient of the refrigerant at low lubricating oil concentrations [123, 134, 137, 140]. Therefore, it is essential to understand how the lubricating oil concentration affects the flow boiling heat transfer,

two-phase pressure drop and flow pattern characteristics and to predict the flow boiling heat transfer coefficient and two-phase frictional pressure drop of such mixtures properly.

A number of lubricants for CO₂ have been studied over the past years. According to the studies of lubricants for CO₂ by Kaneko et al. [124] and Ikeda [125], PAGs (Polyalkylene-glycols) are the most suitable lubricants used in CO₂ air-conditioning, refrigeration and heat pump systems so far. Unlike R134a, PAGs are immiscible with CO₂. Therefore, it is essential to understand the flow boiling heat transfer and two phase frictional pressure drop behaviors of CO₂-lubricating oil mixtures in the evaporation processes in order to design the evaporators properly.

A literature review of flow boiling heat transfer and two-phase frictional pressure drop of CO₂ with lubricating oil is presented here. The experimental studies on this topic are limited. There are several papers on the effect of lubricating oil on CO₂ flow boiling heat transfer and two-phase frictional pressure drop [127-138]. Of these studies, some are related to flow boiling heat transfer and two-phase frictional pressure drop in macro-scale channels and others are related to flow boiling heat transfer in micro-scale channels. These available studies have been analyzed to obtain useful information for the design of evaporators although the relevant models are limited due to limited experimental data available.

Analysis of these studies on flow boiling and two-phase pressure drop of CO₂-oil mixtures has been carefully conducted to present a state-of-the-art status of the study on these topics. As the lubricating oil (PAG) used in CO₂ air-conditioning, refrigeration and heat pump systems is immiscible with CO₂, emphasis has been placed on evaporation heat transfer and two-phase frictional pressure drop of CO₂ with immiscible oil in micro-scale channels which are of interest to CO₂ air-conditioning and heat pump systems. Unfortunately, there are limited studies of evaporation heat transfer and two-phase frictional pressure drop of CO₂ with immiscible oil in a 3 mm inner diameter tube. With the very limited experimental data available, it is impossible to propose a model for flow boiling heat transfer of CO₂ with immiscible oil. In addition, there is also little information of two-phase frictional pressure drop of CO₂ with lubricating oil in micro-scale channels. Accurate and

systematic experimental data of flow boiling heat transfer and two phase frictional pressure drop of CO₂ lubricating oil mixtures in both macro-scale and microscale tubes are needed. These are the basis for developing relevant prediction methods. Lacking the reliable prediction methods, some empirical methods should be proposed for the design of evaporators.

Katsuta et al. [128] conducted an experimental study of flow boiling heat transfer and two-phase frictional pressure drop of CO₂ and lubricating oil (PAG) mixture in a horizontal tube with an inner diameter of 4.59 mm. The oil concentrations were 1% (wt) and 5% (wt), respectively. The oil concentration had little effect on the two-phase pressure drops. However, the two-phase pressure drops increased with increasing the oil concentrations at vapor qualities larger than 0.6. The possible reason of this trend is that the local oil concentration plays an important role in increasing two-phase pressure drops for the low mass velocities. Figure 25 shows their pressure drop data at two test conditions. It is interesting to see that at a mass velocity of 800 kg/m²s, the pressure drops of CO₂ with 5% oil concentration are slightly lower than those with 1% oil concentration. The oil has little effect on the pressure drops.

Koyama et al. [131, 142] studied flow boiling of CO₂-PAG mixtures inside a horizontal smooth tube with an inner diameter of 4.42 mm and a micro-fin tube with an inner diameter of 4.76 mm. The authors have concluded that the heat transfer coefficient for the smooth tube decreases abruptly with the addition of a very small amount of oil, while the deterioration rate of heat transfer coefficient for the micro-fin tube is smaller than that of the smooth tube. The two-phase pressure drop in the smooth tube increases with increasing the oil concentration especially at high vapor qualities larger than around 0.6 while that of the micro-fin tube increases slightly with increasing the oil concentration.

Katsuta et al. [127, 128] presented the experimental flow boiling heat transfer and two-phase pressure drop data of the lubricating oil concentrations with 0 to 1.1% (wt). For the very low oil concentrations of 0.05% to 0.08% (wt), the flow boiling heat transfer coefficients are decreased about 40% compared to those without oil. This is quite different from the experimental results of Gao and Honda [129, 130] for a 3 mm I.D. tube. According to the study of Gao and Honda, the oil

concentration does not affect the flow boiling heat transfer coefficients if the oil concentration is less than 0.1% (wt). Furthermore, there is no obvious difference between the flow boiling heat transfer coefficients of the oil concentrations of 0.05% to 0.08 % (wt) and those of the oil concentrations with 0.3% to 1.1% (wt). However, when the oil concentration is larger than 1%, heat transfer coefficient decreases greatly.

For all the studies in macro-channels, the oil concentrations were measured by sampling. There is no information on the measurement of the local oil concentration which is of great importance in modeling evaporation heat transfer and two-phase frictional pressure drop.

There are few studies of flow boiling heat transfer in micro-channels and there is no study of two-phase pressure drop in micro-scale channels with oil. Siegismund and Kauffeld [133] only presented a description of their test facility and the data reduction methods in their paper. No experimental data were presented in their paper although the title of their paper is the influence of lubricant oil on CO₂ evaporation heat transfer in mini-channel tubes.

Gao and Honda [129, 130] conducted an experimental study on flow boiling heat transfer of CO₂ and oil (PAG) mixtures inside a horizontal tube with an inner diameter of 3 mm. Figure 30 shows the effect of lubricating oil on the local heat transfer coefficient at the indicated test conditions [129, 130]. The local evaporation heat transfer coefficient falls considerably when the lubricating oil concentration is larger than 1% (wt). Furthermore, when the lubricating oil concentration increases, the change of heat transfer coefficient with vapor quality becomes small. Therefore, when the oil concentration is larger than 1% (wt), the evaporation heat transfer coefficient is not greatly affected by further increasing the oil concentration. Three oil concentrations were used in their study: less than 0.1% (wt), 1% (wt) and 2% (wt). When the concentration of the lubricating oil is more than 1% (wt), the local heat transfer coefficient was much lower than that without the lubricating oil. According to the authors' analysis, the reason for this decrease is considered due to the nucleate boiling being suppressed by the oil film. Therefore, the evaporation heat transfer is considered to change from the nucleate boiling dominated mechanism to the convective evaporation dominated mechanism. The

dryout vapor quality decreases with increasing mass velocity and is a little influenced by the saturation temperature and the lubricating oil concentration. The experimental heat transfer data of the oil concentration less than 0.1% (wt) were already used in the database in our previous study of the CO₂ evaporation heat transfer model [31]. As independent experimental flow boiling heat transfer data, the flow pattern based evaporation heat transfer model of Cheng et al. [30, 31] predicts well the evaporation heat transfer data of the oil concentration less than 0.1% (wt). Therefore, it can be concluded that the oil does not affect the heat transfer when the oil concentration is less than 0.1%.

Zhao et al. [130] conducted an experimental study of flow boiling heat transfer of CO₂ with miscible oil in multi micro-channels with an inner diameter of 0.86 mm (an equivalent diameter of 1.15 mm). Figure 31 shows their results of the oil effect on heat transfer coefficient at the indicated test conditions. The lubricating oil with a concentration less than 3% may increase the flow boiling heat transfer coefficients for at vapor qualities less than 0.4. The authors attributed this to a foaming effect that increases wall-wetting. In addition, they concluded that increasing mass flux also improved the heat transfer coefficient in the presence of oil since the average vapor quality decreased for constant heat flux and inlet vapor quality. On the other hand, they concluded that increasing the vapor quality and the saturation temperature decreased the heat transfer coefficient in the presence of oil. It must be pointed out here that the authors did not mention what kind of oil was used in their study. It was a miscible oil. Apparently, the effect of the miscible oil on the heat transfer characteristics of CO₂ is quite different from that of an immiscible oil. According to the analysis, for the study of flow boiling heat transfer and two-phase pressure drop of CO₂ with an immiscible oil (PAG) in micro-scale channels, there is no such information in the literature so far.

From the available studies, it can be concluded that very small amount of the lubricating oil (< 0.5% wt) seems to have little effect while larger concentrations (> 1% wt) tend to dramatically reduce flow boiling heat transfer coefficients. For two-phase pressure drops, the effect of lubricating oil only occurs at vapor qualities larger than around 0.6.

Based on this analysis, it is recommended that further experimental studies on flow boiling heat transfer and two-phase frictional pressure drop of CO₂ and oil mixtures in both macro- and micro-channels be conducted over a wide range of test conditions to provide more experimental data on these aspects. In order to understand the evaporation heat transfer mechanisms of CO₂ and immiscible oil mixtures, flow visualization and local measurement of oil concentration are also suggested to be done. It should be mentioned that Mastrullo et al. [6] have recently presented a comprehensive review on the oil effect on the CO₂ flow boiling heat transfer in their review paper from different viewpoints. It is valuable to contribute to understanding the current research, mechanisms and prediction methods on this topic. Furthermore, they assessment several heat transfer correlations considering the effect of oil, which may help to select the proper correlations and for further development of solid prediction methods in future. The current review analyze the phenomena in different viewpoint but both are very useful in understanding the fundamentals and applications of the topic.

6.2. Analysis the oil effect on CO₂ flow boiling heat transfet and two-phase pressure drop prediction methods

As the flow boiling heat transfer [31] model predicts well the independent experimental heat transfer data of the lubricating oil concentration less than 0.1 % (wt) by Gao and Honda [129, 130] only using the physical properties of pure CO₂, it is expected that the flow boiling heat transfer model may be modified to handle evaporation heat transfer of CO₂-immiscible lubricating oil mixtures. For the prediction of the two-phase pressure drops of CO₂-immiscible lubricating oil mixtures, the flow pattern based two-phase frictional pressure drop model of Cheng et al. [30] for pure CO₂ may be a good basis to start from when accurate and sufficient experimental data become available.

As for the prediction methods for flow boiling heat transfer and two-phase pressure drop with CO₂ and lubricant oil mixtures, the flow pattern based flow boiling heat transfer and two-phase pressure drop models of Cheng et al. [30, 31] may be used to simulating the oil effect on the heat

transfer and pressure drop by adopting the physical properties of CO₂ lubricating oil mixtures in the models.

A review on the oil effects on the flow boiling heat transfer, flow regimes and two phase pressure drops is presented in [135]. The evaluation methods for the physical properties are detailed in this paper. For using the flow pattern based models, first, the physical properties are evaluated using the methods in [135]. Then, apply the physical properties of oil and refrigerant mixtures in the models to obtain the heat transfer and pressure drop results. Simulation results of the oil effects on the flow boiling heat transfer and two phase frictional pressure drops are illustrated here, using the flow pattern based models of Wojtan et al. and Moreno-Quibén et al. Figure 27 shows the predicted flow boiling heat transfer results of R134a-oil using the heat evaporation transfer model of Wojtan et al. [48, 49] and Figure 28 shows the predicted pressure drop results using the Moreno-Quibén-Thome [63, 64] pressure drop model with a correct factor. These simulations show the effect of oil concentrations on evaporation heat transfer coefficients and two-phase pressure drops. It seems the simulated results are quite similar to those of the existing experimental results.

Due to the immiscibility of lubricant oil and CO₂, whether these methods for miscible oil can be applied to CO₂-lubricant oil or not still need to be further verified. Therefore, extensive experimental data are needed to verify the available methods or to develop new prediction methods for CO₂.

7. CO₂ evaporator simulation and engineering design

As a natural working fluid, CO₂ is used in refrigeration, air-conditioning and heat pump systems for environmental safety. Most commonly used feed methods for CO₂ are pumped liquid and direct expansion. Various structures of CO₂ evaporators are used in the practical applications, e.g. fin-tube evaporator, tube-in-tube evaporator and plate-fin evaporator etc. CO₂ evaporation occurs inside the tubes and the other side of heat transfer may be air flow, water flow or other waste heat resources. Both macro-scale and micro-scale tubes are used in CO₂ evaporators. The prediction of evaporation

heat transfer and two-phase pressure drops inside tubes is critical but difficult due to the effects of various fluid properties and channel sizes [11-14, 28- 31, 49-52, 53-57, 61, 136, 139]. Therefore, proper flow boiling heat transfer and two-phase frictional pressure drop models are needed to predict the heat transfer coefficients, two phase pressure drops and the related flow patterns. Once these are obtained properly. The generally used principles and methods for designing heat exchangers apply for CO₂ evaporators.

7.1. CO₂ evaporation and evaporator modeling

Over the last decades, the Cheng et al. [28-31] CO₂ flow patterns, flow boiling heat transfer and two phase frictional pressure drop models have been proved to favorably agree with the observed flow patterns and measured flow boiling heat transfer and pressure drop data. They are widely used in evaporator design and simulation [139, 14-53-158], for example, Gao [137] has found that the Cheng et al. flow pattern map [28, 30] can predict the flow patterns in micro-fin tubes properly. It can also be used for predicting flow patterns with the effect of oil [140].

Cheng and Thome [11] used the CO₂ flow boiling heat transfer and two phase flow models to predict the thermal performance of CO₂ in a silicon multi-microchannel evaporator having 67 parallel channels with a width of 0.223 mm, a height of 0.68 mm and a length of 20 mm for cooling of a microprocessor as shown in Fig. 29. Simulations of the base temperatures of the silicon multi-microchannel evaporator using CO₂ were performed for the conditions of base heat fluxes from 20 to 100 W/cm², a mass flux of 987.6 kg/m²s and a saturation temperature of 25 °C. The results show that the base temperatures using CO₂ are much lower than the measured temperatures using R236fa. Compared to R236fa, CO₂ has much higher heat transfer coefficients and lower pressure drops in the multi-microchannel evaporator. Figure 30 shows the comparison of the simulated base temperatures of CO₂ evaporation and the measured base temperature of R236fa evaporation in the same silicon multi-microchannel evaporator at a mass flux of 987.6 kg/m²s and a saturation temperature of 25 °C

for base heat fluxes in the range from 20 to 100 W/cm². It can be seen that CO₂ can achieve lower base temperatures than R236fa by 4 - 6 K. Based on the simulation and analysis, CO₂ appears to be a promising coolant for microprocessors at low operating temperatures. However, the operation pressure of CO₂ is much higher than that of R236fa and it presents a great technological challenge like other new cooling technologies.

Marcinichen et al. [141] developed sophisticated simulation tool including the latest prediction methods and oil effects and then used this tool to investigate methods to find a much more compact CO₂ evaporator design with a significantly smaller charge of CO₂ for its operation. Compared to an actual CO₂ evaporator design, the new one proposed here reduces the CO₂ charge by 58.7% and also reduces the size (volume) of the CO₂ evaporator by one-half, meaning the refrigeration system becomes much more compact and lighter in weight. Thus, these benefits can be explored to take advantage of a much lower space within the cabinet of the beverage machine for the refrigeration system and also potentially lower manufacturing costs. In their simulation, the leading two-phase flow pattern map and physically-based prediction models for evaporation of CO₂ developed by Cheng et al. [30, 31] were used. They were also used for modelling oil effects on CO₂ evaporation. The effects of tube size, shape and wettability for significant performance improvements, miscible oil concentration, etc., were addressed while staying within the industry's fabrication and operational limits. The adverse influence of oil was found to reduce the mean CO₂ side heat transfer coefficient and to increase the CO₂ pressure drop by up to 11% and 94%. Figures 31 and 32 show the considerable negative and escalating impact of these oil concentrations observed on the evaporation heat transfer coefficient and on the two-phase pressure gradient according to the simulation results using the Cheng et al. models. The evaporation heat transfer coefficient decreases significantly at large vapor qualities while the two phase pressure drops increases significantly in the mean time for higher concentration of oil. Thus, it is suggested that the oil concentration should be kept below 1% to avoid too large of oil penalty.

Marcinichen et al [145] presented the simulation results of the design of the evaporators with two different types of fins: plain versus wavy fins. A corrugation angle of 12.5° was assumed for the wavy fin while the fin pitch and thickness remained the same. Also, here the air volumetric flow was fixed to be $250 \text{ m}^3/\text{h}$ for the simulations. Figure 33 shows the better performance of the evaporator with wavy fins in terms of local heat transfer per unit of tube length and outlet air temperature. Also, it is clear to see that only two rows of tubes were more than sufficient to transfer the desired 600 W of heat load. The necessary mass of CO_2 was reduced from 11.47 g to 10.43 g when changing from plain fins to wavy fins, which means an additional reduction of about 9.1% . On the other hand, the air-side pressure drop increased from 10.5 Pa to 13.6 Pa . In summary, one can say that the wavy-fin tube evaporator showed the best results in terms of the main design parameters, with the exception of its higher air-side pressure drop and thus special attention is highlighted here for the selection of the fan (not in their study).

7.2. Simulations of CO_2 thermal systems using the Cheng et al. models

The Cheng et al. flow pattern based evaporation heat transfer and two phase frictional pressure drop models for have been widely used for simulations of CO_2 refrigeration, air-conditioning and heat pump systems by a number of researchers [142 - 145, 154 - 158]. For example, in order to improve the system performance of the CO_2 heat pump, it is necessary to develop an optimum design and a control method for the CO_2 heat pump water heater.

Yamaguchi et al. [142] have developed a high-precision and general-purpose system simulation model for the CO_2 heat pump water heater and investigated the validity of the model with detailed experiments. Figure 34 shows the system flow diagram of the CO_2 heat pump water heater in their study. This system consists of a gas cooler, an evaporator, an internal heat exchanger, a compressor, and an expansion valve. In the internal heat exchanger, the refrigerant from the evaporator cools the refrigerant that flows in from the gas cooler, and then flows into the compressor, where its pressure

and temperature are increased. The heated refrigerant then flows into the gas cooler, where it heats up the supplied water. Subsequently, it flows into the internal heat exchanger and is expanded by the expansion valve. Finally, the refrigerant flows into the evaporator. In the evaporator, the refrigerant absorbs heat from the ambient air, after which it flows back to the internal heat exchanger. In this system, a cross-finned tube heat exchanger with smooth plate fins is adapted for use in the evaporator as shown in Fig. 34.

A cross-finned tube heat exchanger with smooth plate fins is adapted for use in the evaporator in the heat pump system. In the development of their model, the local heat transfer coefficient and two phase frictional pressure drop inside the tubes are calculated using the Cheng et al. [30, 31] flow pattern based evaporation heat transfer model. These models were developed specifically for CO₂ to predict the evaporation heat transfer coefficient and the two phase frictional pressure drop on the basis of the flow pattern map for CO₂. They also considered the oil effect on the performance. According to study of the PAG oil effect on heat transfer by Yoshioka et al. [147], the heat transfer coefficient of the evaporator with 5.0 wt.% PAG oil was almost 25% lower than that of the evaporator without oil. This value was used in their study. In comparison of predicted and measured values, it is confirmed that the predicted values are in good agreement with the measured values totally. For evaporator, the results show good agreement between the measured and predicted heat transfer rate. This means that the Cheng et al. models work well in this study. The maximum difference between the predicted and measured COP is 5.4%, and the average difference is 0.9%.

Considering the actual heat transfer processes of heat exchangers and characteristics of components adopted in the cycle of air-source trans-critical CO₂ heat pump water heater system, Wang et al. [143] conducted simulation for the heat pump cycle. In their simulation model, the Cheng et al. flow pattern based evaporation model was adopted in the evaporator model in their simulation. It shows good agreement with the experimental results. Faria et al. [144] investigated the behavior of the solar evaporator and expansion valve assembly of a transcritical CO₂ heat pump in transient and steady conditions. The dynamic behavior of systems using CO₂ as a refrigerant is significantly

influenced by the dynamics of the heat transfer mechanisms. The solar evaporator model is based on the equations of conservation of mass, momentum, and energy. The model validation is realized by comparing simulation results with the Cheng et al. models and the experimental data. The model is a useful tool for analyzing the behavior in transient and steady conditions simulating various operating conditions of the heat pump including solar radiation, ambient temperature, wind speed and atmospheric conditions. Yang et al. [145] investigated experimentally a prototype of combined R134a and transcritical CO₂ heat pump. The experimental results demonstrated that the combined system could operate reliably and supply stable temperature hot water over a wide range of ambient temperatures and feed water temperatures. The experimental results also showed that ambient temperature had a large effect on the system performance. Furthermore, they investigated the improvement of the combined system in comparison to the standard transcritical CO₂ heat pump, a simple mathematical model was developed and validated by the experimental data. The comparison results showed that the combined system could offer higher system coefficient of performance (COP) at experimental ambient and feed water temperatures. In their evaporator model, the Cheng et al. models were used in the simulations. In general, the Cheng et al. [30, 31] flow pattern-based evaporation heat transfer and two phase pressure drop models show good agreement with the experimental data in the existing studies when used in modeling the evaporators in these systems.

7.3. CO₂ evaporator design and selection criteria

Using the proper flow boiling heat transfer models is the key to the thermal design of CO₂ evaporators. The oil effect on the evaporation heat transfer and two-phase pressure drops should be considered as the fouling resistance if the oil presents. The Cheng et al. [30, 31] flow boiling heat transfer and pressure drop models should be used to evaluate the heat transfer coefficients and two-phase pressure drops for the working conditions. The heat transfer coefficients on the other side of the evaporators should be evaluated with the proper correlations [151-152, 159]. Once the tube

material, diameter and wall thickness are selected, the overall heat transfer coefficient may be determined. The conventional heat exchanger design methods may be applied for the CO₂ evaporator. For more accurate evaluation of the heat transfer rate, local heat transfer may be evaluated using the relevant model.

In the thermal design of a evaporator, the Number of Transfer Units (NTU) and the LMTD calculation methods are used. The evaporators should be divided into zones. Each zone is related to a fraction of the total surface of the exchanger. CO₂ evaporators have a two-phase zone for evaporation and a single-phase zone for superheating. The CO₂ evaporator are divided into many small sections to take into account of the heat transfer coefficient changes in different flow regimes. Just for one example, for the design and simulation of evaporator for a CO₂ automobile air conditioning system, Jin et al. [159] adopted the method of Kim and Bublard [160] to predict the performance of an evaporator for a CO₂ mobile air-conditioning system. Based on the finite volume method, the model has been developed using mass and energy conservation equations, with emphasis placed on the refrigerant-side heat transfer and pressure drop characteristics. Figure 35. Shows the schematic illustration of evaporator model segment discretization. The in-tube refrigerant flow was divided into two-phase region and superheated region, and both dry and wet conditions were considered. Using the newly developed refrigerant-side heat transfer model of Cheng et al. [31], the model can predict the performance of evaporator with a reasonable accuracy compared with the experimental data. For the air-side heat transfer and pressure drop methods, details may be found in [160, 161] (not the part of this review).

Besides the thermal design of a CO₂ evaporator, other aspects such as material selection, operation pressure, optimum minimum mass flow rate and defrost etc. should be considered in selection/design of the evaporator. The process of designing/selecting air cooling evaporators to operate in CO₂ refrigeration, air conditioning and heat pump systems is very similar to designing/selecting evaporators for ammonia and other refrigerants according to the ASHRAE standard [161]. Typically, the following inputs are required for properly selecting CO₂ evaporators:

- (1) Elevation, (b) Return air ('Air on') temperature, (c) Return air relative humidity, (d) Evaporating temperature, (e) Type of feed, (f) Overfeed rate (if pumped feed), (g) Liquid pressure and temperature at the expansion valve (if direct expansion), (h) Required cooling duty, (i). Type of defrost, (j) Supply voltage, (k) Materials of construction, (l) Required MAWP (Maximum Allowable Working Pressure).
- (2) Other inputs may include: (m) Maximum allowable air velocity, (n) Minimum air flow rate, (o) Maximum allowable fan speed, (p) Maximum allowable sound pressure (usually in dB(A)), (q) Minimum air throw distance, (r) Minimum number of fans, (s) Dimensional constraints (maximum height or length limitations).
- (3) The Output data typically includes: (t) Actual cooling duty, (u) Air flow rate and air velocity, (v) Leaving air temperature, (w) Leaving air relative humidity, (x) Sound pressure level, (y) Air throw distance, (z) Dimensional characteristics and (aa) Electrical characteristics.

There are many similarities in evaporator rating methods and construction for ammonia and other refrigerants, however, the very different thermodynamic and chemical characteristics of CO₂ compared to ammonia and other refrigerants require special attention with regard to the following aspects:

- **Material Compatibility:** CO₂ can be used safely with copper and copper-bearing alloys. Actually, dry CO₂ is quite inert and can be used with all commonly used base metals, copper, carbon steel, stainless steel, and aluminum. Care must be taken to select materials with sufficient strength to withstand the higher maximum allowable working pressure (MAWP) required for CO₂. This normally rules out the use of aluminum with CO₂.
- **Pressure:** CO₂ evaporators will operate at significantly higher pressures than ammonia and other refrigerants for a given temperature.
- **Heat Transfer:** Thermodynamic and transport properties are very different for CO₂ compared to ammonia and other refrigerants and result in very different evaporator

circuiting arrangements to achieve equivalent cooling capacity. The Cheng et al. models [28-31] are recommended for calculation of evaporation heat transfer coefficient.

Both copper and stainless steel tubing and pipe are recommended for use in CO₂ evaporators provided the diameters and wall thicknesses meet the required design pressures. When using copper, a non-phosphorous bearing brazing alloy is recommended. This is needed to limit the risk of leaks caused by acidic conditions resulting from the presence of carbonic acid. Carbon steel is not recommended for use in CO₂ evaporators due to (a) susceptibility to corrosion in the presence of carbonic acid, and (b) embrittlement at low temperatures. Aluminum is not recommended for use in CO₂ evaporators due to its lower yield and tensile strength characteristics. ASHRAE Standard 15 [161] establishes the design pressure requirements for CO₂ systems:

- ASHRAE Standard 15 requires the design pressure for CO₂ evaporators to be "...at least 20% higher than the saturation pressure corresponding to the warmest location in the circuit." The "warmest location in the circuit" is interpreted as the warmest anticipated room temperature in which the evaporator(s) will operate. Although minimum tube wall thicknesses are recommended [161], the evaporator manufacturer must insure that all pressure bearing components in the coil, including headers and pipe connections, are designed correctly.
- The temperature used to establish design pressure must be carefully selected to account for conditions which include (but are not necessarily limited to) those shown here: (a) Startup conditions, (b) Peak load operation, (c) Abnormal loads (process temperature excursions) and (d) Standby conditions that occur frequently (i) Power outages limited in time duration but which may happen with some frequency and (ii) Shutdown during cleanup.

Reducing the overfeed rate in pumped refrigerant systems is desirable because pumping power will be reduced by the cube of the ratio of the reduction in flowrate. As the liquid overfeed rate is reduced, however, the risk of operating evaporators with the refrigerant in separated flow patterns (stratified/wavy) increases. The heat transfer becomes poor due to if vapor and liquid is separated. Cooling capacity of the evaporator falls off dramatically when this occurs. Therefore, it is essential to maintain the minimum mass flow rate in the evaporators. For instance, with CO₂ in an evaporator having 5/8" tubes, a minimum mass flux of 200 kg/m²-s is required to avoid stratified/wavy flow. Optimum Overfeed Rates are recommended as follows:

- Pumped CO₂ systems can be successfully operated with lower overfeed rates compared to ammonia and other refrigerants.
- Recommended overfeed rates for pumped CO₂ evaporators are 1.5:1 for coolers and 2:1 for freezers.

CO₂ evaporators can be operated with direct expansion feed. Care must be taken by the evaporator manufacturer to circuit the coil in such a way that the refrigerant mass flux is kept above 200 kg/m²-s in order to avoid stratified/wavy flow. This becomes challenging with larger diameter tubes (greater than 5/8"). At very low temperatures, enhanced tubes (microfin copper) are recommended as a way to mitigate separated flow patterns and improve performance.

Defrost is another important aspect in CO₂ evaporator design and selection. CO₂ evaporators are commonly defrosted using the following methods: (a) Air, (b) Water and (c) Electric Resistance. Control valve groups for these methods of defrost are very simple and low cost. Hot gas defrost with CO₂ evaporators is not commonly used. In a cascade system, the intermediate CO₂ temperature/pressure is normally too low to allow the CO₂ from that circuit to be used for defrost. This then requires a separate high pressure (capable of 50 bar) compressor with sufficient capacity to be installed expressly for purposes of providing hot gas for defrost. Other means of generating hot

CO₂ gas for defrost include use of a heat-driven boiler vessel, typically heated by discharge gas from the high side of the cascade system. The complexity and added expense of hot gas defrost with CO₂ has limited its application.

8. Potential application of CO₂ in cooling and thermal energy Systems

As an excellent coolant, CO₂ may be used in electronic cooling [11], two-phase thermosyphon loop [146] and evaporative CO₂ cooling system for the upgrade of the CMS pixel detector [150] etc. and it presents a great technological challenge like other new cooling technologies. Furthermore, new applications with CO₂ in various thermal systems with microscale channel evaporators should be further explored to improve the energy efficiency and environmental safe. CO₂ may also be used for renewable energy system such as geothermal energy [148, 149], solar energy utilization and recovery of industrial waste heat using CO₂ as a working fluid in various thermal systems. Hybrid power and heat systems using CO₂ as a working fluid should also be investigated.

Using the proper heat transfer models is the key to the thermal design of CO₂ evaporators for various thermal energy systems such as heat pump, refrigeration and air-conditioning systems. For more accurate evaluation of the heat transfer rate, local heat transfer may be evaluated using the proper model. To this end, the Cheng et al. [30, 31] models are recommended. The oil effect on the flow boiling heat transfer and two-phase pressure drops should be considered as the fouling resistance if the oil presents. The heat transfer coefficients on the other side of the evaporators should be evaluated with the proper correlations [151, 152, 159, 160]. Once the tube material, diameter and wall thickness are selected, the overall heat transfer rate may be determined by segmenting the evaporator into many small volumes and applying the heat exchanger design methods to the small volumes and then integrate the heat transfer rates to obtain the total heat transfer rate for the CO₂ evaporator.

9. Concluding remarks and future research recommendations

Fundamentals, engineering applications and design of CO₂ flow boiling in macro- and micro-channel evaporators have been reviewed. The main conclusions are summarized as follows:

The research on CO₂ flow boiling and two phase flow phenomena and mechanisms in macro- and micro-channel evaporators have been extensively analyzed and discussed. The available experimental results have shown different flow boiling heat transfer and two-phase flow characteristics of CO₂ at high and low reduced pressures. The evaporation heat transfer and two-phase flow of CO₂ at saturation temperatures ranging from 0 to 25°C show different characteristics from those of conventional refrigerants. The flow boiling heat transfer mechanisms are the dominance of the nucleate boiling at low/moderate vapor qualities prior to dryout and the occurrence of dryout in CO₂ at relatively lower vapor qualities than conventional refrigerants. The experimental data from the different independent studies show somewhat different evaporation heat transfer trends at similar test conditions. This might be caused by large measurement uncertainties. Therefore, more accurate experimental data are needed for CO₂ evaporation in both macro- and micro-channels through well designed test facilities and careful experiments. In particular, a wide range of test conditions should be designed to meet the practical needs in industry.

The prediction methods for flow patterns, heat transfer and pressure drop are analyzed. It is essential to develop mechanistic prediction methods according to the physical phenomena and mechanisms. In this aspect, the Cheng et al. [30, 31] generalized flow pattern map and flow pattern based flow boiling heat transfer model for CO₂ reasonably predicts the observed flow patterns and experimental heat transfer coefficients and also capture properly the parametric trends. However, for the dryout and mist flow regimes with partially or all dry perimeters, the heat transfer model is only partially satisfactory. Therefore, more careful experiments are needed in these two regimes to provide more accurate heat transfer data. More accurate experimental CO₂ two phase pressure drop data should be obtained to further test or improve the model for pressure drop in the future. Furthermore, the available studies of flow boiling of CO₂ in enhanced channels are limited in the literature. Quite

different results have been obtained in the available studies. It is difficult to reach generally acceptable conclusions from these studies. It is essential to conduct feasibility of applicability of enhanced channels for CO₂ flow boiling according to the mechanisms of heat transfer enhancement and mechanisms.

Oil has significant effects on CO₂ evaporation heat transfer and two-phase pressure drops. In general, very small amounts of the lubricating oil (< 0.5% wt) seem to have little effect while larger concentrations (> 1% wt) tend to dramatically reduce flow boiling heat transfer coefficients. For two-phase pressure drops, the effect of lubricating oil only occurs at vapor qualities larger than around 0.6. Further experimental studies on evaporation heat transfer and two-phase frictional pressure drops of CO₂- oil mixtures in both macro- and micro-channels should be conducted over a wide range of test conditions to provide more experimental data on these aspects. In order to understand the heat transfer mechanisms of evaporation with CO₂ and immiscible oil, flow visualization and local measurement of oil concentration are also suggested to be done. Due to the immiscibility of lubricant oil and CO₂, whether the available methods for miscible oil can be applied to CO₂-lubricant oil or not still need to be further verified. Therefore, extensive experimental data are needed to verify the available methods or to develop new methods for CO₂.

CO₂ has also been investigated in heat pump, refrigeration and air-conditioning systems. Design methods and selection criteria of CO₂ evaporators have been discussed. Furthermore, other practical applications such as electronic chips cooling, evaporative CO₂ cooling system for the upgrade of the CMS pixel detector and so on. It has potential applications in renewable energy utilization such as geothermal and solar thermal systems, recovery of industrial waste heat and hybrid heating and power systems. It is recommended that fundamentals, engineering applications and design in the relevant systems should be further conducted. New applications using CO₂ thermal systems should be explored.

Nomenclature

A	cross-sectional area of flow channel, m ² ;
A_L	cross-sectional area occupied by liquid-phase, m ²
CO	Confinement number
D	internal tube diameter, m
$Fr_{V,Mori}$	vapor Froude number [$G^2/(\rho_v(\rho_L - \rho_v)gD_{eq})$]
f	friction factor
G	total vapor and liquid two-phase mass flux, kg/m ² s
g	gravitational acceleration, 9.81 m/s ²
h	heat transfer coefficient, W/m ² K
h_{LV}	latent heat of vaporization, J/kg
j	segment
k	thermal conductivity, W/mK
L	channel length, m
M	molecular weight, kg/kmol
N	number of data points
Pr	Prandtl number [$c_p\mu/k$]
p	pressure, bar
p_r	reduced pressure [p/p_{crit}]
q	heat flux, W/m ²
Re_H	homogeneous Reynolds number $\{(GD_{eq}/\mu_v)[x + \rho_v/\rho_L(1-x)]\}$
Re_M	Reynolds number [$GD_{eq}/(\mu_H)$] defined in mist flow
Re_v	vapor phase Reynolds number [$GxD_{eq}/(\mu_v\varepsilon)$]
S	nucleate boiling suppression factor

T	temperature, °C
u	mean velocity, m/s
W	absolute humidity of moist air, kg/kg
We_L	liquid Weber number [$G^2 D_{eq}/(\rho_L \sigma)$] defined by Eq. (17); [$\rho_L u_L^2 D_{eq}/\sigma$]
We_V	vapor Weber number [$G^2 D_{eq}/(\rho_V \sigma)$] defined
x	vapor quality
Y	correction factor

Greek symbols

Δp	pressure drop, Pa
δ	liquid film thickness, m
ε	cross-sectional vapor void fraction
ε_{IA}	vapor void fraction at $x = x_{IA}$
μ	dynamic viscosity, Ns/m ²
θ_{dry}	dry angle of tube perimeter, rad
θ_{dry}^*	dimensionless dry angle [$\theta_{dry}/(2\pi)$]
θ_{wet}	wet angle of the tube perimeter, rad
ρ	density, kg/m ³
σ	surface tension, N/m; standard deviation, %
ξ_i	relative error, %
$\bar{\xi}$	average error, %
$ \bar{\xi} $	mean error, %

Subscripts

A	annular flow
-----	--------------

<i>ai</i>	air inlet
<i>ao</i>	air outlet
<i>cb</i>	convective boiling
<i>crit</i>	critical
<i>de</i>	dryout completion
<i>di</i>	dryout inception
<i>dry</i>	dry
<i>dryout</i>	dryout region
<i>eq</i>	equivalent
<i>f</i>	frictional
<i>g</i>	gas
<i>H</i>	homogeneous
<i>h</i>	hydraulic
<i>I</i>	intermittent flow
<i>IA</i>	intermittent flow to annular flow transition
<i>in</i>	tube inlet
<i>j</i>	j segment
<i>L</i>	liquid
<i>LO</i>	considering the total vapor-liquid flow as liquid flow
<i>LV</i>	liquid-vapor
<i>M</i>	mist flow
<i>m</i>	momentum
<i>nb</i>	nucleate boiling
<i>out</i>	tube outlet
<i>ri</i>	refrigerant inlet
<i>ro</i>	refrigerant outlet

<i>Slug</i>	slug flow
<i>SW</i>	stratified-wavy flow
<i>sat</i>	saturation
<i>static</i>	static
<i>total</i>	total
<i>tp</i>	two-phase flow
<i>V</i>	vapor
<i>wet</i>	wet perimeter

References

- [1] Lorentzen, G. Revival of carbon dioxide as a refrigerant. *Int. J. Refrig.* 1994, vol. 17, 292-30.
- [2] Lorentzen, G. The use of natural refrigerants: a complete solution to the CFC/HCFC predicament. *Int. J. Refrig.* 1995, vol. 18, 190-197.
- [3] Kandlikar, S.G., A roadmap for implementing minichannels in refrigeration and air-conditioning systems - current status and future directions, *Heat Transfer Eng.* 2007, vol. 28(12), 973–985, 2007
- [4] Bansal, P., A review - status of CO₂ as a low temperature refrigerant: Fundamentals and R&D opportunities. *Appl. Therm. Eng.* 2012, vol. 41, 18-29.
- [5] Thome, J. R.; Ribatski, G. State-of-the-art of two-phase flow and flow boiling heat transfer and pressure drop of CO₂ in macro- and micro-channels. *Int. J. Refrig.* 2005, vol. 28, 1149-1168.
- [6] Mastrullo, R., Mauro, A.W., Viscito, L., Flow boiling of carbon dioxide: Heat transfer for smooth and enhanced geometries and effect of oil. state of the art review. *Int. J. Refrig.* 2019, vol. 108, 311 – 335.
- [7] Cheng, L., Ribatski, G., Thome, J. R. Analysis of supercritical CO₂ cooling in macro- and micro-channels. *Int. J. Refrig.* 2008, vol. 31, 1301-1316.

- [8] Cheng, L., Xia, G., Li, Q. CO₂ Evaporation Process Modeling: Fundamentals and Engineering Applications, *Heat Transfer Eng.* DOI: 10.1080/01457632.2021.190529, 2021, 1-21.
- [9] Kim, M. H.; Pettersen, J.; Bullard, C. W. Fundamental process and system design issues in CO₂ vapor compression systems. *Prog. Energy Combust. Sci.* 2000, vol. 30, 119-174.
- [10] Sawalha, S. Using CO₂ in supermarket refrigeration. *ASHRAE J.* 2005, vol. 47, no. 8, 26-30.
- [11] Cheng, L.; Thome, J. R. Cooling of microprocessors using flow boiling of CO₂ in micro-evaporators: Preliminary analysis and performance comparison. *Appl. Therm. Eng.* 2009, vol. 29, 2426-2432.
- [12] Karayiannis, T.G., Mahmoud M.M. Flow boiling in microchannels: Fundamentals and applications, *Appl. Therm. Eng.* 2017, vol. 115, 1372-1397.
- [13] Cheng, L.; Xia, G. Fundamental issues, mechanisms and models of flow boiling heat transfer in microscale channels, *Int. J. Heat Mass Transfer.* 2017, vol. 108 (Part A), 97-127.
- [14] Cheng, L. Fundamental issues of critical heat flux phenomena during flow boiling in microscale-channels and nucleate pool boiling in confined spaces. *Heat Transfer Eng.* 2013, vol. 34, issue 13, 1011-1043.
- [15] Kandlikar, S.G., Grande, W.J. Evolution of microchannel flow passages - Thermohydraulic performance and fabrication technology. *Heat Transfer Eng.* 2003, vol. 24 (1), 3-17,
- [16] Kandlikar, S. G. Fundamental issues related to flow boiling in minichannels and microchannels. *Exp. Therm. Fluid Sci.* 2002, vol. 26, 389-407.
- [17] Cheng, L.; Mewes, D. Review of two-phase flow and flow boiling of mixtures in small and mini channels. *Int. J. Multiphase Flow.* 2006, vol. 32, 183-207.
- [18] Cheng, L. Microscale Flow Patterns and Bubble Growth in Microchannels, in *Microchannel Phase Change Heat Transfer*, Editor: Sujoy Kumar Saha, Elsevier Publisher, 2016, pp.91-140.
- [19] Cheng, L. Flow Boiling Heat Transfer with Models in Microchannels, in *Microchannel Phase Change Heat Transfer*, Editor: Sujoy Kumar Saha, Elsevier Publisher, 2016, pp.141-191.

- [20] Kew, P. A.; Cornwell, K. Correlations for the prediction of boiling heat transfer in small-diameter channels. *Appl. Therm. Eng.* 1997, *vol.* 17, 705-715.
- [21] Mehendale, S. S.; Jacobi, A. M.; Ahah, R. K. Fluid flow and heat transfer at micro- and meso-scales with application to heat exchanger design. *ASME Appl. Mech. Rev.* 2000, *vol.* 53, 175-193.
- [22] Cheng, L.; Ribatski, G.; Thome, J. R. Gas-liquid two-phase flow patterns and flow pattern maps: fundamentals and applications. *ASME Appl. Mech. Rev.* 2008. *vol.* 61, 050802-1-050802-28.
- [23] REFPROP. NIST Refrigerant Properties Database 23. Gaithersburg, MD, 2013, Version 9.1.
- [24] REFPROP. NIST Refrigerant Properties Database 23. Gaithersburg, MD, 2002, Version 7.0.
- [25] REFPROP. NIST Refrigerant Properties Database 23. Gaithersburg, MD, 1998, Version 6.01.
- [26] EES, Engineering Equation Solver. F-Chart Software Inc., Wisconsin (USA), 2005..
- [27] Thome, J. R., Hajal, J. Flow boiling heat transfer to carbon dioxide: general prediction method, *Int. J. Refrig.* 2004, *vol.* 27, 294–301
- [28] Cheng, L.; Ribatski, G.; Wojtan, L.; Thome, J. R. New flow boiling heat transfer model and flow pattern map for carbon dioxide evaporating inside horizontal tubes. *Int. J. Heat Mass Transfer.* 2006, *vol.* 49, 4082-4094.
- [29] Cheng, L.; Ribatski, G.; Wojtan, L.; Thome, J. R. Erratum to: New flow boiling heat transfer model and flow pattern map for carbon dioxide evaporating inside tubes, [Heat Mass Transfer 49 (21-22) (2006) 4082-4094]. *Int. J. Heat Mass Transfer.* 2007, *vol.* 50, 391.
- [30] Cheng, L.; Ribatski, G.; Moreno Quibén, J.; Thome, J. R. New prediction methods for CO₂ evaporation inside tubes: Part I - A general two-phase flow pattern map and development of a phenomenological model of two-phase flow frictional pressure drop. *Int. J. Heat Mass Transfer.* 2008, *vol.* 51, 111-124.
- [31] Cheng, L.; Ribatski, G.; Thome, J. R. New prediction methods for CO₂ evaporation inside tubes: Part II - A general flow boiling heat transfer model based on flow patterns, *Int. J. Heat Mass Transfer.* 2008, *vol.* 51, 125-135.

- [32] Pettersen, J. Flow vaporization of CO₂ in microchannel tubes. *Exp. Therm. Fluid Sci.* 2004, vol. 28, 111-121.
- [33] Yun, R.; Kim, Y.; Kim, M. S.; Choi, Y. Boiling heat transfer and dryout phenomenon of CO₂ in a horizontal smooth tube. *Int. J. Heat Mass Transfer.* 2003, vol. 46, 2353-2361.
- [34] Yun, R.; Kim, Y.; Kim, M. S. Flow boiling heat transfer of carbon dioxide in horizontal mini tubes. *Int. J. Heat Fluid Flow.* 2005, vol. 26, 801-809.
- [35] Hihara, E; Tanaka, S. Boiling heat transfer of carbon dioxide in horizontal tubes. In: *Preliminary Proceedings of IIR Gustav Lorentzen Conference on Natural Working Fluids*, Purdue, 2000, pp. 279-284.
- [36] Yoon, S. H.; Cho, E. S.; Hwang, Y. W.; Kim, M. S.; Min, K.; Kim, Y. Characteristics of evaporative heat transfer and pressure drop of carbon dioxide and correlation development. *Int. J. Refrig.* 2004, vol. 27, 111-119.
- [37] Yun, R.; Kim, Y.; Kim, M. S. Convective boiling heat transfer characteristics of CO₂ in microchannels. *Int. J. Heat Mass Transfer.* 2005, vol. 48, 235-242.
- [38] Koyama, S.; Kuwahara, K.; Shinmura, E.; Ikeda, S. Experimental study on flow boiling of carbon dioxide in a horizontal small diameter tube. In: *IIR Commission B1 Meeting*, Paderborn, Germany, 2001, pp. 526-533.
- [39] Hihara, E. Fundamental technology for carbon dioxide operated heat pumps. In: *JSAE Automotive Air-Conditioning Symposium*. 2006, pp.243-262.
- [40] Bredesen, A.; Hafner, A.; Pettersen, J.; Neksa, P.; Aflekt, K. Heat transfer and pressure drop for in-tube evaporation of CO₂. In: *Proceedings of the International Conference on Heat Transfer Issues in Natural Refrigerants*, University of Maryland, USA, 1997, pp. 1-15.
- [41] Knudsen, H. J.; Jensen, R. H. Heat transfer coefficient for boiling carbon dioxide. In: *Workshop Proceedings - CO₂ Technologies in Refrigeration, Heat Pumps and Air Conditioning Systems*, Trondheim, Norway, 1997, pp. 319-328.

- [42] Zhao, X.; Bansal, P.K. Flow boiling heat transfer characteristics of CO₂ at low temperatures. *Int. J. Refrig.* 2007, vol. 30, 937-945.
- [43] Park, C. Y.; Hrnjak, P. S. Flow boiling heat transfer of CO₂ at low temperatures in a horizontal smooth tube. *J. Heat Transfer.* 2005, vol. 127, 1305-1312.
- [44] Park, C. Y.; Hrnjak, P. S. CO₂ and R410A flow boiling heat transfer, pressure drop, and flow pattern at low temperatures in a horizontal smooth tube. *Int. J. Refrig.* 2007, vol. 30, 166 -178.
- [45] Koyama, S., Lee, S., Ito, D., Kuwahara, K., Ogawa, H. Experimental study on flow boiling of pure CO₂ and CO₂-oil mixtures inside horizontal smooth and micro-fin copper tubes. In: *Proceedings of 6th IIT-Gustav Lorentzen Conference*, Glasgow, UK, 2004.
- [46] Zhao, X, Bansal, P. Experimental Investigation on flow boiling heat transfer of CO₂ at low temperatures, *Heat Transfer Eng.* 2009, vol. 30(1-2):2-11.
- [47] Choi, K-I., Pamitrana, A.S., Oh, Ch-Y., Oh, J-T. Boiling heat transfer of R-22, R-134a, and CO₂ in horizontal smooth minichannels. *Int. J. Refrig.* 2007, vol. 30, 1336 -1346.
- [48] Wojtan, L.; Ursenbacher, T.; Thome, J. R. Investigation of flow boiling in horizontal tubes: Part I – A new diabatic two-phase flow pattern map. *Int. J. Heat Mass Transfer.* 2005, vol. 48, 2955-2969.
- [49] Wojtan, L.; Ursenbacher, T.; Thome, J. R. Investigation of flow boiling in horizontal tubes: Part II – Development of a new heat transfer model for stratified-wavy, dryout and mist flow regimes. *Int. J. Heat Mass Transfer,* 2005, vol. 48, 2970-2985.
- [50] Kattan, N.; Thome, J. R.; Favrat, D. Flow boiling in horizontal tubes. Part 1: Development of a diabatic two-phase flow pattern map. *J. Heat Transfer.* 1998, vol. 120, 140-147.
- [51] Kattan, N.; Thome, J. R.; Favrat, D. Flow boiling in horizontal tubes: Part 2-New heat transfer data for five refrigerants. *J. Heat Transfer.* 1998, vol. 120, 148-155.
- [52] Kattan, N.; Thome, J. R.; Favrat, D. Flow boiling in horizontal tubes: Part-3: Development of a new heat transfer model based on flow patterns. *J. Heat Transfer.* 1998, vol. 120, 156-165.

- [53] Chen, J. C. Correlation for boiling heat transfer to saturated fluids in convective flow. *Ind. Chem. Eng. Des. Dev.* 1966, vol. 5, 322-339.
- [54] Shah, M. M. Chart correlation for saturated boiling heat transfer: equations and further study. *ASHRAE Trans.* 1982, vol. 88, 185-196.
- [55] Gungor, K. E.; Winterton, R. H. S. A general correlation for flow boiling in tubes and annuli. *Int. J. Heat Mass Transfer.* 1986, vol. 29, 351-358.
- [56] Kandlikar, S. G. A general correlation for saturated two-phase flow boiling heat transfer inside horizontal and vertical tubes. *J. Heat Transfer.* 1990, vol. 112, 219-228.
- [57] Liu, Z.; Winterton, R. H. S. A general correlation for saturated and subcooled flow boiling in tubes and annuli based on a nucleate pool boiling equation. *Int. J. Heat Mass Transfer.* 1991, vol. 34, 2759-2766.
- [58] Fang, X., Zhou, Z., Li, D. Review of correlations of flow boiling heat transfer coefficients for carbon dioxide. *Int. J. Refrig.* 2013, vol. 36, 2017-2039.
- [59] Fang, X. A new correlation of flow boiling heat transfer coefficients for carbon dioxide. *Int. J. Heat Mass Transfer.* 2013, vol. 64, 802-807.
- [60] Fang, X., Wu, Q., Yuan, Y. A general correlation for saturated flow boiling heat transfer in channels of various sizes and flow directions. *Int. J. Heat Mass Transfer.* 2017, vol. 107, 972-981.
- [61] Kim, S-M, Mudawar, I. Review of databases and predictive methods for heat transfer in condensing and boiling mini/micro-channel flows. *Int. J. Heat Mass Transfer.* 2014, vol. 77, 627 - 652
- [62] Ould-Didi, M. B.; Kattan, N.; Thome, J. R. Prediction of two-phase pressure gradients of refrigerants in horizontal tubes. *Int. J. Refrig.* 2002, vol. 25, 935-947.
- [63] Moreno Quibén, J.; Thome, J. R. Flow pattern based two-phase frictional pressure drop model for horizontal tubes, Part I: diabatic and adiabatic experimental study. *Int. J. Heat Fluid Flow.* 2007, vol. 28, 1049-1059.

- [64] Moreno Quibén, J.; Thome, J. R. Flow pattern based two-phase frictional pressure drop model for horizontal tubes, Part II: new phenomenological model. *Int. J. Heat Fluid Flow*. 2007, vol. 28, 1060-1072.
- [65] Baker, O. Design of pipe lines for simultaneous flow of oil and gas. *Oil and Gas J.* 1954, vol. 53, 185-190.
- [66] Taitel, Y.; Dukler, A. E. A model for predicting flow regime transitions in horizontal and near horizontal gas-liquid flow. *AIChE J.* 1976, vol. 22, 47-55.
- [67] Hashitume, K. Flow pattern and void fraction of refrigerant two-phase flow in a horizontal pipe. *Bulletin of the JSME*. 1983, vol. 26, 1597-1602.
- [68] Steiner, D. VDI-Wärmeatlas, Verein Deutscher Ingenieure VDI-Gesellschaft Verfahrenstechnik und Chemieingenieurwesen (GCV), Düsseldorf, Ch. Hbb, 1993.
- [69] Moreno Quibén, J.; Cheng, L.; da Silva Lima, R. J.; Thome, J. R. Flow boiling in horizontal flattened tubes: Part I — Two-phase frictional pressure drop results and model, *Int. J. Heat Mass Transfer*. 2009, vol. 52, 3634-3644.
- [70] Moreno Quibén, J.; Cheng, L.; da Silva Lima, R. J.; Thome, J. R. Flow boiling in horizontal flattened tubes: Part II — Flow boiling heat transfer results and model, *Int. J. Heat Mass Transfer*. 2009, vol. 52, pp. 3645-3653.
- [71] Thome, J. R.; El Hajal, J. Two-phase flow pattern map for evaporation in horizontal tubes: Latest version. In: *1st International Conference on Heat Transfer, Fluid Mechanics and Thermodynamics*, Kruger Park, South Africa, April 8-10, 2002, pp. 182-188.
- [72] Rouhani, Z., Axelsson, E. Calculation of volume void fraction in a subcooled and quality region. *Int. J. Heat Mass Transfer*. 1970, vol. 17, 383-393.
- [73] Biberg, D. An explicit approximation for the wetted angle in two-phase stratified pipe flow. *Canadian J. Chem. Eng.* 1999, vol. 77, 1221-1224.

- [74] Mori, H., Yoshida, S., Ohishi, K., Kokimoto, Y. Dryout quality and post dryout heat transfer coefficient in horizontal evaporator tubes. In: *Proceeding of 3rd European Thermal Sciences Conference*, 2000, pp. 839-844.
- [75] Kutateladze, S. S. On the transition to film boiling under natural convection. *Kotloturbostroenie*, 1948, vol. 3, 10-12.
- [76] Gasche, J. L. Carbon dioxide evaporation in a single micro-channel. *J. Braz. Soc. Mech. Sci. Eng.* 2006, vol. 28, 69-83.
- [77] Dittus, F. W.; Boelter, L. M. K. Heat transfer in automobile radiator of the tubular type. *Univ. Calif. Publ. Eng.* 1930, vol. 2, 443-461.
- [78] Cooper, M. G. Saturation nucleate pool boiling: a simple correlation. In: 1st U.K. National Conference on Heat Transfer, 1984, vol. 2, pp. 785-793.
- [79] El Hajal, J.; Thome, J. R.; Cavallini, A. Condensation in horizontal tubes, part 2: New heat transfer model based on flow regimes. *Int. J. Heat Mass Transfer*. 2003, vol. 46, 3365-3387.
- [80] Groeneveld, D. C. Post dry-out heat transfer at reactor operating conditions. In: *ANS Topical Meeting on Water Reactor Safety*, Salt Lake City, 1973.
- [81] Cheng, L.; Ribatski, G.; Thome, J. R. On the Prediction of Flow Boiling Heat Transfer of CO₂. In: *The 22nd IIR International Congress of Refrigeration*, Beijing, P.R. China, August 21-26, 2007.
- [82] Yun, R.; Choi, C.; Kim, Y. Convective boiling heat transfer of carbon dioxide in horizontal small diameter tubes. In: *IIR/IIF-Commission B1, B2, E1 and E2-Guangzhou*, China, 2002, pp. 293-303.
- [83] Tanaka, S.; H. Daiguji, H.; Takemura, F.; Hihara, E. Boiling heat transfer of carbon dioxide in horizontal tubes. In: *38th National Heat Transfer Symposium of Japan*, 2001, pp. 899-900.
- [84] Shinmura, E.; Take, K.; Koyama, S. Development of high-performance CO₂ evaporator. In: *JSAE Automotive Air-conditioning Symposium*, 2006, pp. 217-227.

- [85] Jeong, S.; Cho, E.; Kim, H. Evaporative heat transfer and pressure drop in a microchannel tube. In: *Proceedings of the 3rd International Conference on Microchannels and Minichannels*, Toronto, Ontario, Canada, Part B, 2005, pp. 103-108.
- [86] Zhao, Y.; Molki, M.; Ohadi, M. M.; Dessiatoun, S. V. Flow boiling of CO₂ in microchannels. *ASHRAE Trans.* 2000, vol. 106, Part I, pp. 437-445.
- [87] Zhao, Y.; Molki, M.; Ohadi, M. M. Heat transfer and pressure drop of CO₂ flow boiling in microchannels. In: *Proceedings of the ASME Heat Transfer Division*, 2000, vol. 2, pp. 243-249.
- [88] Pettersen, J., Vestbøstad, K. Heat transfer and pressure drop for flow of supercritical and subcritical in microchannel tubes. In: *Workshop Proceedings-Selected Issue on CO₂ as Working Fluid in Compression System*, Trondheim, Norway, 2000, pp. 101-114.
- [89] Yun, R.; Kim, Y. Two-phase pressure drop of CO₂ in mini tubes and microchannels. In: *First International Conference on Microchannels and Minichannels*, Rochester, NY, 2003, pp. 507-511.
- [90] Cho, J. M.; Kim, M. S. Experimental studies on the evaporative heat transfer and pressure drop of CO₂ in smooth and micro-fin tubes of the diameters of 5 and 9.52 mm. *Int. J. Refrig.* 2007, vol. 30, 986-994.
- [91] Grauso, S.; Mastrullo, R.; Mauro, A. W.; Vanoli, G. P. Flow boiling of R410A and CO₂ from low to medium reduced pressures in macro channels: Experiments and assessment of prediction methods. *Int. J. Heat Mass Transfer.* 2013, vol. 56, Issues 1–2, 107-118.
- [92] Mastrullo, R.; Mauro, A. W.; Rosato, A.; Vanoli, G. P. Carbon dioxide local heat transfer coefficients during flow boiling in a horizontal circular smooth tube. *Int. J. Heat Mass Transfer.* 2009, vol. 52, Issues 19–20, 4189-4194.
- [93] R. Mastrullo, A.W. Mauro, G.P. Vanoli, Carbon dioxide heat transfer coefficients and pressure drops during flow boiling: Assessment of prediction methods, *Int. J. Refrig.* 2010, vol. 33, 1068–1085.

- [94] Grauso, S., Mastrullo, R., Mauro, A. W., Vanoli, G. P. CO₂ and propane blends: Experiments and assessment of predictive methods for flow boiling in horizontal tubes. *Int. J. Refrig.* 2011, vol. 34, 1026 - 11039
- [95] Wu, J., Koettig, T., Franke, Ch., Helmer, D., Eisel, T., Haug, F., Bremer, J. Investigation of heat transfer and pressure drop of CO₂ two-phase flow in a horizontal minichannel. *Int. J. Heat Mass Transfer.* 2011, vol. 54, Issues 9–10, 154-2162
- [96] Jiang, L, Liu, J., Zhang, L., Liu, Q, Xu, X. A research on the dryout characteristics of CO₂'s flow boiling heat transfer process in mini-channels. *Int. J. Heat Mass Transfer.* 2017, vol. 108, 131 - 142.
- [97] Jiang, L, Liu, J., Zhang, L., Liu, Q, Xu, X. Characteristics of heat transfer for CO₂ flow boiling at low temperature in mini-channel, *Int. J. Heat Mass Transfer*, vol. 108, Part B, 2017, 2120 - 2129.
- [98] Mastrullo, R., Mauro, A. W., Thome, J.R., Toto, Vanoli, G.P. Flow pattern maps for convective boiling of CO₂ and R410A in a horizontal smooth tube: experiments and new correlations analyzing the effect of the reduced pressure. *Int. J. Heat Mass Transfer.* 2012, vol. 55, 1519 - 1528.
- [99] Grauso, S., Mastrullo, R., Mauro, A.W., Vanoli, G.P. Flow boiling of R410A and CO₂ from low to medium reduced pressures in macro channels: Experiments and assessment of prediction methods. *Int. J. Heat Mass Transfer.* 2013, vol. 56, 107–118.
- [100] Mastrullo, R., Mauro, A.W., Thome, J.R., Vanoli, G.P., CO₂ and R410A: Two-phase flow visualizations and flow boiling measurements at medium (0.50) reduced pressure, *Appl. Therm. Eng.* 49 (2012) 2 -8.
- [101] Ozawa, M., Ami, T, Ishihara, I., Umekawa, H., Matsumoto, R., Tanaka, Y., Yamamoto, T., Ueda, Y. Flow pattern and boiling heat transfer of CO₂ in horizontal small-bore tubes, *Int. J. Multiphase Flow* 35 (2009) 699–709.

- [102]Del Col, D. Flow boiling of halogenated refrigerants at high saturation temperature in a horizontal smooth tube, *Exp. Therm. Fluid Sci.* 2010, vol. 34, 234–245.
- [103]Jung, D.S., Mclinden, M., Radermacher, R., Didion, D. A study of flow boiling heat transfer with refrigerant mixtures. *Int. J. Heat Mass Transfer.* 1989, vol. 32,1751– 1764.
- [104]Hihara, E., Tanaka, S. Boiling heat transfer of carbon dioxide in horizontal tubes, In: Proceedings of the 4th IIR Gustav Lorentzen Conference on Natural Working Fluids, 2000, pp. 279–284.
- [105]Revellin, R., Thome, J.R. A new type of diabatic flow pattern map for boiling heat transfer in microchannels, *J. Micromech. Microeng.* 2007, vol, 17, 788-796
- [106]Dang, C., Haraguchi, N., Hihara, E., Flow boiling heat transfer of carbon dioxide inside a small-sized microfin tube, *Int. J. Refrig.* 33 (2010) 655–663.
- [107] Wu, X., Zhu, Y., Tang, Y. New experimental data of CO₂ flow boiling in mini tube with micro fins of zero helix angle. *Int. J. Refrig.* 2015, vol. 59. 281–294
- [108]Jeong, S., Park, D., Evaporative heat transfer of CO₂ in a smooth and a micro-grooved miniature channel tube, *Heat Transfer Eng.* vol. 30, iss. 7 (2009) 582-589
- [109]Zhang, L., Jiang, L., Liu, J., Zhao, Y. Investigation of flow boiling heat transfer characteristics of CO₂ in horizontal mini-tube. *Int. J. Therm. Sci.* 2019, vol.138, 109–115.
- [110]Oh, H-K, Son, C-H, Flow boiling heat transfer and pressure drop characteristics of CO₂ in horizontal tube of 4.57-mm inner diameter. *Appl. Therm. Eng.* 2011, vol. 31, 163-172.
- [111]Yuna, R., Kim, Y. Post-dryout heat transfer characteristics in horizontal mini-tubes and a prediction method for flow boiling of CO₂. *Int. J. Refrig.* 2009, vol. 32, 1085–1091.
- [112]Ducoulombier, M., Colasson, S., Bonjour, J., Haberschill, P. Carbon dioxide flow boiling in a single microchannel – Part I: Pressure drop. *Exp. Therm. Fluid Sci.* 2011, vol. 35, 581–596.
- [113]Ducoulombier, M., Colasson, S., Bonjour, J., Haberschill, P. Carbon dioxide flow boiling in a single microchannel – Part II: Heat transfer, *Exp. Therm. Fluid Sci.* 2011, vol. 35, 597–611.

- [114]Kenia, K., Mazzellib, F., Garimella, S. Experimental investigation of carbon dioxide flow boiling in a single microchannel. *Int. J. Heat Mass Transfer*. 2020, vol. 159, 120100.
- [115]Zhang, L., Jiang, L., Liu, J., Yuan, Y., Zhang, J. Research on pressure drop characteristics of CO₂ flow boiling based on flow pattern in horizontal minichannel. *Heat Mass Transfer*, 2020, vol. 56, 2939–2952.
- [116]Kneer, A., Wirtz, M., Laufer, T., Nestler, B., Barbe, S. Experimental investigations on pressure loss and heat transfer of two phase carbon dioxide flow in a horizontal circular pipe of 0.4 mm diameter. *Int. J. Heat Mass Transfer*. 2018, vol. 119, 828–840.
- [117]Yun, R., Kim, Y. Two-phase pressure drop of CO₂ in mini tubes and microchannels: *Microscale Thermophysical Eng.* 2004, vol. 8, 259-270.
- [118]Chisholm, D. Pressure gradients due to friction during the flow of evaporating two-phase mixtures in smooth tubes and channels. *Int. J. Heat Mass Transfer*. 1973, vol. 16, 347–358.
- [119]Friedel, L. Improved friction drop correlations for horizontal and vertical two-phase pipe flow. In: *European Two-phase Flow Group Meeting*, Ispra, Italy, 1979, paper E2.
- [120]Grønnerud, R. Investigation of liquid hold-up, flow-resistance and heat transfer in circulation type of evaporators, part IV: two-phase flow resistance in boiling refrigerants. In: *Annexe 1972-1, Bull. De l'Inst. Du Froid*, 1979.
- [121]Müller-Steinhagen, H., Heck, K. A simple friction pressure drop correlation for two-phase flow in pipes. *Chem. Eng. Process*. 1986, vol. 20, 297-308.
- [122]Ciccitti, A.; Lombardi, C.; Silvestri, M. ; Soldaini, G.; Zavattarelli, R. Two-phase cooling experiments—pressure drop, heat transfer and burnout measurements. *Energia Nucleare*. 1960, vol. 7, no. 6, 407–425.
- [123]Zhao, X., Bansal, P. Critical review of flow boiling heat transfer of CO₂–lubricant mixtures. *Int. J. Heat and Mass Transfer*. 2009, vol. 52, 870–879.

- [124] Kaneko, M., Ikeda, H.; Kawaguchi, Y.; Suto, H.; Schweim, E. The development of capped-PAG refrigeration lubricants for automotive A/C with CO₂ and HFC152a. In: *SAE 5th Alternate Refrigerant Systems Symposium*, 2004.
- [125] Ikeda, H., Kaneko, M., Tokiai, T., Yoshii, A., Suto, H. Evaluation of lubricants for carbon dioxide automobile A/C system. In: *SAE 7th Alternate Refrigerant System Symposium*, 2006.
- [126] Katsuta, M.; Takeo, N.; Kamimura, I.; Mukaiyama, H. A study on the evaporator of refrigerant cycle: characteristics of heat transfer coefficient and pressure drop on mixing CO₂ and oil (PAG). *Transaction. of the Japan Society of Refrigerating and Air conditioning Engineers (JSRAE)*. 2003, vol. 20, no. 3, 397-405.
- [127] Katsuta, M.; Kinpara, H.; Aoyagi, T.; Yagi, S.; Kamimura, I.; Mukaiyama, H. The effect of oil contamination on evaporator heat transfer characteristics of CO₂ refrigeration cycle. In: *40th National Heat Transfer Symposium of Japan*, 2003.
- [128] Katsuta, M., Kinpara, H., Yagi, S., Mukaiyama, H. The effect of oil contamination on evaporator heat transfer characteristics of CO₂ refrigeration cycle. *Transaction of the Japan Society of Refrigerating and Air conditioning Engineers (JSRAE)*. 2004, vol. 21, no. 3, 275-283.
- [129] Gao, L., Honda, T. Effects of lubricant oil on boiling heat transfer of CO₂ inside a horizontal smooth tube. In: *42nd National Heat Transfer Symposium of Japan*, 2005, pp. 261-270.
- [130] Gao, L., Honda, T. An experimental study on flow boiling heat transfer of carbon dioxide and oil mixtures inside a horizontal smooth tube. In: *IIR 2005 Vicenza Conference-Thermophysical Properties and Transfer Processes of Refrigerants*, Vicenza, Italy, 2005, pp. 237-243.
- [131] Koyama, S., Lee, S. M., Ito, D., Kuwahara, K., Ogawa, H. Experimental study on flow boiling of pure CO₂ and CO₂-oil mixture inside horizontal smooth and micro-fin tubes. In: *6th IIR-Gustav Lorentzen Conference, Glasgow, UK, Aug. 29 –Sept. 1st, 2004*.
- [132] Koyama, S., Ito, D., Lee, S. M., Kuwahara, K.; Saeki, C., Ogawa, H. Experimental investigation for flow boiling of pure CO₂ and CO₂-oil mixture inside horizontal copper tubes. In: *IIR 2005*

Vicenza Conference-Thermophysical Properties and Transfer Processes of Refrigerants,
Vicenza, Italy, 2005.

- [133] Siegismund, V., Kauffeld, M. Influence of lubricant oil on CO₂ heat transfer in minichannel tubes. In: *6th IIR-Gustav Lorentzen Conference, Glasgow, UK, Aug. 29 –Sept. 1st, 2004*.
- [134] Zhao, Y., Molki, M., Ohadi, M. M., Fanca, F. H. R., Radermacher, R., Cho, K. Flow boiling of CO₂ with miscible oil in microchannels. *ASHRAE Trans.* 2002, vol. 108, Part I, 135-144.
- [135] Bandarrra Filho, E. P., Cheng, L.; Thome, J. R. Flow boiling characteristics and flow pattern visualization of refrigerant/lubricant oil mixtures. 2009, *Int. J. Refrig.* vol. 32, 185-2002.
- [136] Cheng, L., Cheng, T. Comparison of six typical correlations for upward flow boiling heat transfer with kerosene in a vertical smooth tube, 2000, *Heat Transfer Eng.* vol. 21, no. 5, 27-34.
- [137] Gao, L., Watanabe Y., Honda, T. CO₂ Flow boiling in small diameter smooth and micro-fin tubes. *Journal of JSME.* 2011, vol. 11, SS66-SS72.
- [138] Kim, S., Hrnjak, P.S., Effect of oil on flow boiling heat transfer and flow patterns of CO₂ in 11.2 mm horizontal smooth and enhanced tube, Proceedings of the International Refrigeration and Air Conditioning Conference at Purdue (2012), July 16-19
- [139] Patiño J., Llopis, R., Sánchez, D; Sanz-Kock, C.; Cabello, R.; Torrella, E. A comparative analysis of a CO₂ evaporator model using experimental heat transfer correlations and a flow pattern map. *Int. J. Heat Mass Transfer.* 2014, vol. 71. 361-375.
- [140] Wetzal, M., Dietrich, B., Wetzal, T. Influence of oil on heat transfer and pressure drop during flow boiling of CO₂ at low temperatures. *Exp. Therm. Fluid Sci.* 2014, vol. 59, 202-212.
- [141] Marcinichen, J. B., Thome, J. R., Pereira, R. H. Working fluid charge reduction, part 1: CO₂ fin tube evaporator designed for light commercial appliances utilizing flow pattern based phenomenological prediction models. *Int. J. Refrig.* 2016, vol. 65, 258–272.
- [142] Yamaguchi, S., Kato, D., Saito, K.; Kawai, S. Development and validation of static simulation model for CO₂ heat pump. *Int. J. Heat Mass Transfer.* 2011, vol. 54, 1986-1906.

- [143] Wang, S., Tuo, H., Cao, F., Xing, Z., Experimental investigation on air-source transcritical CO₂ heat pump water heater system at a fixed water inlet temperature. *Int. J. Refrig.* 2013, vol. 36, 701-716.
- [144] Faria, R. N., Nunes, R. O., Koury, R. N. N.; Machado, L. Dynamic modeling study for a solar evaporator with expansion valve assembly of a transcritical CO₂ heat pump. *Int. J. Refrig.* 2016, vol. 64, 203–213.
- [145] Yang, D., Song, Y., Cao, F.; Jin, L., Wang, X. Theoretical and experimental investigation of a combined R134a and transcritical CO₂ heat pump for space heating. *Int. J. Refrig.* 2016, vol. 72, 156-170.
- [146] Tong, Z., Liu, X. H., Li, Z., Jiang, Yi. Experimental study on the effect of fill ratio on an R744 two-phase thermosyphon loop. *Appl. Therm. Eng.* 2016, vol. 99, 302–312.
- [147] Yoshioka, S., Kim, H. Y., Kasai, K. Heat transfer performance and oil behaviour for R744 with PAG oil in air-cooled heat exchanger, in: *8th IIR Gustav Lorentzen Conference on Natural Working Fluids*, 2008, pp. 389–396.
- [148] Pruess, K. Enhanced geothermal systems (EGS) using CO₂ as working fluid—A novel approach for generating renewable energy with simultaneous sequestration of carbon. *Geothermics*, 2006, vol. 35, 351–367
- [149] Pruess, K. On production behavior of enhanced geothermal systems with CO₂ as working fluid, *Energy Conv. Manag.* 2008, vol. 49, 1446–1454
- [150] Daguin, J., Arndt, K., Bertl, W., Noite, J., Petagna, P., Postema, H., Tropea, P., Verlaat, B. Evaporative CO₂ cooling system for the upgrade of the CMS pixel detector at CERN, 13th InterSociety Conference on Thermal and Thermomechanical Phenomena in Electronic Systems, 30 May-1 June 2012. <https://ieeexplore.ieee.org/abstract/document/6231499>
- [151] Bergman, T. L., Lavine, A., Incropera, F. P., DeWitt, D. P. *Fundamentals of Heat and Mass Transfer*. 8th Edition, John Wiley, 2017.
- [152] Thulukkanam, K. *Heat Exchanger Design Handbook*, 2nd Edition, CRC Press, 2013.

- [153] Yun, R., Chasik, Park, Y. Numerical analysis on a microchannel evaporator designed for CO₂ air-conditioning systems. *Appl. Therm. Eng.* 2007, vol. 27, 1320–1326.
- [154] Yokoyama, R., Shimizua, T., Ito, K, Takemura, K. Influence of ambient temperatures on performance of a CO₂ heat pump water heating system. *Energy.* 2007, vol. 32, 388–398
- [155] Silvia Minetto, Theoretical and experimental analysis of a CO₂ heat pump for domestic hot water, *Int. J. Refrig.* 2011, vol. 34, 742-751.
- [156] Sarkar, J., Bhattacharyya, S., Ram Gopal, M., Simulation of a transcritical CO₂ heat pump cycle for simultaneous cooling and heating applications. *Int. J. Refrig.* 2006, vol. 29, 735–743.
- [157] Lin, K.-H., Kuo, C.-S., Hsieh, W.-D., Wang, C.-C. Modeling and simulation of the transcritical CO₂ heat pump system. *Int. J. Refrig.* 2013, vol. 36, 2048–2064.
- [158] Byrne, P., Miriel, J., Lenat, Y. Design and simulation of a heat pump for simultaneous heating and cooling using HFC or CO₂ as a working fluid, *Int. J. Refrig.* 2009, vol. 32, 1711-1723.
- [159] Kim, M., Bullard, C.W., Development of a microchannel evaporator model for a CO₂ air-conditioning, *Energy.* 2001, vol. 26, 931–948.
- [160] Jin, J., Chen, J., Chen, Z. Development and validation of a microchannel evaporator model for a CO₂. *Appl. Therm. Eng.* 2011, vol. 31, 137-146
- [161] ASHRAE, ANSI/ASHRAE Standard 15-2013. “Safety Standard for Refrigeration Systems”. American Society of Heating Refrigerating and Air-Conditioning Engineers. Atlanta, GA, 2013.

List of table captions

Table 1. Selected experimental studies on flow boiling heat transfer of CO₂ inside channels for the analysis of the mechanisms and comparison before 2007 [31].

Table 2. Selected experimental studies on flow boiling heat transfer and two phase flow of CO₂ inside macro- and micro-channels after 2007.

Table 3. Selected research on evaluation of flow boiling heat transfer correlations and development of new flow boiling heat transfer correlations.

Table 4. Flow pattern visualizations for CO₂ at a reduced pressure of 0.50, different mass fluxes and vapor qualities compared to flow pattern predictions according the Cheng et al. [30] flow pattern map for CO₂ by Mastrullo et al. [100].

Table 5. Selected studies of CO₂ two phase pressure drop inside channels before 2007 [30].

Table 6. Selected research on evaluation of two phase frictional pressure drop correlations and development of new pressure drop correlations.

Table 7. Statistical analysis of the two-phase frictional pressure drop predictions for all data points in the database in table 6 [30].

List of figure captions

Figure 1. Pressure-enthalpy diagrams of CO₂ and R134a in automobile air-conditioning systems.

Figure 2. Schematic of ammonia-CO₂ in secondary loop of an indirect refrigeration system.

Figure 3. Comparison of the definitions of macro- and micro-scale channels for CO₂ according to Kandlikar and Grande [15] and Kandlikar [16] and the Confinement number Co [20].

Figure 4 Simulated results by the Cheng et al. model [30, 31] using various physical properties of EES, REFPROP 6.01, REFPROP 7.0 and REFPROP 9.1: (a) Simulated flow boiling heat transfer coefficients of CO₂ versus vapor quality at the indicated working conditions; (b) The corresponding flow pattern map (I represents intermittent flow, A represents annular flow, D represents dryout region, M represents mist flow, SW represents stratified-wavy flow, S represents stratified flow and SLUG represents slug flow): the vertical dash line represents the I to A transition using EES, REFPROP 7.0 and REFPROP 9.1 and the solid vertical line represents the I to A transition using REFPROP 6.01.

Figure 5 Simulated results using physical properties of REFPROP 6.01 and REFPROP 9.1: (a) Comparison of simulated flow boiling heat transfer coefficients and the experimental data of [90] at the indicated working conditions; (b) The corresponding flow pattern map: the dash lines represent flow pattern transitions using the physical properties of REFPROP 9.1 and the solid lines represent the flow pattern transitions using the physical properties of REFPROP 6.01.

Figure 6 Simulated results using physical properties of REFPROP 6.01 and REFPROP 9.1: (a) Comparison of simulated flow boiling heat transfer coefficients and the experimental data of [91] at the indicated working conditions; (b) The corresponding flow pattern map: the dash lines represent flow pattern transitions using the physical properties of REFPROP 9.1 and the solid lines represent the flow pattern transitions using the physical properties of REFPROP 6.01.

Figure 7 Simulated results using physical properties of REFPROP 6.01 and REFPROP 9.1: (a) Comparison of simulated flow boiling heat transfer coefficients and the experimental data of [91] at the indicated working conditions; (b) The corresponding flow pattern map: the dash lines represent

flow pattern transitions using the physical properties of REFPROP 9.1 and the solid lines represent the flow pattern transitions using the physical properties of REFPROP 6.01.

Figure 8 Simulated results using physical properties of REFPROP 6.01 and REFPROP 9.1: (a) Comparison of simulated flow boiling heat transfer coefficients and the experimental data of [95] at the indicated working conditions; (b) The corresponding flow pattern map: the dash lines represent flow pattern transitions using the physical properties of REFPROP 9.1 and the solid lines represent the flow pattern transitions using the physical properties of REFPROP 6.01.

Figure 9 Simulated results using physical properties of REFPROP 6.01 and REFPROP 9.1: (a) Comparison of simulated flow boiling heat transfer coefficients and the experimental data of [114] at the indicated working conditions; (b) The corresponding flow pattern map: the dash lines represent flow pattern transitions using the physical properties of REFPROP 9.1 and the solid lines represent the flow pattern transitions using the physical properties of REFPROP 6.01.

Figure 10. The experimental heat transfer coefficients in two different studies showing two opposite trends with the increase of saturation temperature. Arrow 1 showing the trend of the experimental flow boiling heat transfer coefficients (solid symbols) of Pettersen [32]: $D_h = 0.8$ mm, $G = 280$ kg/m²s and $q = 10$ W/m² at 0, 20 and 25 °C. Arrow 2 showing the trend of the experimental flow boiling heat transfer coefficients (hollow symbols) of Yoon et al. [36]: $D_h = 7.53$ mm, $G = 318$ kg/m²s and $q = 16.4$ W/m² at 5, 15 and 20 °C.

Figure 11. The experimental flow boiling heat transfer coefficients in the same study showing different results with a very little change of hydraulic diameters from 1.53 mm to 1.54 mm. Solid symbols showing the experimental flow boiling heat transfer coefficients of Yun et al. [37]: $D_h = 1.53$ mm, $G = 300$ kg/m²s, $T_{sat} = 5$ °C and $q = 20$ W/m². Hollow symbols showing the experimental flow boiling heat transfer coefficients of Yun et al. al. [37]: $D_h = 1.54$ mm, $G = 300$ kg/m²s, $T_{sat} = 5$ °C and $q = 20$ W/m².

Figure 12. Observed flow pattern of CO₂, $D_p = 2.0$ mm by Ozawa et al. [101].

Figure 13. Observed flow pattern of CO₂, $D_p = 1.0$ mm by Ozawa et al. [101].

Fig. 14. Flow pattern map of CO₂ in 2-mm tube Solid lines: Cheng et al. [30] (dashed lines: Revellin and Thome [105], IB: isolated bubble, CB: coalescing bubble, A: annular flow) by Ozawa et al. [101].

Figure 15. Dynamic progress of CO₂ bubble growth in a microchannel with a diameter of 1.5 mm by Zhang et al. [115].

Figure 16. Simulation of flow boiling model and flow pattern map or 3 mm channel at the conditions: $q = 20 \text{ kW/m}^2$, $T_{sat} = 10^\circ\text{C}$ and $G = 390 \text{ kg/m}^2\text{s}$ with indicated value at $x = 0.70$. [83].

Figure 17. Comparison of the Cheng et al. mechanistic flow boiling heat transfer model with the experimental database before dryout by Zhang et al. [109].

Figure 18. Comparison of the Cheng et al. mechanistic flow boiling heat transfer model with the experimental database after dryout by Zhang et al. [109].

Figure 19. Comparison of the several leading methods to the experimental data of Bredesen et al. [40] at the experimental conditions: $G = 400 \text{ kg/m}^2\text{s}$, $T_{sat} = -10^\circ\text{C}$, $D_{eq} = 7 \text{ mm}$ and $q = 6 \text{ kW/m}^2$; 1 - The Moreno-Quibén and Thome model [63, 64]; 2 - The Friedel method [92]; 3 - The Grönnerud method [93]; 4 - The Müller-Steighagen-Heck method [94]; 5 - The Chisholm method [91].

Figure 20. (a) Comparison of the new CO₂ pressure drop model to the experimental data of Bredesen et al. [40] at the experimental conditions: $G = 400 \text{ kg/m}^2\text{s}$, $T_{sat} = -10^\circ\text{C}$, $D_{eq} = 7 \text{ mm}$ and $q = 3 \text{ kW/m}^2$; (b) The corresponding flow pattern map at the same experimental condition as that in (a) (I represents intermittent flow, A represents annular flow, D represents dryout region, M represents mist flow, S represents stratified flow and SW represents stratified-wavy flow).

Figure 21. Comparison of the predicted frictional pressure gradients by the new model to the entire database (74.7% of the data are predicted within $\pm 30\%$) [30]: 1–Bredesen et al. [40], 2–Yun and Kim

[89, 117], 3– Pettersen [32] and Pettersen and VestbØstad [88] and 4–Zhao et al. [86, 87] (Note that 2, 3 and 4 are the data of micro-channels).

Figure 22. Experimental two phase frictional pressure drop data for CO₂ flow boiling at $T_{\text{sat}} = -10\text{ }^{\circ}\text{C}$, $G = 400\text{ kg}/(\text{m}^2\text{s})$ and $q = 7.5\text{ kW}/\text{m}^2$ and the corresponding flow patterns on the Cheng et al. flow pattern map by Zhang et al. [115].

Fig. 23. Comparison between the CO₂ flow boiling heat transfer coefficients in micro-fin tube and those in smooth tube: (a) Experimental results in small channel with 2 mm diameter by Dang et al. [104]; (b) Experimental results in large channel with 11.2 mm diameter by Kim and Hrnjak [138].

Figure 24. The effect of the oil on two-phase pressure drop [126]: $G = 400\text{ kg}/\text{m}^2\text{s}$, $q = 10\text{ kW}/\text{m}^2$; (b) $G = 800\text{ kg}/\text{m}^2\text{s}$, $q = 10\text{ kW}/\text{m}^2$.

Figure 25. The effect of oil on heat transfer coefficient [127, 128]: $T_{\text{sat}} = 10\text{ }^{\circ}\text{C}$, $G = 390\text{ kg}/\text{m}^2\text{s}$, $q = 20\text{ kW}/\text{m}^2$.

Figure 26. The effect of oil on heat transfer coefficient [134] ($T_{\text{sat}} = 10\text{ }^{\circ}\text{C}$, $G = 300\text{ kg}/\text{m}^2\text{s}$, $q = 11\text{ kW}/\text{m}^2$).

Figure 27. The oil effect (mass concentration from 0 to 5%) on the evaporation heat transfer coefficient of R134a in a horizontal tube (Simulated results by the flow pattern based heat transfer model of Wojtan et al. [48, 49]): $G = 300\text{ kg}/\text{m}^2\text{s}$, $T_{\text{sat}} = 10\text{ }^{\circ}\text{C}$, $D = 13.84\text{ mm}$ and $q = 7.5\text{ kW}/\text{m}^2$.

Figure 28. The oil effect (mass concentration from 0 to 5%) on two-phase frictional pressure gradient of R134a in a horizontal tube for flow regimes before dryout region (The two-phase frictional pressure gradients were calculated using the flow pattern based two-phase pressure drop model of Moreno-Quiben and Thome [63, 64] for pure R134a with a correction factor of oil effect on two-phase pressure drop): $G = 300\text{ kg}/\text{m}^2\text{s}$, $T_{\text{sat}} = 10\text{ }^{\circ}\text{C}$, $D = 13.84\text{ mm}$ and $q = 7.5\text{ kW}/\text{m}^2$.

Figure 29. Schematic diagram of multi-microchannel evaporators for simulation of electronic chips cooling by Cheng and Thome [11].

Figure 30. Comparisons of simulation results of base temperature of CO₂ and R236fa at the indicated conditions for chips cooling by Cheng and Thome [11].

Figure 31. The oil effect (mass concentration from 0 to 3%) on the evaporation heat transfer coefficient of CO₂ in the evaporator tube using the Cheng et al. heat transfer model [141].

Figure 32. The oil effect (mass concentration from 0 to 3%) on the two-phase frictional pressure gradient of CO₂ in the evaporator tube using the Cheng et al. pressure drop model [149].

Figure 33. The outlet air temperature per row for the plain fin and the wavy fin evaporators (fin type effect) [149].

Figure 34. System flow diagram of CO₂ heat pump and measuring points in the study of Yamaguchi et al. [142].

Figure 35. Schematic illustration of evaporator model segment discretization: (a) evaporator geometry, (b) jth segment. [160]

Table 1. Selected experimental studies on flow boiling heat transfer of CO₂ inside channels for the analysis of the mechanisms and comparison before 2007 [31].

Literature	Channel configuration		Equivalent diameter D_{eq} (mm)	Saturation temperature T_{sat} (°C)	Mass flux G (kg/m ² s)	Heat flux Q (kW/m ²)
Knudsen and Jensen [41]	Single tube	circular	10.06	-28	80	8 - 13
Yun et al. [33]	Single tube	circular	6	5, 10	170 - 340	10 - 20
Yoon et al. [36]	Single tube	circular	7.53	0 - 20	318	12.5 - 18.6
Koyama et al. [38]	Single tube,	circular stainless steel.	1.8	0.26 - 10.88	250 - 260	32.06
Pettersen [32]	Multi-channel with 25 channels	25 circular channels	0.8	0 - 25	190 - 570	5 - 20
Yun et al. [34]	Multi-channels with rectangular channels.	rectangular channels.	1.52 (1.14)* -1.81 (1.54)*	5	200 - 400	10 - 20
Gao and Honda [95, 96]	Single tube	circular	3	-7 - 10	236 - 1179	10 - 21
Tanaka et al. [83]	Single tube	circular	1	15	360	9 - 36
Hihara [35]	Single tube	circular	1	15	720 - 1440	9 - 36
Shinmura et al. [84]	Multi-channel with channels	25 circular channels	0.6	5.83	400	10 - 20
Zhao et al. [86, 87]	Multi-channel with channels	triangular channels	1.15 (0.86)*	10	300	11
Yun et al. [89, 115]	Single channel	circular	0.98 - 2	5 - 10	1000 - 1500	7.2 - 46
Jeong et al. [85]	Multi-channel with channels	rectangular channels	2.3 (2)*	0 - 10	450 - 750	4 - 12

Table 2. Selected experimental studies on flow boiling heat transfer and two phase flow of CO₂ inside macro- and micro-channels after 2007.

Literature	Channel configuration and orientation	Channel diameter D (mm)	Saturation temperature T_{sat} (°C)	Mass flux G (kg/m ² s)	Heat flux Q (kW/m ²)	Main Contents
Cho and Kim [90]	Single circular smooth and microfin tube	5 mm and 9.52 mm	0 - 20	212 - 656	6 - 20	Heat transfer and pressure drop
Zhao and Bansal [46]	Single tube	4.57	-24.3 to 40.6	149 - 250	12- 20.9	Heat transfer
Zhao and Bansal [42]	Single tube	4.57	-29.9 to 28.6	139.5- 230.9	12- 20.9	Heat transfer
Park and Hrnjak [43]	Single tube	6.1	-15, -30	100 - 400	5, 15	Heat transfer and pressure drop
Grauso et al. [91]	Single tube	6.1	0.26 - 10.88	250 - 260	5, 20	Heat transfer
Oh and Son [110]	Single tube/horizontal	4.57	0 - 40	200 - 1000	10 - 40	Heat transfer and pressure drop
Grauso et al. [99]	Single tube/horizontal	6	7, 12	150 - 500	5, 20	Heat transfer
Mastrullo et al. [93]	Single tube	6	7, 12	150 - 500	5, 20	Heat transfer and pressure drop
Mastrullo et al. [92]	Single tube	6	7	200, 350	5, 20	Heat transfer
Choi et al. [45]	Single tube	1.5, 3	10	200 -600	10 - 40	Heat transfer
Ozawa et al. [101]	Single tube	1, 2, 3	6 – 6.7 MPa	300	25	Heat transfer and flow regime
Ducoulombier et al. [113]	Single tube	0.529	-10, -5, 0	200-1299	10, 30	Heat transfer and pressure drop
Wu et al. [99]	Single tube	1.42	-40 to 0	300 - 600	7.5-29.8	Heat transfer and pressure drop
Jiang et al. [97]	Single channel	0.6, 1.5	-40 - 0	300 - 600	2 - 35	Heat transfer
Jiang et al. [94]	Single channel	1, 2	-10 - 15	50 - 1350	7.5 - 30	Heat transfer and dryout
Zhang et al. [109]	Single channel	0.6, 1.5	-40 - 0	200 - 1500	5 - 35	Heat transfer
Zhang et al. [115]	Single channel	01.5	-40 - 0	50 - 600	7.5 - 30	Flow regime and pressure drop
Keniar et al. [114]	Single channel	1.55	15, 22	100 - 500	15 - 72	Heat transfer

Table 3. Selected research on evaluation of flow boiling heat transfer correlations and development of new flow boiling heat transfer correlations.

Literature	Evaluation of heat transfer correlations	Development of heat transfer correlations
Cho and Kim [90]	5 correlations were evaluated. None can predict the data. The Gungor and Winterton [55] and the Liu and Winterton [57] correlations underpredict the data.	No
Zhao and Bansal [46]	7 correlations were evaluated and the Liu and Winterton [57] correlation gives the best prediction.	No
Zhao and Bansal [42]	7 correlations were evaluated with measured database. No correlation predicts the database satisfactorily.	No
Park and Hrnjak [45]	5 correlations were evaluated and the Gungor and Winterton [55] correlation gives the best prediction.	No
Grauso et al. [94]	7 correlations were evaluated and the Cheng et al. [31] heat transfer model gives the best prediction.	No
Oh and Son [111]	correlations were evaluated. The Cheng et al. [31] heat transfer model gives the best prediction.	No
Mastrullo et al. [95]	10 correlations were evaluated. The Cheng et al. [31] heat transfer model gives the best prediction.	No
Choi et al. [46]	7 correlations were evaluated and none of them can predict the data favorably.	Modified the Chen correlation based on their experimental data.
Ducoulombier et al. [123]	15 correlations were evaluated. The correlation of Hihara and Tanaka [16] allowing 74% of the data to be predicted within $\pm 20\%$	Developed prediction methods in three regimes: type I, type II and type III. The Cheng et al. [31] nucleate boiling correlation is used for type I.
Wu et al. [95]	The Cheng et al. [31] model was evaluated with the experimental data. The onset of dryout (peak) is predicted by the model to start at lower vapor quality compared to the presented experimental data. The reason for this difference can be explained by the determination of the onset of dryout during the scanning process of the two-phase region.	No
Jiang et al. [97]	The Cheng et al. [31] model was evaluated with the experimental data. The model predicts the data well before the dryout. The accuracy of prediction is not ideal after the dryout and there is no suitable model to predict heat transfer coefficient after the dryout.	No
Jiang et al. [96]	The Fang et al. [59] correlation was evaluated with the experimental data. The correlation predicts the data well.	No
Jiang et al. [115]	The Cheng et al. [31] model was evaluated with the experimental data. It predicts the data well before the dryout. The accuracy of prediction is not ideal after the dryout.	No
Keniar et al. [114]	12 correlations were evaluated. The Cooper [78] and Cheng et al. [31] nucleate pool boiling correlations give the best prediction.	Developed a suppression factor for the Cheng et al. [31] nucleate boiling correlation based on their own data.

Table 4. Flow pattern visualizations for CO₂ at a reduced pressure of 0.50, different mass fluxes and vapor qualities compared to flow pattern predictions according the Cheng et al. [30] flow pattern map for CO₂ by Mastrullo et al. [100].

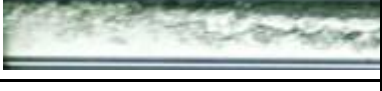
G [kg/(m ² s)]	Vapor quality	Two-phase flow picture	Flow pattern interpretation	Flow pattern prediction
200	0.19		Slug	Transition slug/annular
200	0.85		Dry-out	Dry-out
350	0.18		Slug	Transition slug/annular
350	0.48		Stratified-wavy and asymmetric annular	Annular
350	0.82		Annular	Dry-out

Table 5 Statistical analysis of the predicted flow boiling heat transfer coefficients by the Cheng et al. [30, 31] heat transfer model.

Data used for comparison	Data points	Percentage of predicted points within $\pm 30\%$	Mean error $ \bar{\xi} $	Standard deviation σ
All new data points after 2007	3609	56.9%	40.2%	58.7%
All new data points without the dryout and mist flow data after 2007	2146	81.3%	20.2%	27.2 %
New dryout and mist flow data points after 2007.	1463	21%	71.7%	60.1%
The whole data points including the new data points after 2007 and in [31].	4733	61.7%	67. %	74.5 %
The whole data points without dryout and mist flow data including the new data points after 2007 and in [31]	2919	81.8%	20.3%	29.1%
All dryout and mist including the new data points after 2007 and in [31]	1814	29.3%	70.4 %	107.7%

$$\sigma = \sqrt{\frac{1}{N} \sum_{i=1}^N (\xi_i - \bar{\xi})^2}; \quad |\bar{\xi}| = \frac{1}{N} \sum_{i=1}^N |\xi_i|; \quad \xi_i = \frac{\text{Predicted} - \text{Measured}}{\text{Measured}}$$

Table 6. Selected studies of CO₂ two phase pressure drop inside channels before 2007 [30].

Literature	Channel configuration	Equivalent diameter D_{eq} (mm)	Saturation temperature T_{sat} (°C)	Mass flux G (kg/m²s)	Heat flux Q (kW/m²)
Bredesen et al. [40]	Single circular tube	7	-25 - 5	200 - 400	3 - 9
Pettersen [32]	Multi-channel with 25 circular channels	0.8	0 - 20	190- 380	10
Pettersen and Vestbøstad [88]	Multi-channel with 25 circular channels	0.8	0 - 20	200- 400	10
Zhao et al. [86, 87]	Multi triangular channels	1.15 (0.86)*	10	300	11
Yun and Kim [89, 117]	Multi rectangular channels	1.74 (1.53)*	5	200 - 400	15

Table 7. Statistical analysis of the two-phase frictional pressure drop predictions for all data points in the database in table 6 [30].

Models and data used for comparison	Data points	Percentage of predicted points within $\pm 30\%$	Mean error $\bar{\xi}$	Standard deviation σ
Chisholm model [118]	387	56.1 %	48.6 %	73.8 %
Friedel model [119]	387	71.1 %	30.9 %	55.8 %
Grönnerud model [120]	387	30.2 %	75 %	113.1 %
Müller-Steinhagen and Heck model [121]	387	55.8 %	33.3 %	44.3 %
Modified Chisholm by Yoon et al. model [36]	387	47 %	34.7%	93.7%
Moreno Quibén and Thome model [63, 64]	387	42.4 %	50.1%%	90.6%
New model [30]	387	74.7 %	28.6%	44.3%

$$\sigma = \sqrt{\frac{1}{N} \sum_{i=1}^N (\xi_i - \bar{\xi})^2}; \quad |\bar{\xi}| = \frac{1}{N} \sum_{i=1}^N |\xi_i|; \quad \xi_i = \frac{\text{Predicted} - \text{Measured}}{\text{Measured}}$$

Table 8. Selected research on evaluation of two phase frictional pressure drop correlations and development of new pressure drop correlations.

Literature	Evaluation of pressure drop correlations	Development of pressure correlations	of drop
Cho and Kim [90]	1 correlation was evaluated and does not work.	No.	
Park and Hrnjak [43]	6 correlations were evaluated. The Muller-Steinhagen and Heck [121], and Friedel [119] correlations can predict most of the measured pressure drop.	No.	
Mastrullo et al. [93]	6 correlations were evaluated. The Friedel [119] correlation gives the best prediction overall. For mass fluxes lower than 350 kg/m ² s, the Muller-Steinhagen and Heck correlation captures the experimental trends. For vapor qualities higher than 50% and mass flux near 350 kg/m ² s, the most accurate predictions were given by the Cheng et al. [28] model. The Muller-Steinhagen and Heck [121] correlation gives the best predictions of the vapor quality corresponding to the peak value.	No	
Choi et al. [48]	12 correlations were evaluated and all over predicted the data.	No.	
Ducoulombier et al. [112]	21 correlations were evaluated The Muller-Steinhagen and Heck [121], and Friedel [119] correlations give the best prediction.	Modified the homogenous and Lockhart–Martinelli methods based on own data.	
Jiang et al. [115]	The Cheng et al. [30] model was evaluated with the experimental data. The model predicts the data and capture the trends.	No	
Wu et al. [95]	The Cheng et al. [30] model was evaluated with the experimental data. The maximum experimental frictional pressure drop is determined in the dryout region which derives from the flow partner map.	A modified friction factor in mist flow based on the experimental data has been proposed. The modified model of the two-phase flow frictional pressure drop predicts the experimental data well for all flow regimes.	

Table 9 Statistical analysis of the predicted results for the experimental diabatic two phase frictional pressure drop in table 8

Data used for comparison	Data points	Percentage of predicted points within $\pm 30\%$	Mean error $ \bar{\xi} $	Standard deviation σ
All new data points [91, 93, 108]	463	40.8%	53.4%	64.2%
All new data points without the dryout and mist flow data [91, 93, 108]	287	62.7%	27.3%	34.2%
New dryout and mist flow data points [91, 93, 108]	176	4.6%	96.4%	43%
All data points including new data points and in previous data	850	56.2%	45.5 %	66 %
All data points without the dryout and mist flow data	599	68.9%	25.3%	30.1%
All dryout and mist flow data points including previous data	251	25.6%	82.4 %	35.6%

$$\sigma = \sqrt{\frac{1}{N} \sum_{i=1}^N (\xi_i - \bar{\xi})^2} ; |\bar{\xi}| = \frac{1}{N} \sum_{i=1}^N |\xi_i| ; \xi_i = \frac{Predicted - Measured}{Measured}$$

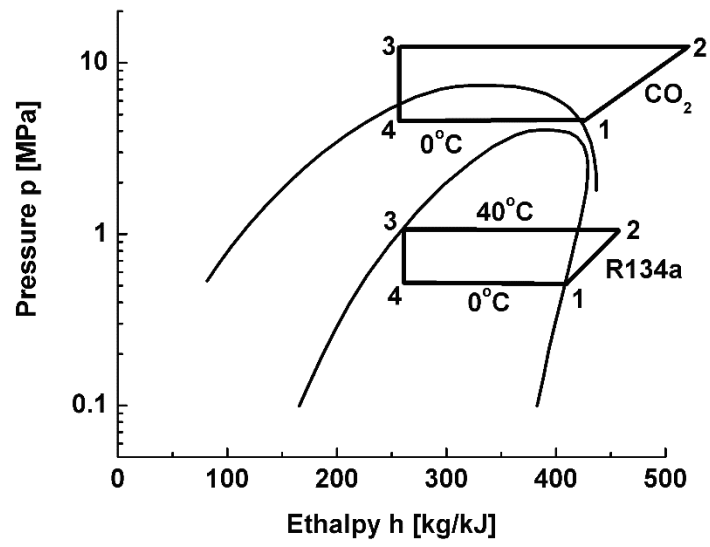


Figure 1. Pressure-enthalpy diagrams of CO_2 and R134a in automobile air-conditioning systems.

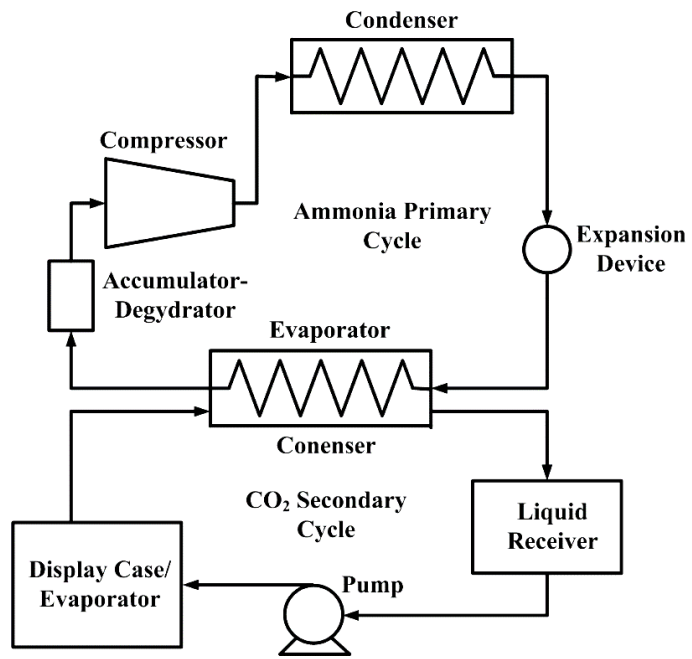


Figure 2. Schematic of ammonia-CO₂ in secondary loop of an indirect refrigeration system.

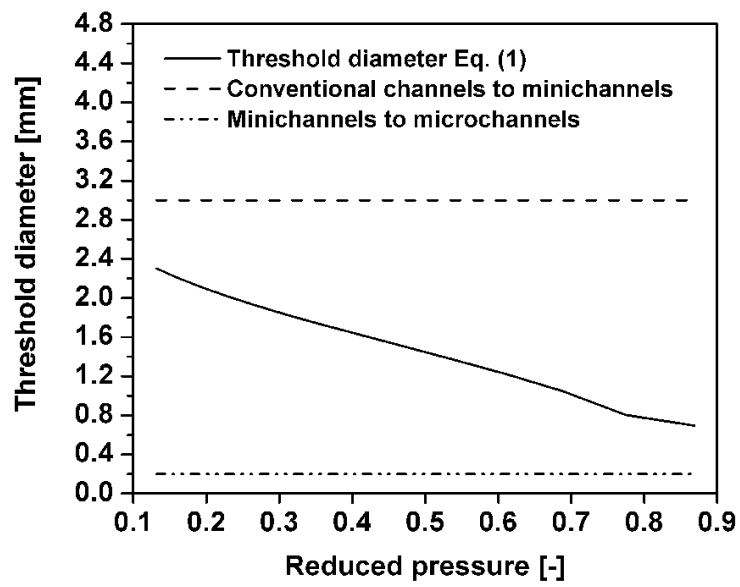


Figure 3. Comparison of the definitions of macro- and micro-scale channels for CO₂ according to Kandlikar and Grande [15] and Kandlikar [16] and the Confinement number Co [20].

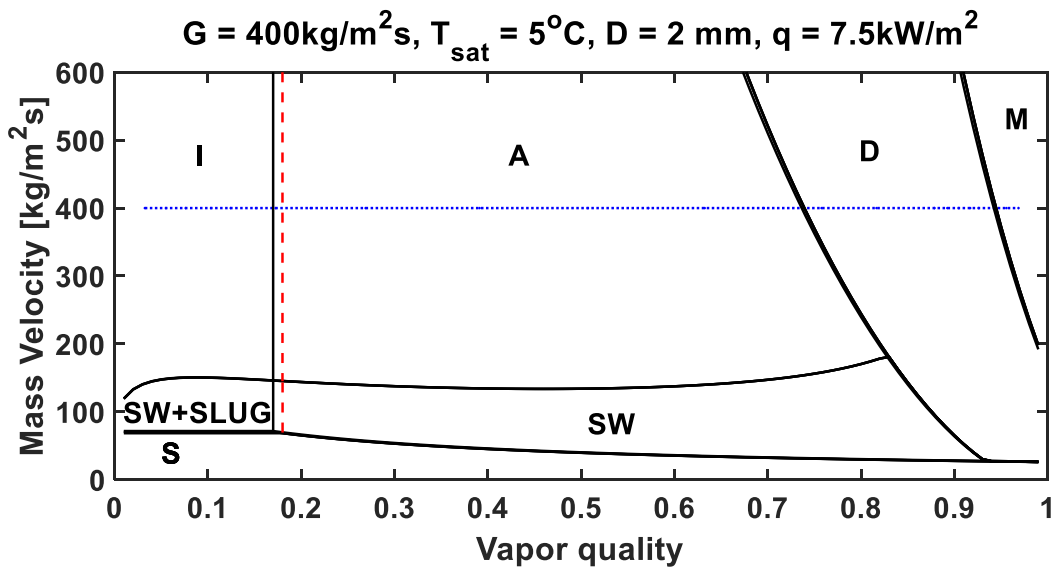
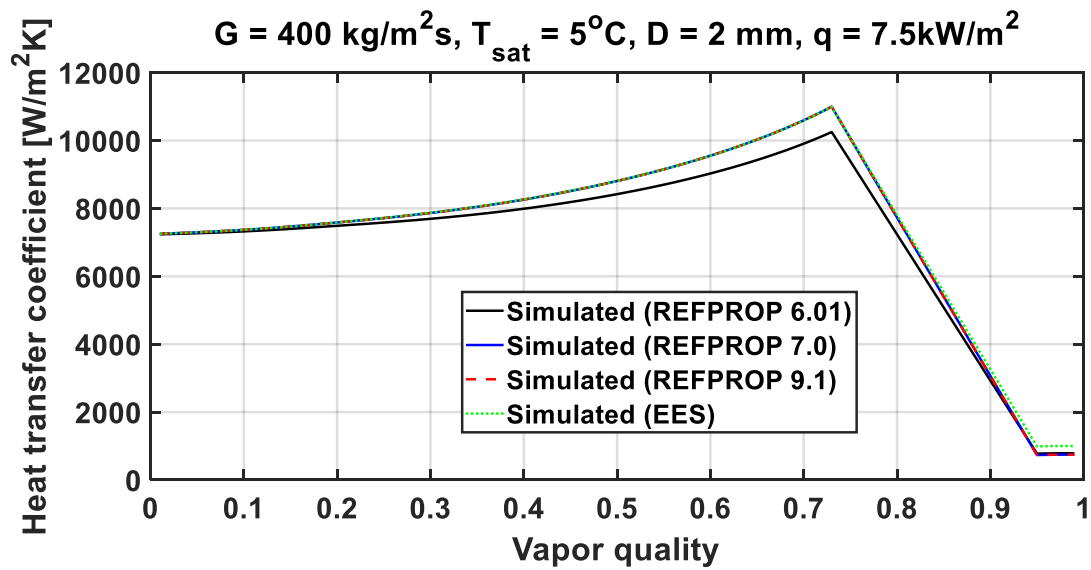


Figure 4 Simulated results by the Cheng et al. model [30, 31] using various physical properties of EES, REFPROP 6.01, REFPROP 7.0 and REFPROP 9.1: (a) Simulated flow boiling heat transfer coefficients of CO₂ versus vapor quality at the indicated working conditions; (b) The corresponding flow pattern map (I represents intermittent flow, A represents annular flow, D represents dryout region, M represents mist flow, SW represents stratified-wavy flow, S represents stratified flow and SLUG represents slug flow): the vertical dash line represents the I to A transition using EES, REFPROP 7.0 and REFPROP 9.1 and the solid vertical line represents the I to A transition using REFPROP 6.01.

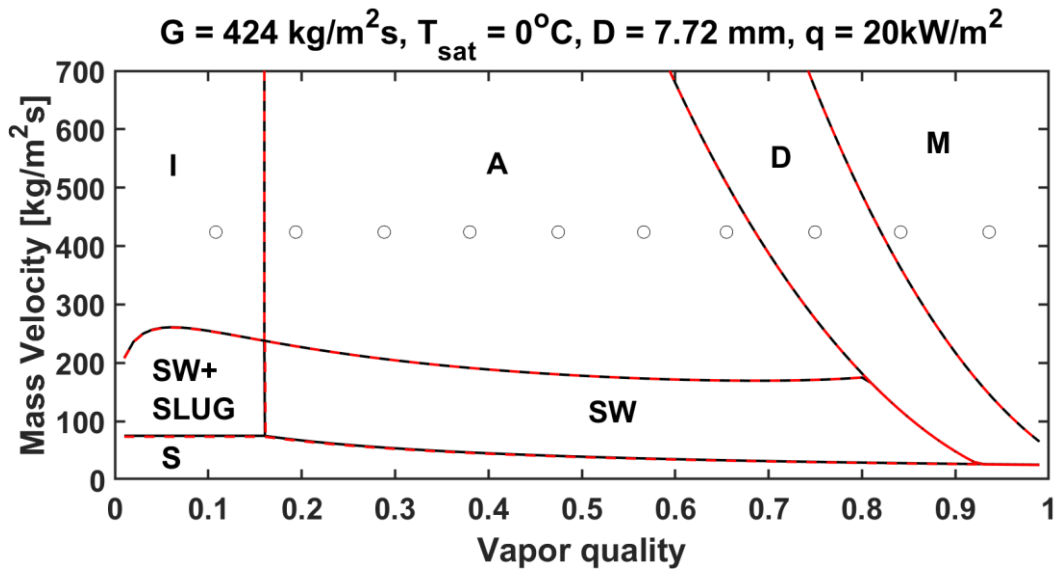
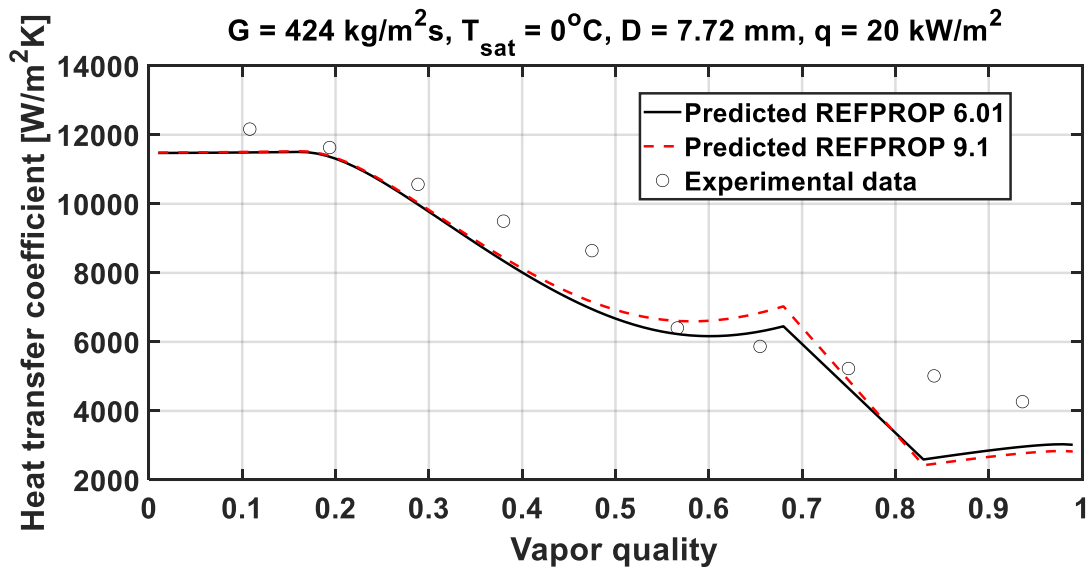


Figure 5 Simulated results using physical properties of REFPROP 6.01 and REFPROP 9.1: (a) Comparison of simulated flow boiling heat transfer coefficients and the experimental data of [90] at the indicated working conditions; (b) The corresponding flow pattern map: the dash lines represent flow pattern transitions using the physical properties of REFPROP 9.1 and the solid lines represent the flow pattern transitions using the physical properties of REFPROP 6.01.

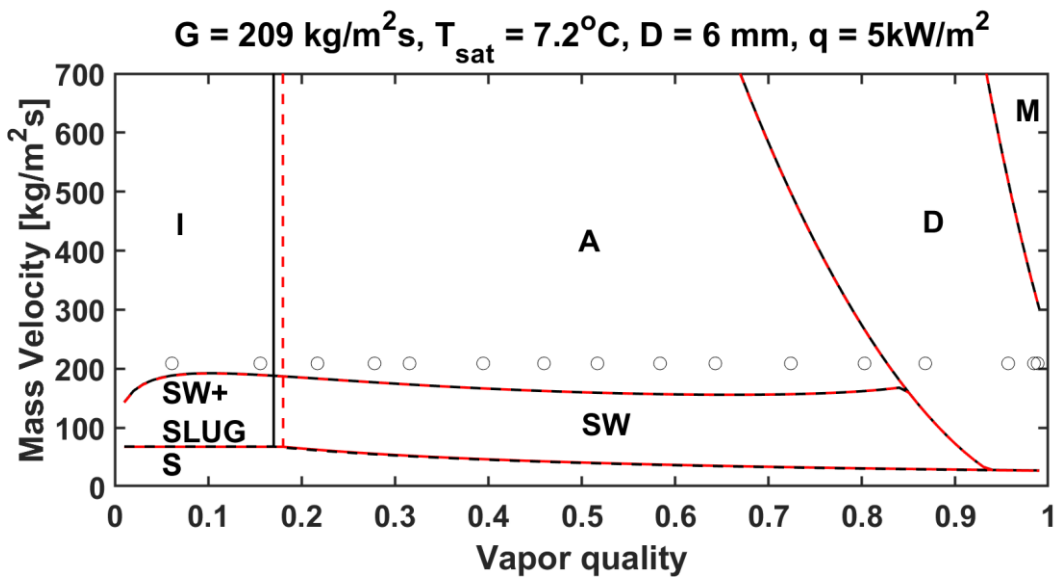
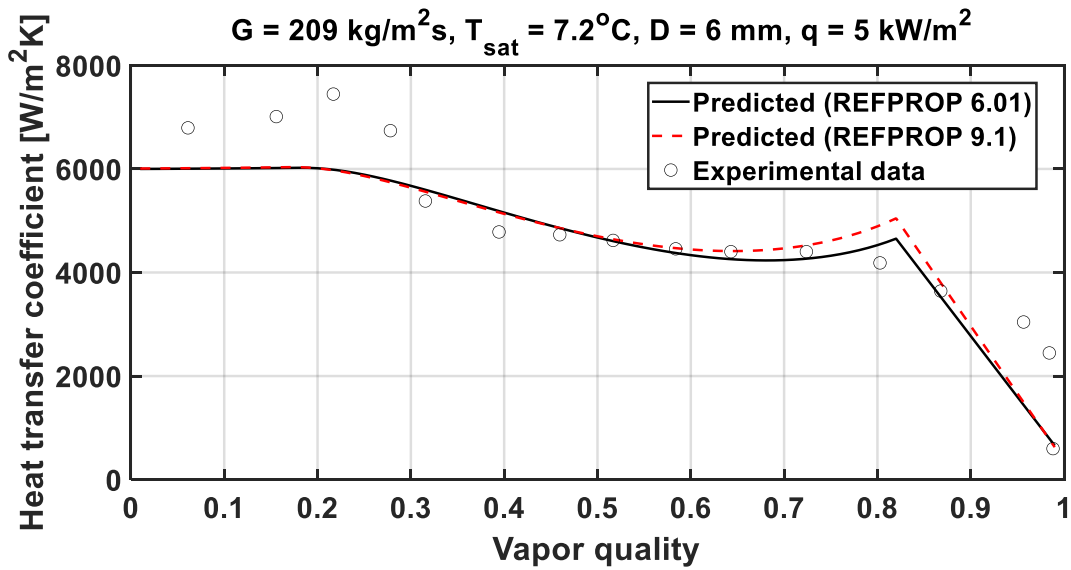


Figure 6 Simulated results using physical properties of REFPROP 6.01 and REFPROP 9.1: (a) Comparison of simulated flow boiling heat transfer coefficients and the experimental data of [91] at the indicated working conditions; (b) The corresponding flow pattern map: the dash lines represent flow pattern transitions using the physical properties of REFPROP 9.1 and the solid lines represent the flow pattern transitions using the physical properties of REFPROP 6.01.

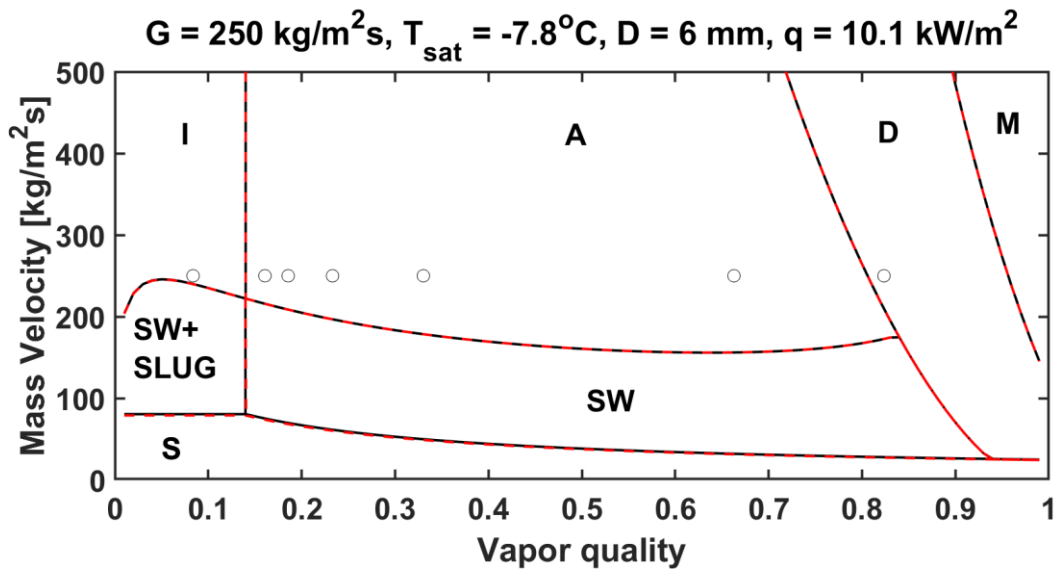
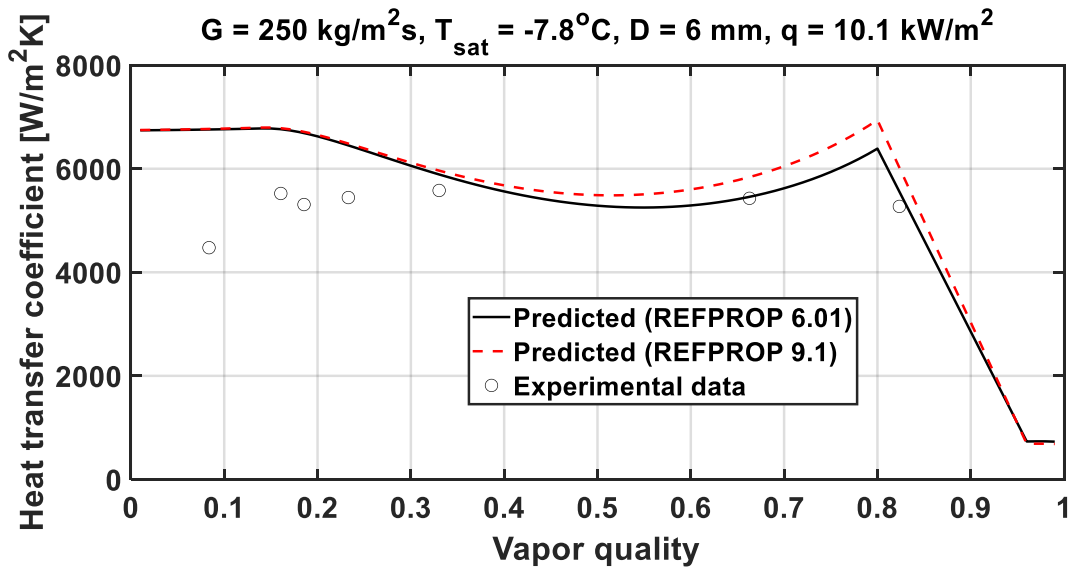


Figure 7 Simulated results using physical properties of REFPROP 6.01 and REFPROP 9.1: (a) Comparison of simulated flow boiling heat transfer coefficients and the experimental data of [91] at the indicated working conditions; (b) The corresponding flow pattern map: the dash lines represent flow pattern transitions using the physical properties of REFPROP 9.1 and the solid lines represent the flow pattern transitions using the physical properties of REFPROP 6.01.

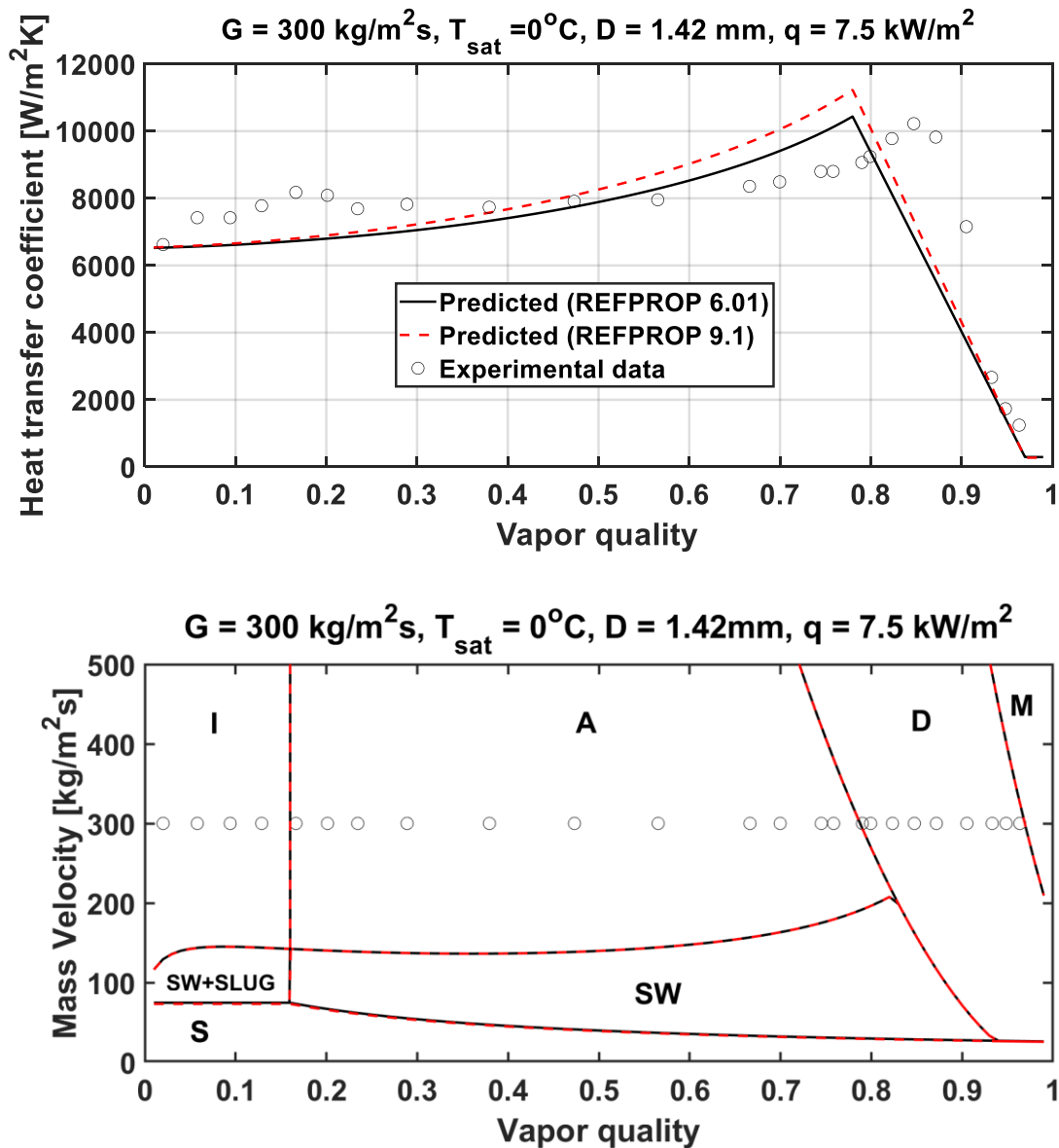


Figure 8 Simulated results using physical properties of REFPROP 6.01 and REFPROP 9.1: (a) Comparison of simulated flow boiling heat transfer coefficients and the experimental data of [95] at the indicated working conditions; (b) The corresponding flow pattern map: the dash lines represent flow pattern transitions using the physical properties of REFPROP 9.1 and the solid lines represent the flow pattern transitions using the physical properties of REFPROP 6.01.

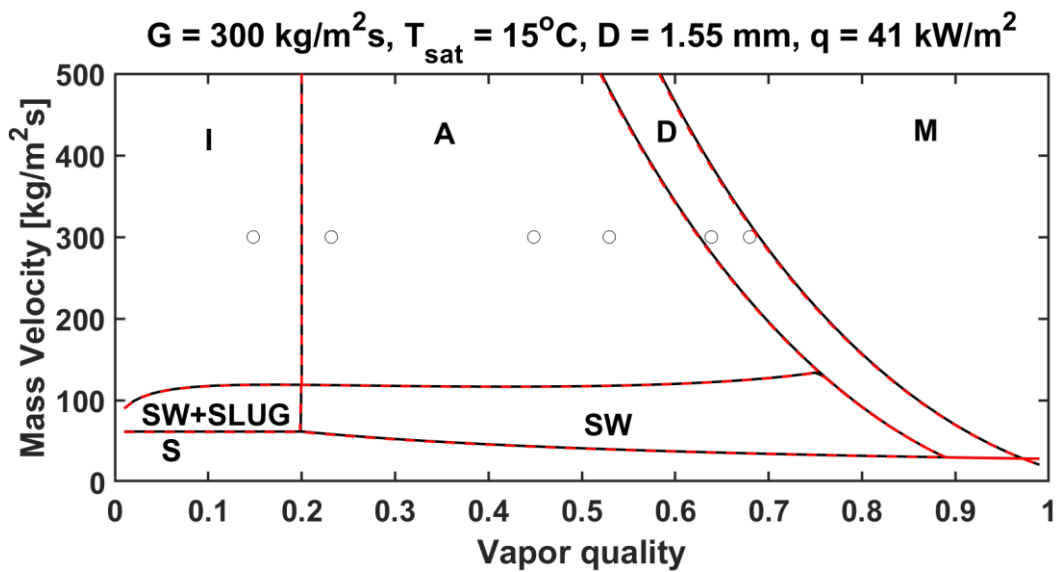
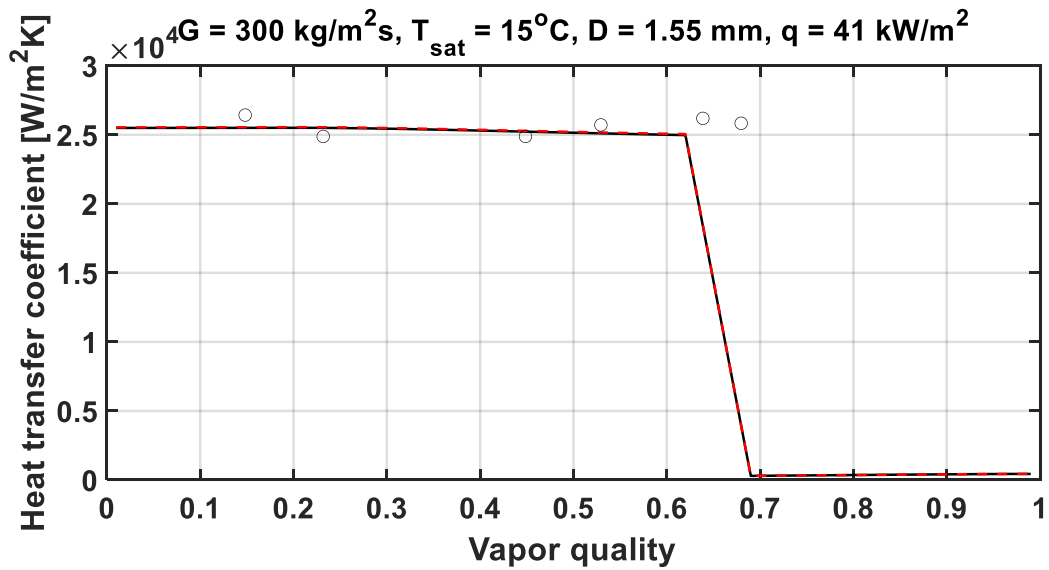


Figure 9 Simulated results using physical properties of REFPROP 6.01 and REFPROP 9.1: (a) Comparison of simulated flow boiling heat transfer coefficients and the experimental data of [114] at the indicated working conditions; (b) The corresponding flow pattern map: the dash lines represent flow pattern transitions using the physical properties of REFPROP 9.1 and the solid lines represent the flow pattern transitions using the physical properties of REFPROP 6.01.

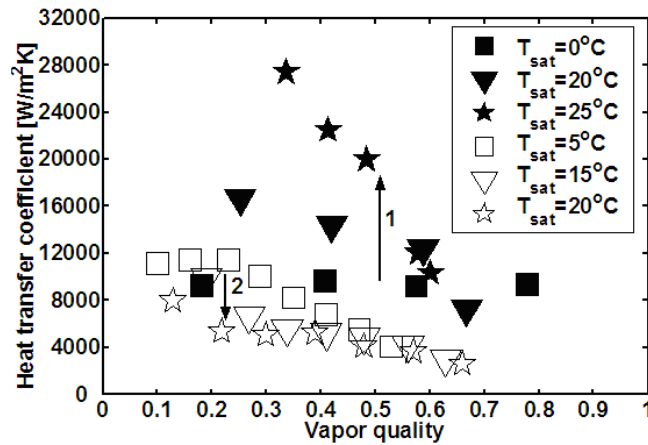


Figure 10. The experimental heat transfer coefficients in two different studies showing two opposite trends with the increase of saturation temperature. Arrow 1 showing the trend of the experimental flow boiling heat transfer coefficients (solid symbols) of Pettersen [32]: $D_h = 0.8$ mm, $G = 280$ kg/m²s and $q = 10$ W/m² at 0, 20 and 25 °C. Arrow 2 showing the trend of the experimental flow boiling heat transfer coefficients (hollow symbols) of Yoon et al. [36]: $D_h = 7.53$ mm, $G = 318$ kg/m²s and $q = 16.4$ W/m² at 5, 15 and 20 °C.

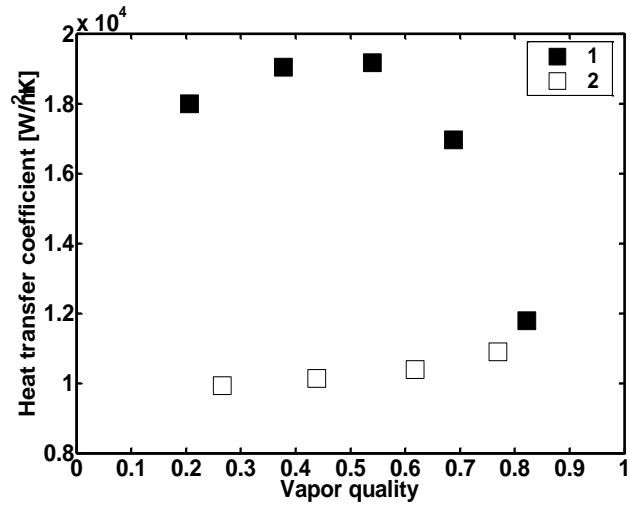


Figure 11. The experimental flow boiling heat transfer coefficients in the same study showing different results with a very little change of hydraulic diameters from 1.53 mm to 1.54 mm. Solid symbols showing the experimental flow boiling heat transfer coefficients of Yun et al. [37]: $D_h = 1.53$ mm, $G = 300$ kg/m²s, $T_{sat} = 5$ °C and $q = 20$ W/m². Hollow symbols showing the experimental flow boiling heat transfer coefficients of Yun et al. al. [37]: $D_h = 1.54$ mm, $G = 300$ kg/m²s, $T_{sat} = 5$ °C and $q = 20$ W/m².

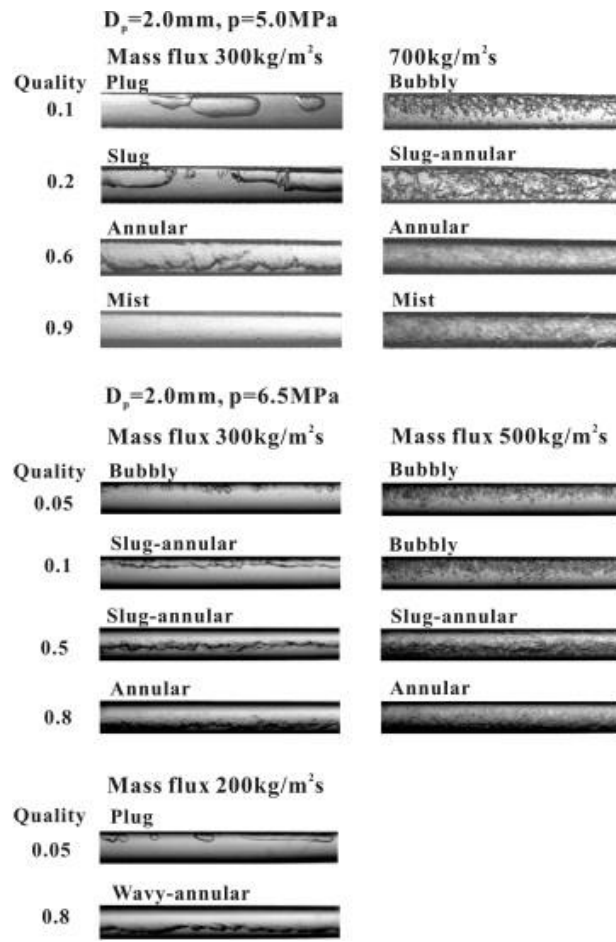


Figure 12. Observed flow pattern of CO₂ in a channel with a diameter of 2 mm by Ozawa et al. [101].

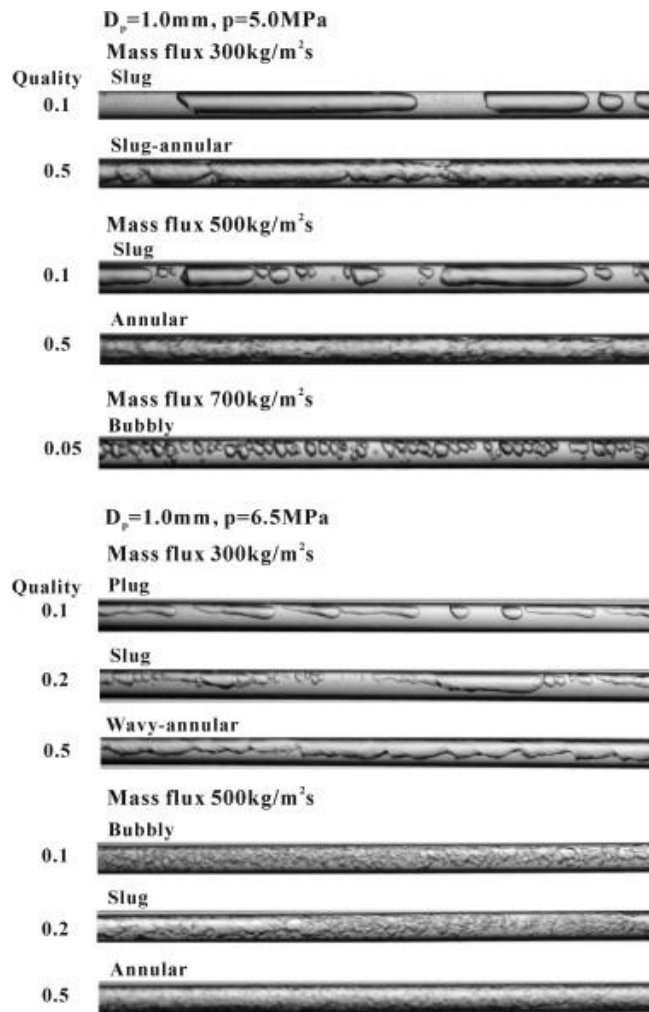


Figure 13. Observed flow pattern of CO_2 in a channel with a diameter of 1 mm by Ozawa et al. [101].

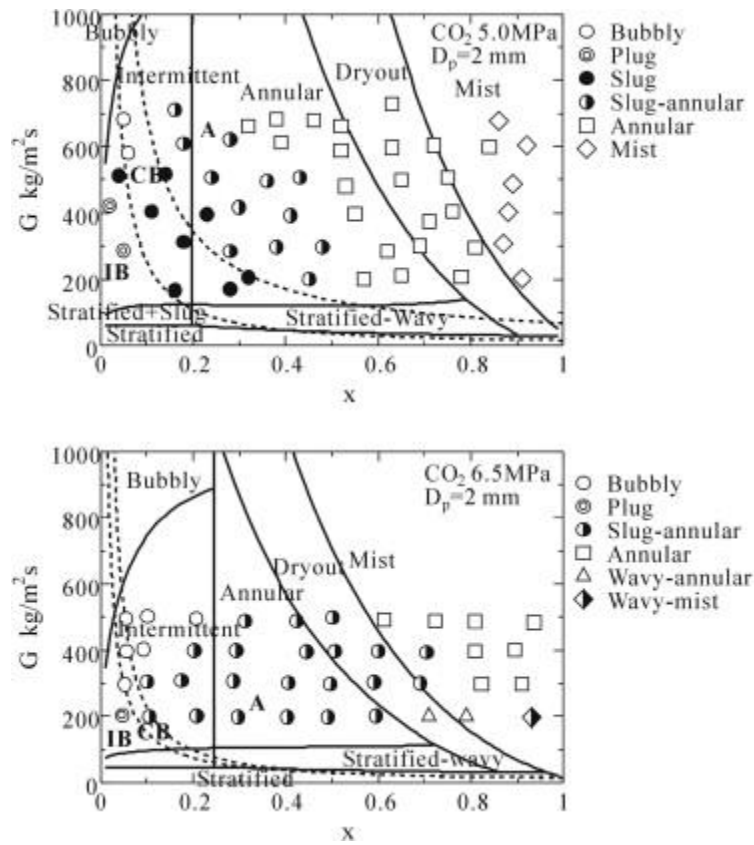


Figure 14. Flow pattern map of CO₂ in 2-mm tube Solid lines: Cheng et al. [30] (dashed lines: Revellin and Thome [105], IB: isolated bubble, CB: coalescing bubble, A: annular flow) by Ozawa et al. [101].

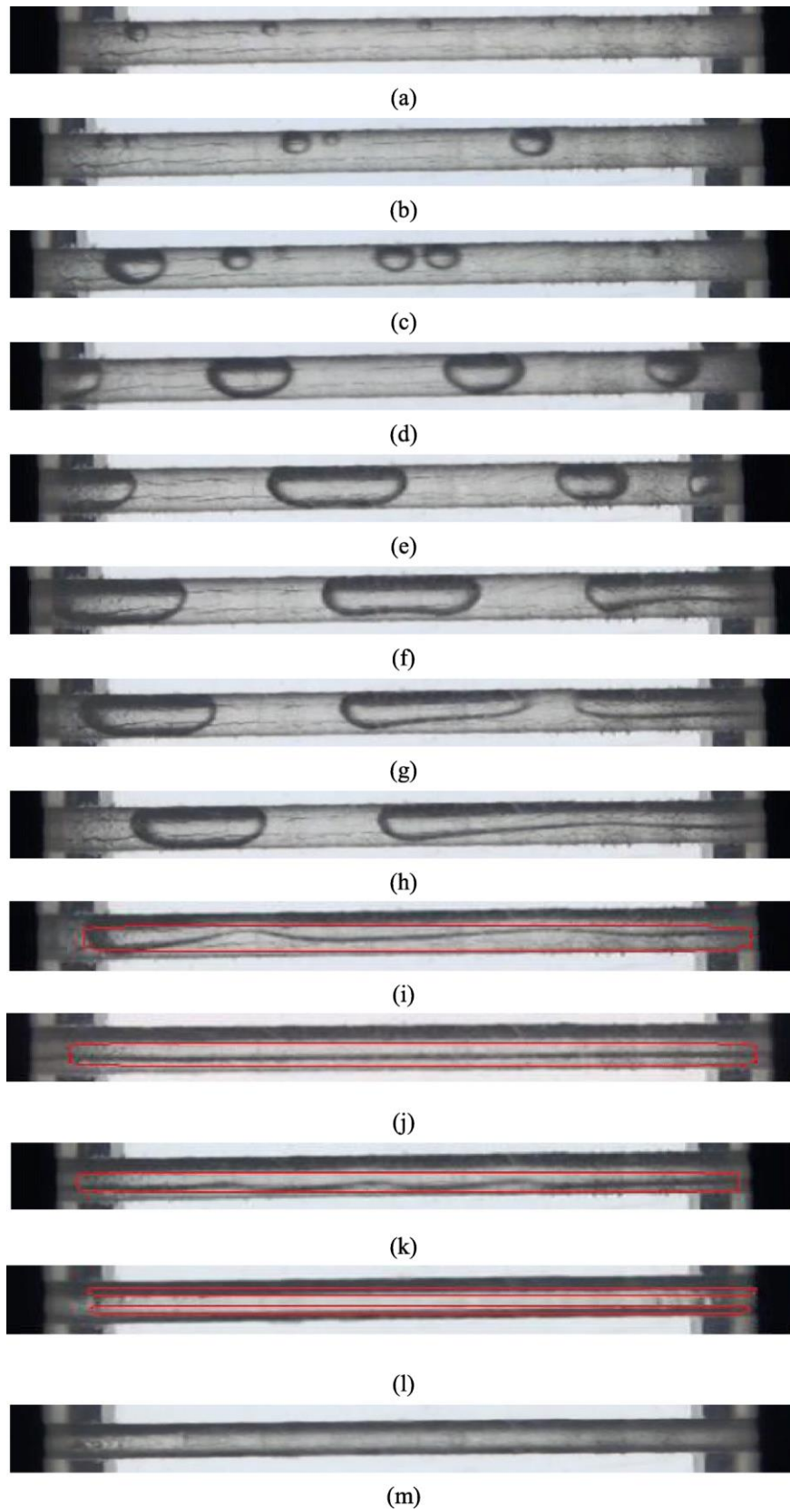


Figure 15. Dynamic progress of CO₂ bubble growth in a microchannel with a diameter of 1.5 mm by Zhang et al. [115].

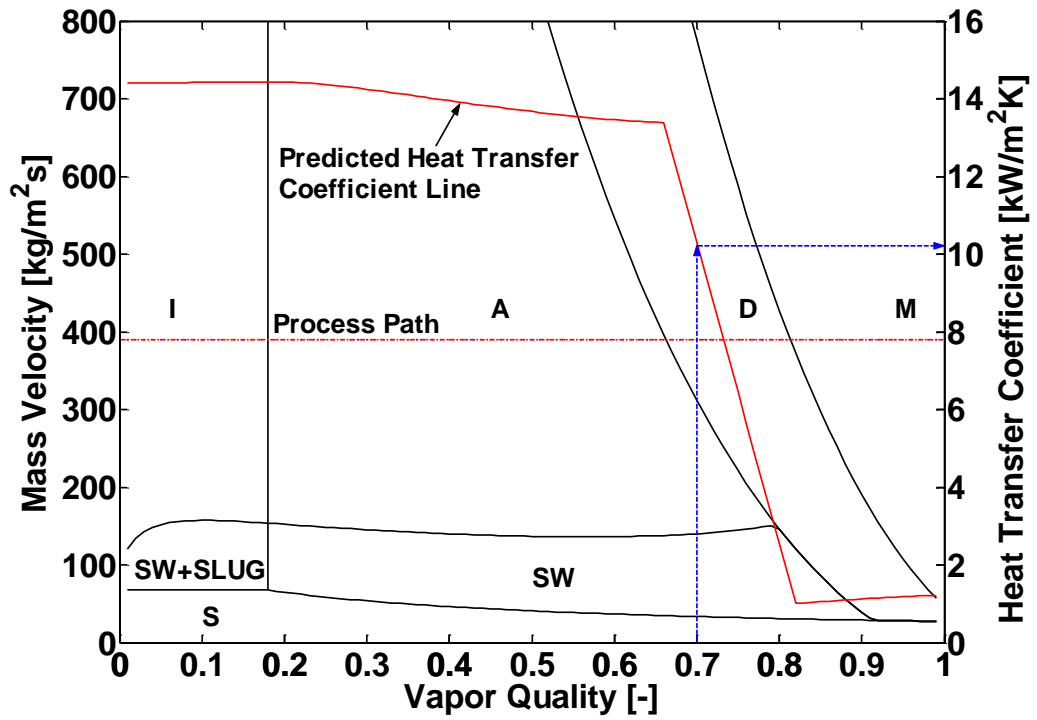


Figure 16. Simulation of flow boiling model and flow pattern map or 3 mm channel at the conditions: $q = 20 \text{ kW/m}^2$, $T_{sat} = 10^\circ\text{C}$ and $G = 390 \text{ kg/m}^2\text{s}$ with indicated value at $x = 0.70$. [83].

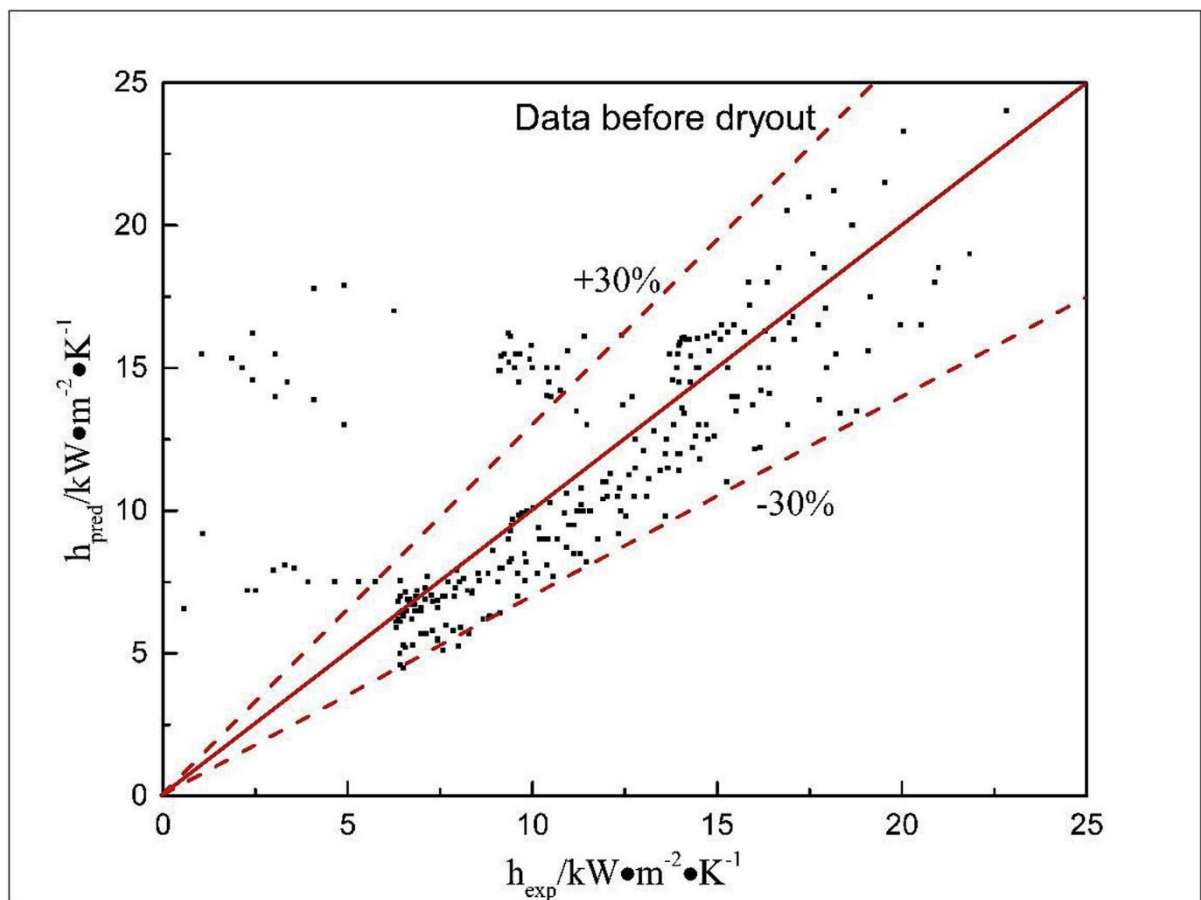


Figure 17. Comparison of the Cheng et al. mechanistic flow boiling heat transfer model with the experimental database before dryout by Zhang et al. [109].

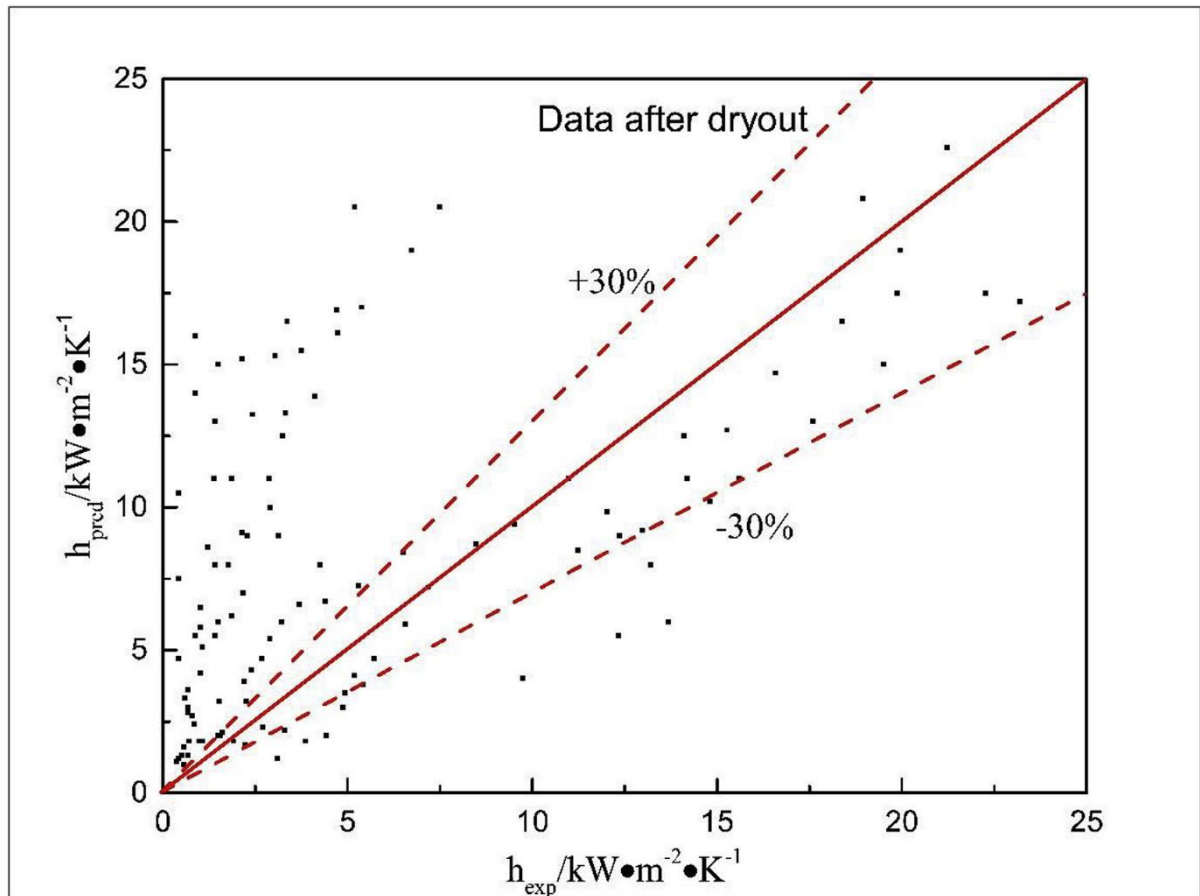


Figure 18. Comparison of the Cheng et al. mechanistic flow boiling heat transfer model with the experimental database after dryout by Zhang et al. [109].

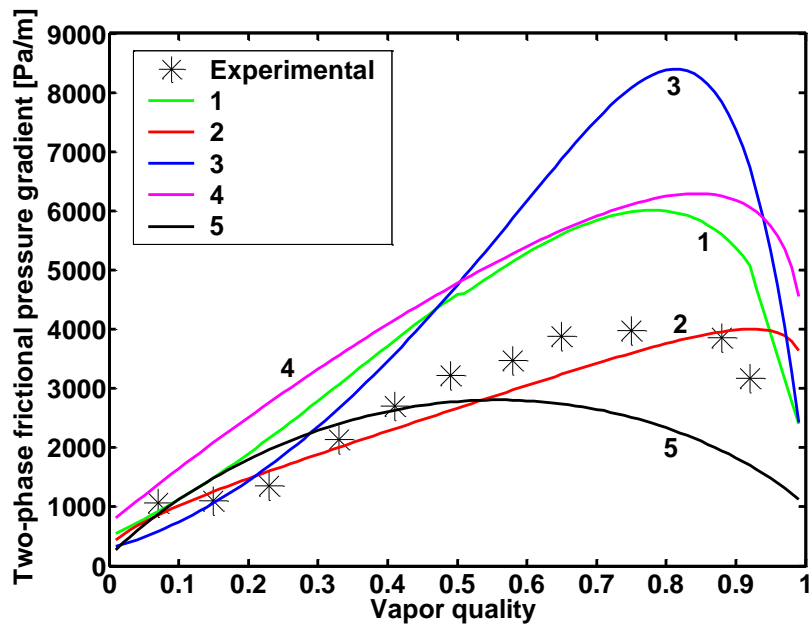
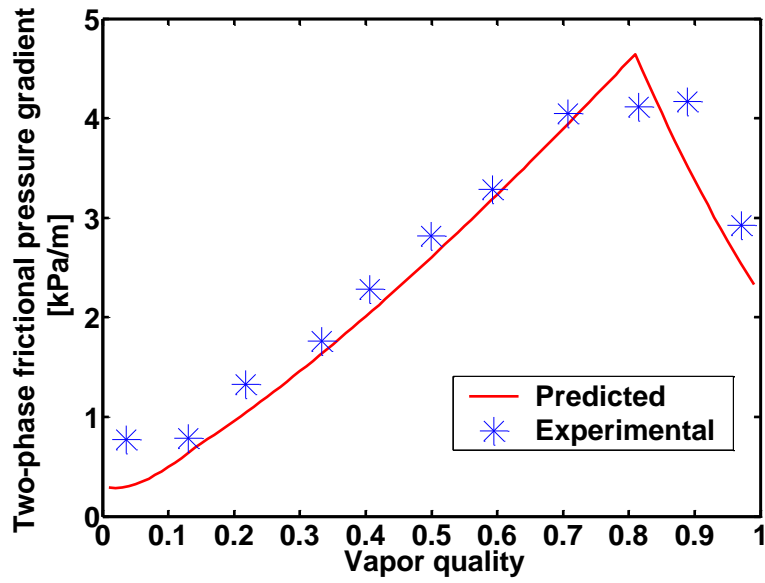
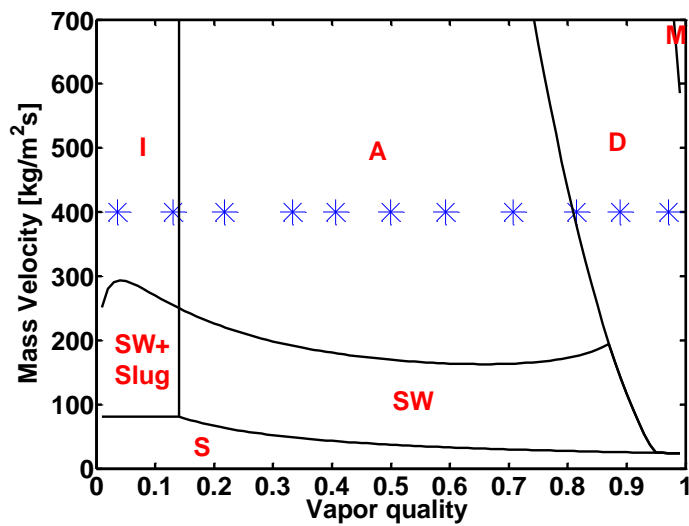


Figure 19. Comparison of the several leading methods to the experimental data of Bredesen et al. [40] at the experimental conditions: $G = 400 \text{ kg/m}^2\text{s}$, $T_{\text{sat}} = -10 \text{ }^\circ\text{C}$, $D_{\text{eq}} = 7 \text{ mm}$ and $q = 6 \text{ kW/m}^2$; 1 - The Moreno-Quibén and Thome model [63, 64]; 2 - The Friedel method [92]; 3 - The Grönnerud method [93]; 4 - The Müller-Steighagen-Heck method [94]; 5 - The Chisholm method [91].



(a)



(b)

Figure 20. (a) Comparison of the new CO₂ pressure drop model to the experimental data of Bredesen et al. [40] at the experimental conditions: $G = 400 \text{ kg/m}^2\text{s}$, $T_{\text{sat}} = -10 \text{ }^\circ\text{C}$, $D_{\text{eq}} = 7 \text{ mm}$ and $q = 3 \text{ kW/m}^2$; (b) The corresponding flow pattern map at the same experimental condition as that in (a) (I represents intermittent flow, A represents annular flow, D represents dryout region, M represents mist flow, S represents stratified flow and SW represents stratified-wavy flow).

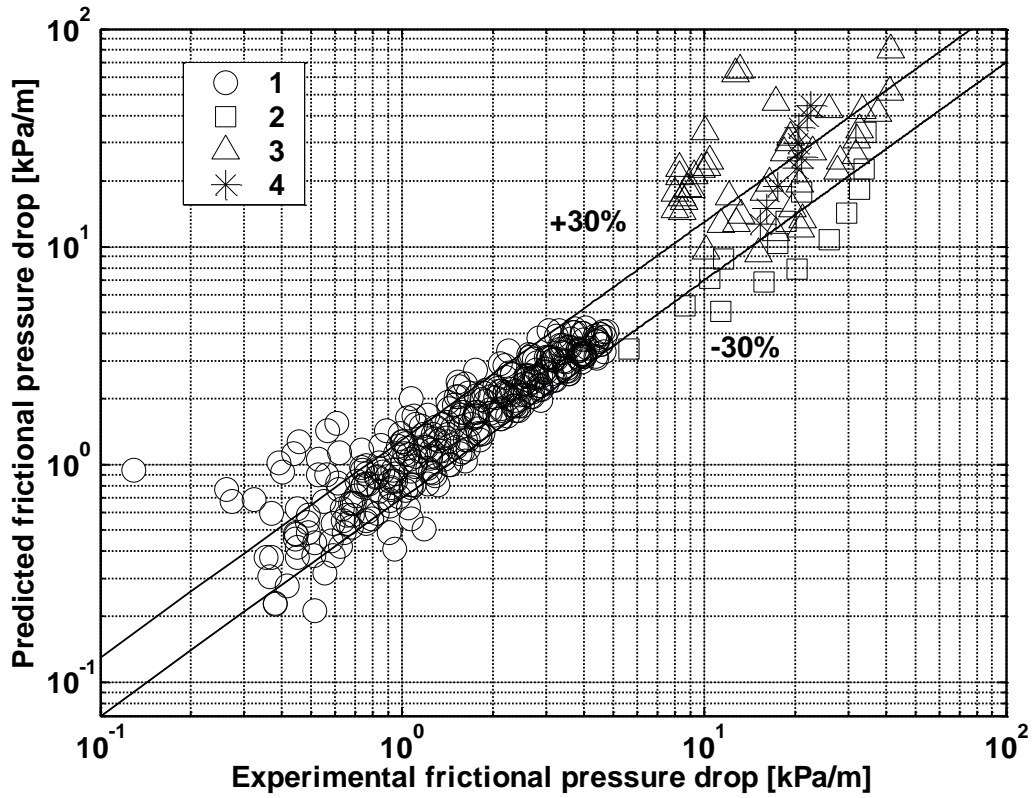


Figure 21. Comparison of the predicted frictional pressure gradients by the new model to the entire database (74.7% of the data are predicted within $\pm 30\%$) [30]: 1–Bredesen et al. [40], 2–Yun and Kim [89, 117], 3– Pettersen [32] and Pettersen and VestbØstad [88] and 4–Zhao et al. [86, 87] (Note that 2, 3 and 4 are the data of micro-channels).

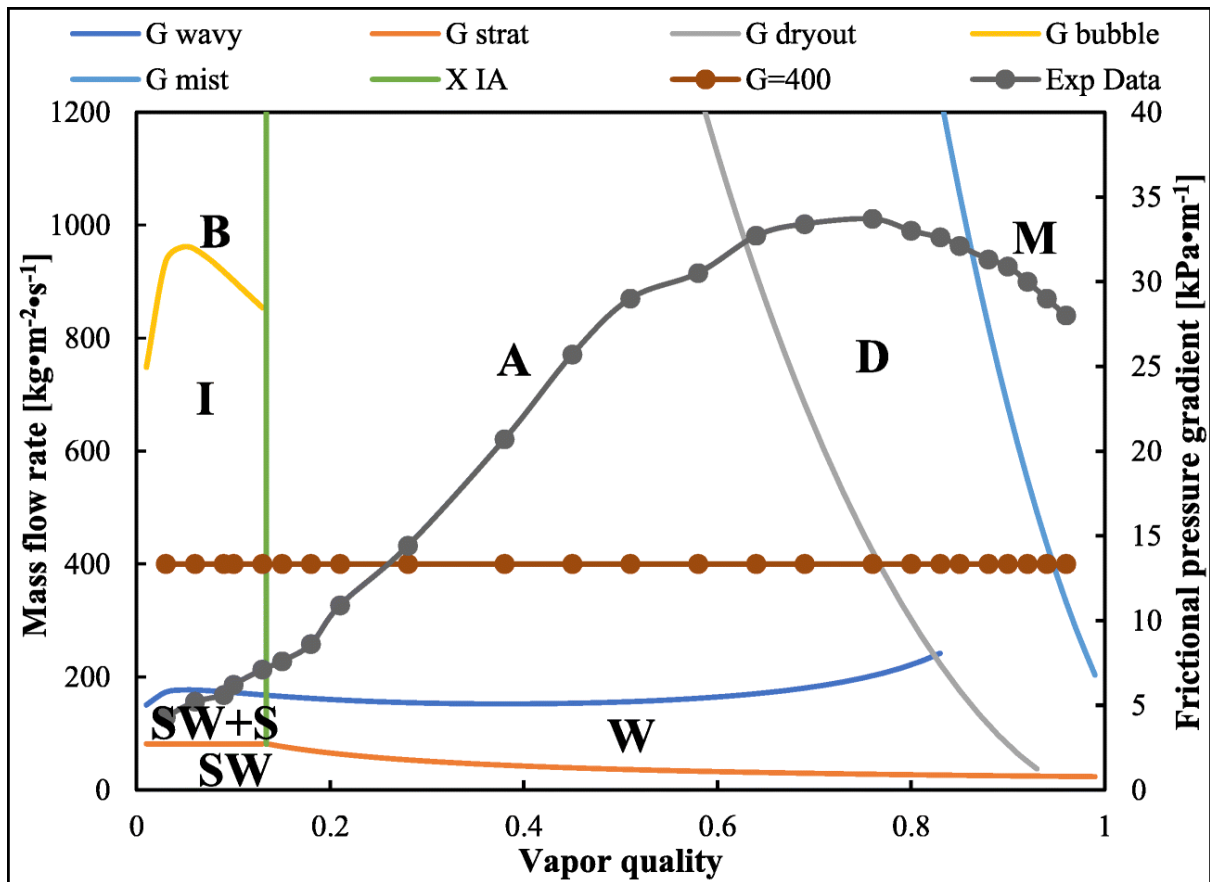
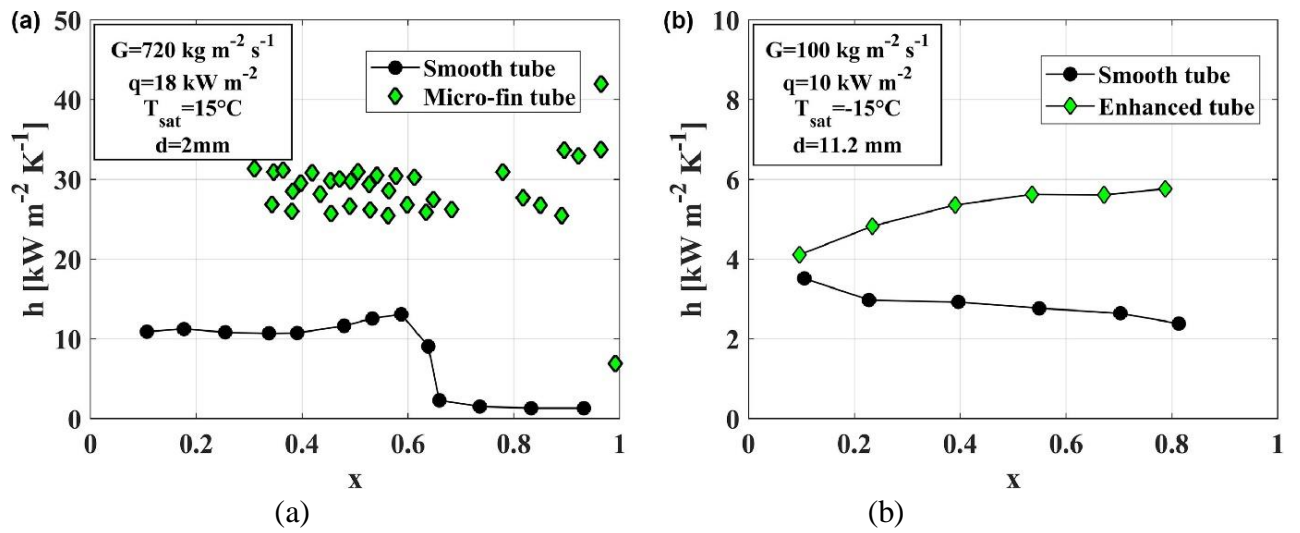
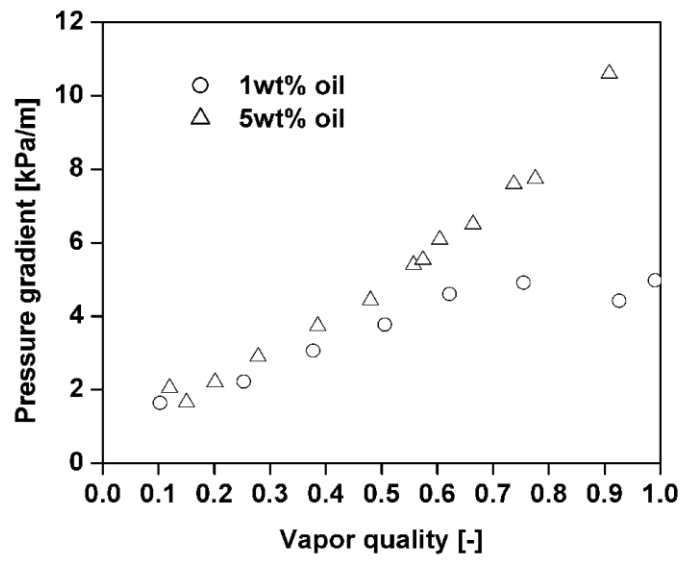


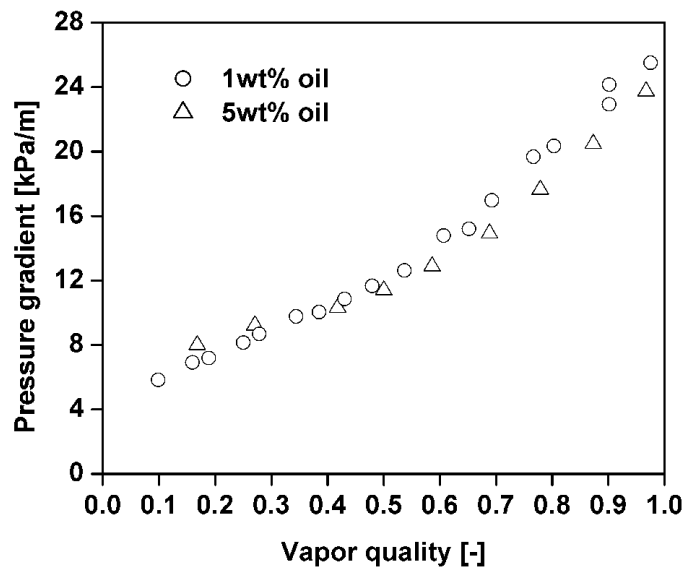
Figure 22. Experimental two phase frictional pressure drop data for CO_2 flow boiling at $T_{\text{sat}} = -10\text{ }^\circ\text{C}$, $G = 400\text{ kg}/(\text{m}^2\text{s})$ and $q = 7.5\text{ kW}/\text{m}^2$ and the corresponding flow patterns on the Cheng et al. flow pattern map by Zhang et al. [115].



Figur 23. Comparison between the CO₂ flow boiling heat transfer coefficients in micro-fin tube and those in smooth tube: (a) Experimental results in small channel with 2 mm diameter by Dang et al. [106]; (b) Experimental results in large channel with 11.2 mm diameter by Kim and Hrnjak [138].



(a)



(b)

Figure 24. The effect of the oil on two-phase pressure drop [130]: $G = 400 \text{ kg/m}^2\text{s}$, $q = 10 \text{ kW/m}^2$; (b) $G = 800 \text{ kg/m}^2\text{s}$, $q = 10 \text{ kW/m}^2$.

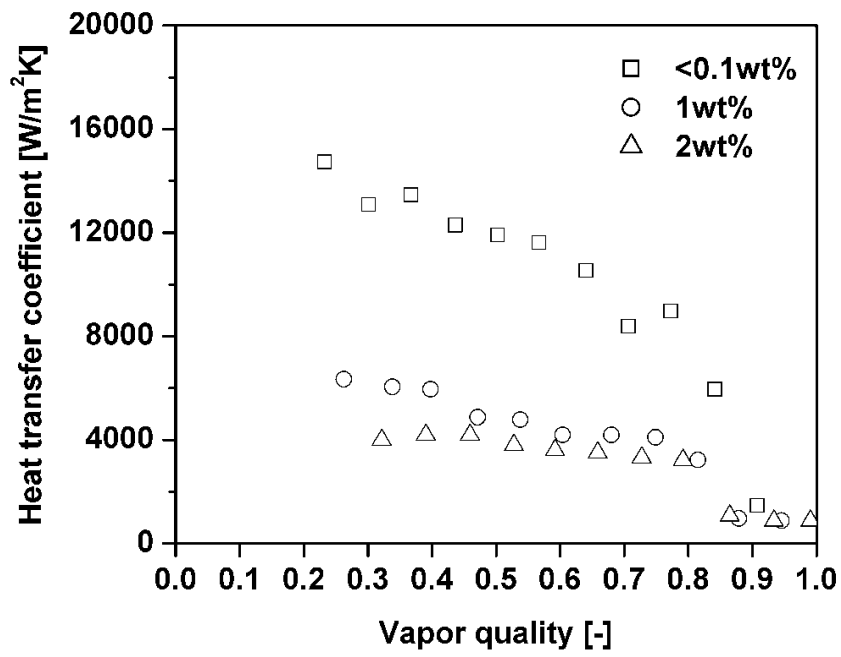


Figure 25. The effect of oil on heat transfer coefficient [131, 132]: $T_{\text{sat}} = 10^{\circ}\text{C}$, $G = 390 \text{ kg/m}^2\text{s}$, $q = 20 \text{ kW/m}^2$.

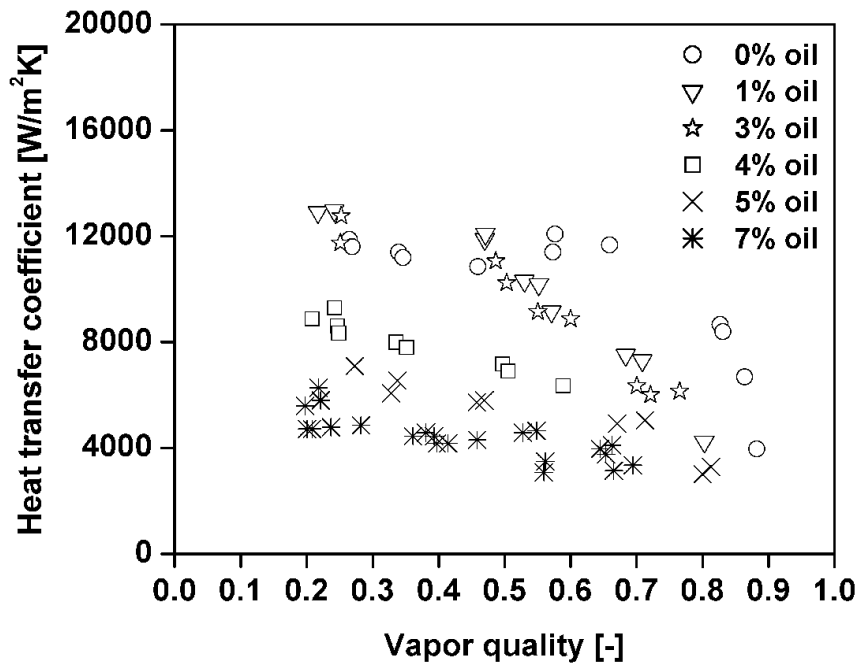


Figure 26. The effect of oil on heat transfer coefficient [138] ($T_{\text{sat}} = 10^{\circ}\text{C}$, $G = 300 \text{ kg/m}^2\text{s}$, $q = 11 \text{ kW/m}^2$).

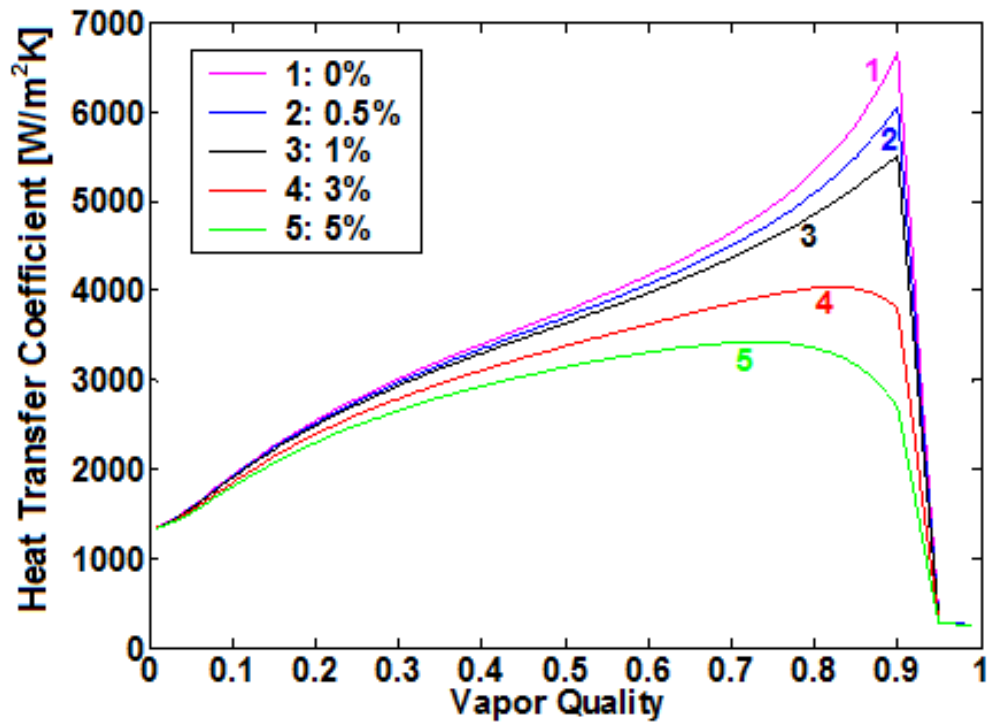


Figure 27. The oil effect (mass concentration from 0 to 5%) on the evaporation heat transfer coefficient of R134a in a horizontal tube (Simulated results by the flow pattern based heat transfer model of Wojtan et al. [48, 49]): $G = 300 \text{ kg/m}^2\text{s}$, $T_{\text{sat}} = 10^\circ\text{C}$, $D = 13.84 \text{ mm}$ and $q = 7.5 \text{ kW/m}^2$.

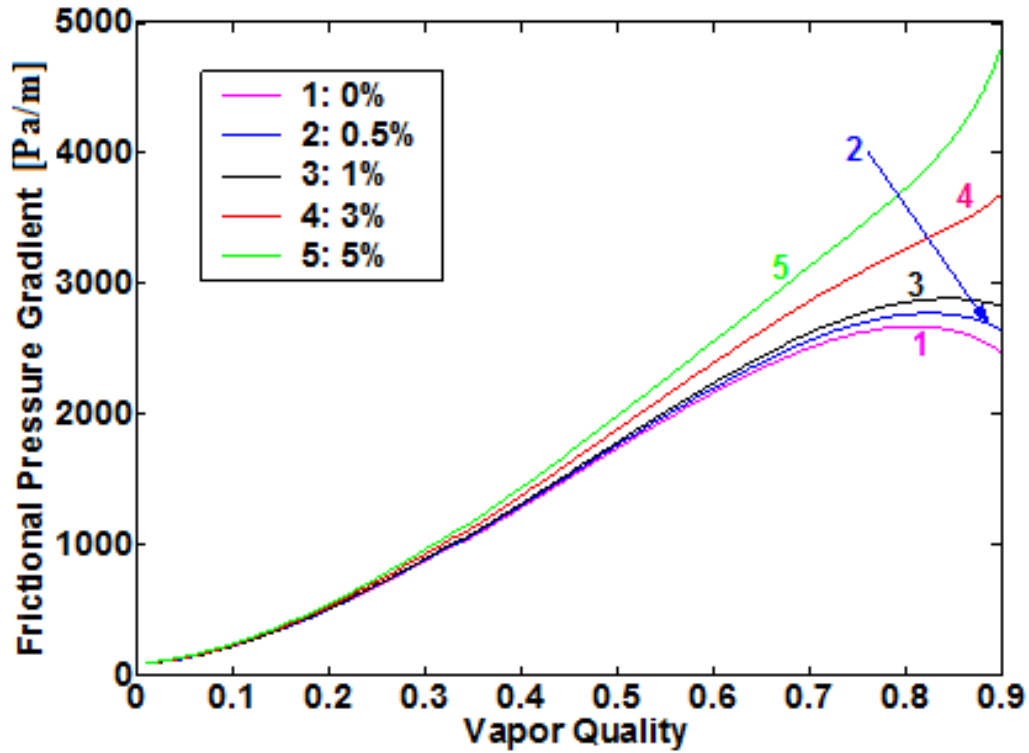
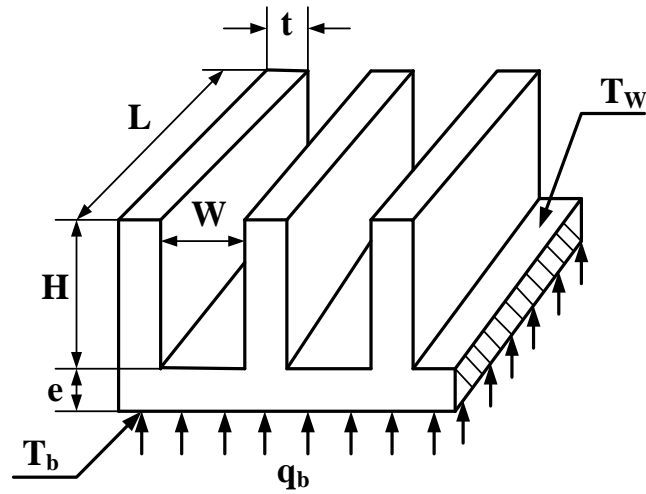


Figure 28. The oil effect (mass concentration from 0 to 5%) on two-phase frictional pressure gradient of R134a in a horizontal tube for flow regimes before dryout region (The two-phase frictional pressure gradients were calculated using the flow pattern based two-phase pressure drop model of Moreno-Quiben and Thome [63, 64] for pure R134a with a correction factor of oil effect on two-phase pressure drop): $G = 300 \text{ kg/m}^2\text{s}$, $T_{\text{sat}} = 10^\circ\text{C}$, $D = 13.84 \text{ mm}$ and $q = 7.5 \text{ kW/m}^2$.



L (mm)	H (mm)	W (mm)	t (mm)	e (mm)	N	D (mm)
20	0.68	0.223	0.08	0.32	67	0.336* 0.44**

Figure 29. Schematic diagram of multi-microchannel evaporators for simulation of electronic chips cooling by Cheng and Thome [11].

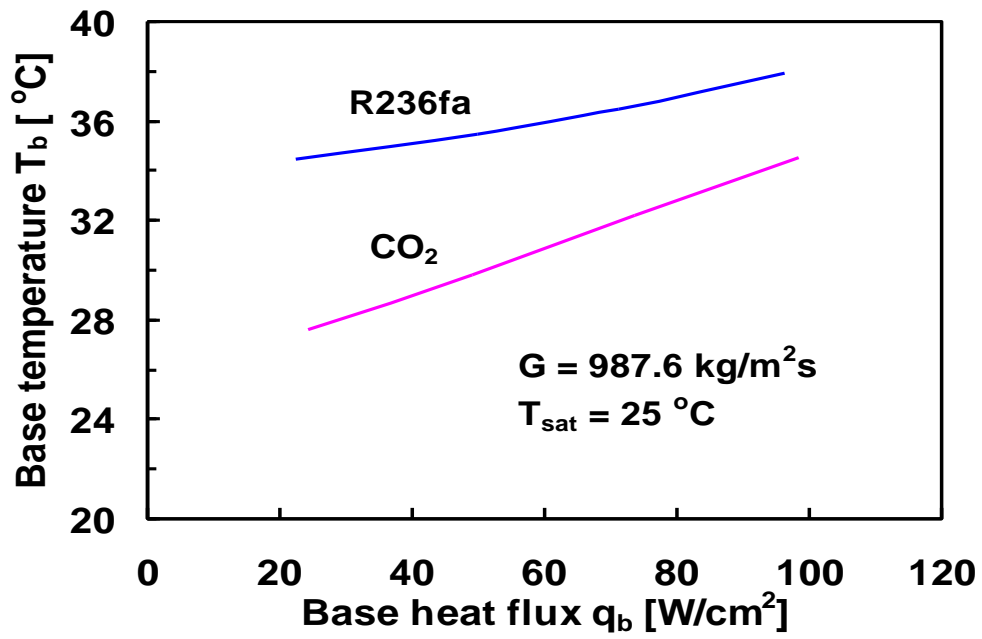


Figure 30. Comparisons of simulation results of base temperature of CO₂ and R236fa at the indicated conditions for chips cooling by Cheng and Thome [11].

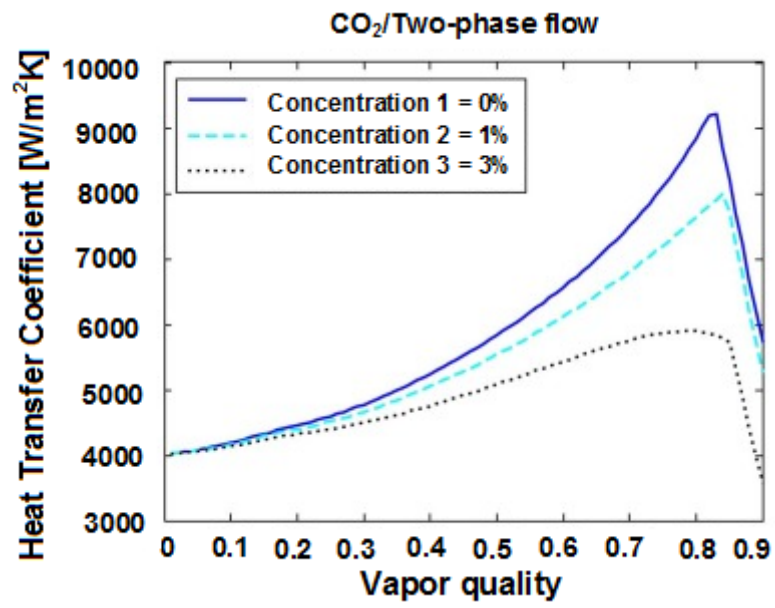


Figure 31. The oil effect (mass concentration from 0 to 3%) on the evaporation heat transfer coefficient of CO₂ in the evaporator tube using the Cheng et al. [31] heat transfer model [141].

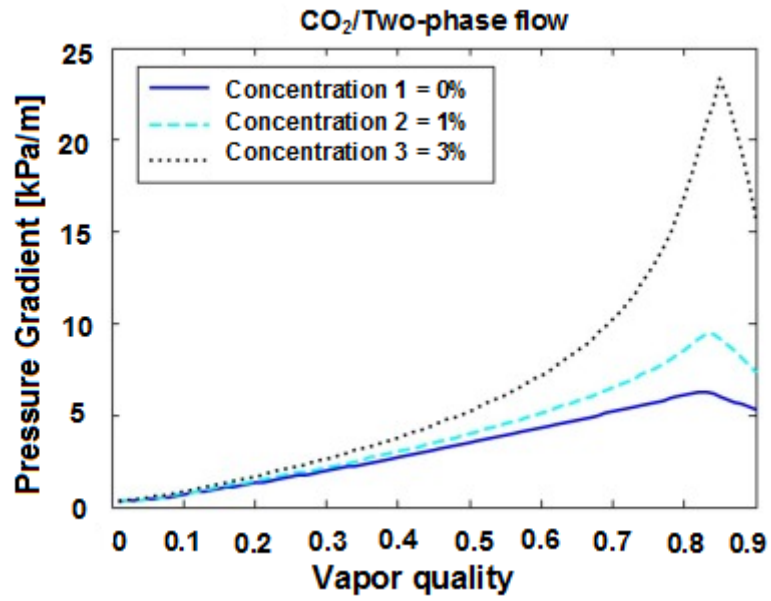


Figure 32. The oil effect (mass concentration from 0 to 3%) on the two-phase frictional pressure gradient of CO₂ in the evaporator tube using the Cheng et al. [31] pressure drop model [141].

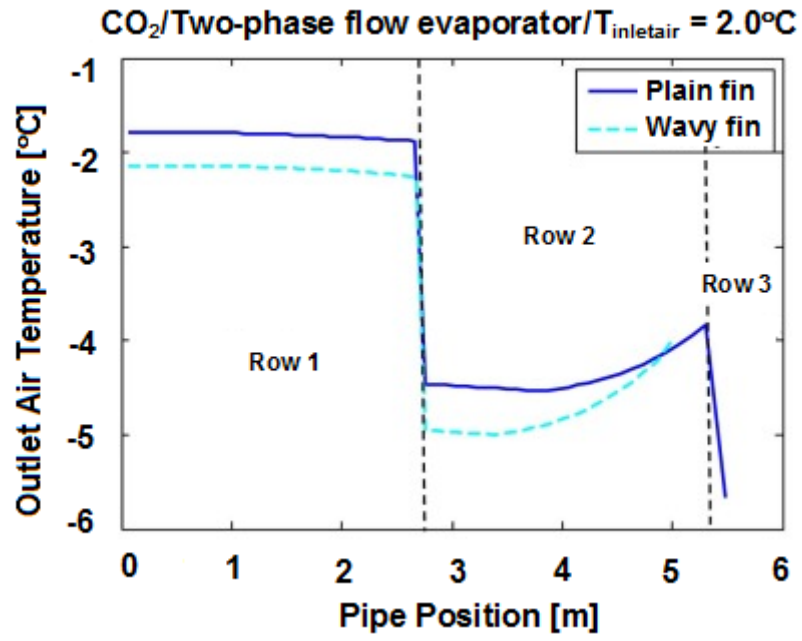


Figure 33. The outlet air temperature per row for the plain fin and the wavy fin evaporators (fin type effect) [141].

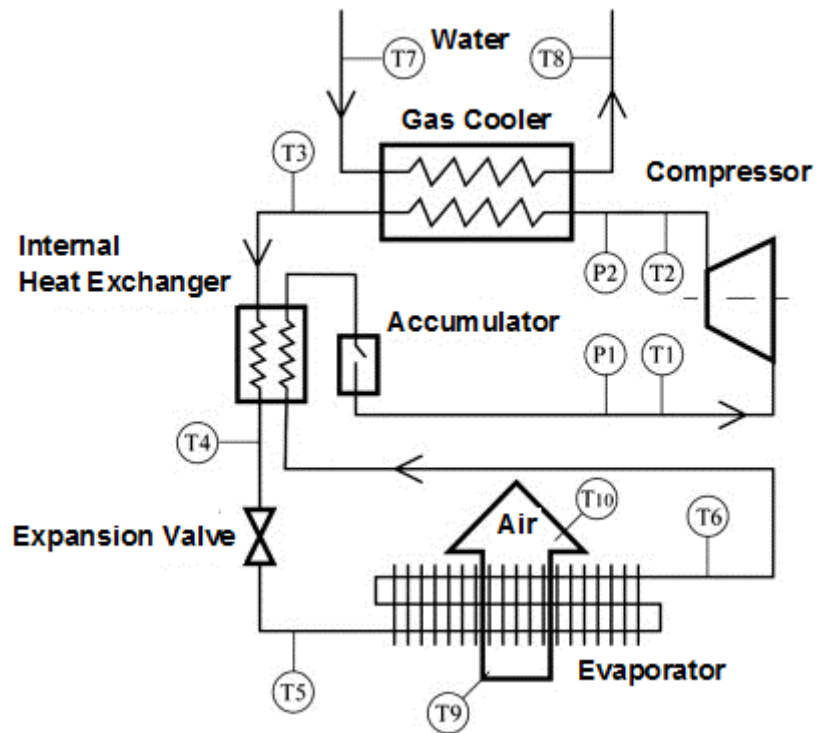


Figure 34. System flow diagram of CO₂ heat pump and measuring points in the study of Yamaguchi et al. [142].

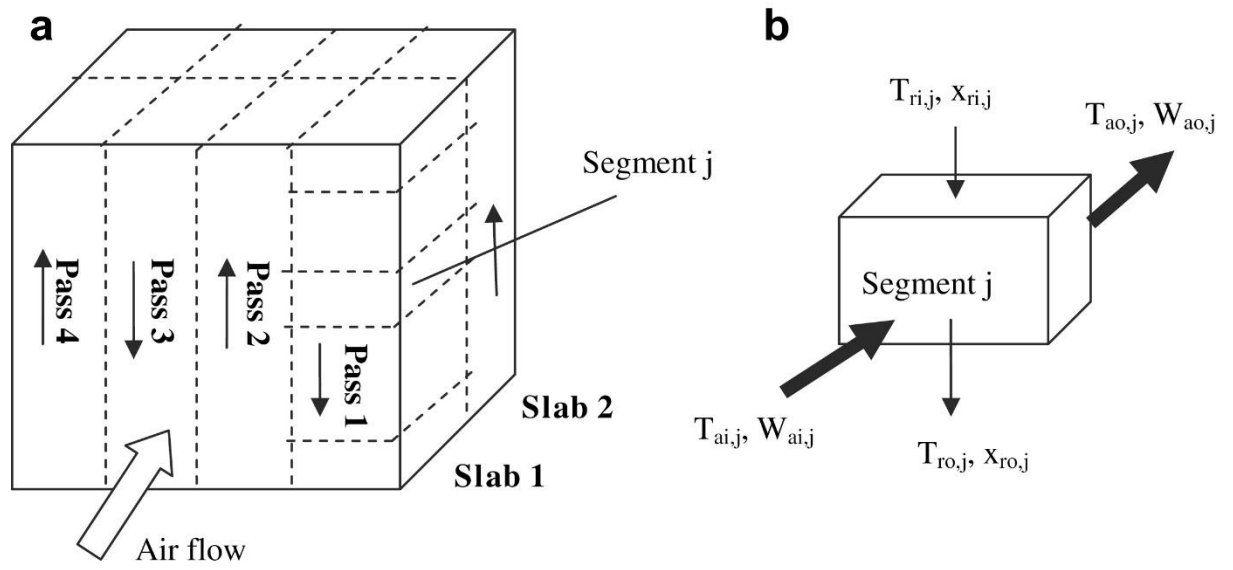


Figure 35. Schematic illustration of evaporator model segment discretization: (a) evaporator geometry, (b) j th segment. [160]